Towards a new geological time scale: A template for improved rock-based subdivision of pre-Cryogenian time

Graham A. Shields[1*], Robin A. Strachan[2], Susannah M. Porter[3], Galen P. Halverson[4], Francis A. Macdonald[3], Kenneth A. Plumb[5], Carlos J. de Alvarenga[6], Dhiraj M. Banerjee[7], Andrey Bekker[8], Wouter Bleeker[9], Alexander Brasier[10], Partha P. Chakraborty[7], Alan S. Collins[11], Kent Condie[12], Kaushik Das[13], Evans, D.A.D.[14], Richard Ernst[15], Anthony E. Fallick[16], Hartwig Frimmel[17], Reinhardt Fuck[6], Paul F. Hoffman[18], Balz S. Kamber[19], Anton Kuznetsov[20], Ross Mitchell[21], Daniel G. Poiré[22], Simon W. Poulton[23], Robert Riding[24], Mukund Sharma[25], Craig Storey[2], Eva Stueeken[26], Rosalie Tostevin[27], Elizabeth Turner[28], Shuhai Xiao[29], Shuanhong Zhang[30], Ying Zhou[1], Maoyan Zhu[31]

[1]Department of Earth Sciences, University College London, UK; g.shields@ucl.ac.uk
[2]School of the Environment, Geography and Geosciences, University of Portsmouth, UK
[3]Department of Earth Science, University of California at Santa Barbara, USA
[4]Department of Earth and Planetary Sciences, McGill University, Canada
[5]Geoscience Australia (retired), Canberra, Australia
[6]Instituto de Geociências, Universidade de Brasilia, Brazil
[7]Department of Geology, University of Delhi, India
[8]Department of Earth and Planetary Sciences, University of California, Riverside, USA
[9]Geological Survey of Canada , Ottawa, Canada
[10]School of Geosciences, University of Aberdeen, UK
[11]Department of Earth Sciences, The University of Adelaide, Australia
[12]New Mexico Institute of Mining and Technology, USA
[13]Department of Earth and Planetary System Sciences, Hiroshima University, Japan
[14]Department of Earth and Planetary Sciences, Yale University, USA
[15]Department of Earth Sciences, Carleton University, Canada; Faculty of Geology and Geography, Tomsk State University, Tomsk, Russia
[16]Isotope Geosciences Unit S.U.E.R.C., East Kilbride, UK
[17]Institute of Geography and Geology, University of Würzburg, Germany
[18]Department of Earth and Planetary Sciences, Harvard University, USA; University of Victoria, Canada
[19]School of Earth and Atmospheric Sciences, Queensland University of Technology, Brisbane, Australia
[20]Institute of Precambrian Geology and Geochronology, St. Petersburg, Russia
[21]Institute of Geology and Geophysics, Beijing, China
[22]Centro de Investigaciones Geológicas–CONICET–FCNyM, (UNLP), La Plata, Argentina
[23]School of Earth and Environment, University of Leeds, UK
[24]Department of Earth and Planetary Sciences, University of Tennessee, Knoxville, USA
[25]Birbal Sahni Institute of Palaeobotany, Lucknow, India
[26]Department of Earth Sciences, University of St. Andrews, UK
[27]Department of Earth Sciences, University of Cape Town, South Africa

[28]Laurentian University, Sudbury, Canada
[29]Department of Geosciences, Virginia Tech, USA
[30]Institute of Geomechanics, Chinese Academy of Geological Sciences, China
[31]Nanjing Institute of Geology and Palaeontology, Nanjing, China

Abstract

Four eon- and nine era-level units continue to provide intuitive subdivision of geological time. Major Earth system transitions occurred at approximately 2.5-2.3, 1.8-1.6, 1.0-0.8 and 0.7-0.5 Ga, and so future rock record-based subdivision of pre-Cryogenian time, eventually by use of global stratotypes (GSSPs), will likely require only modest deviation from current chronometric era boundaries. Here we argue that removal of GSSAs could be expedited by establishing event-based concepts and provisional, approximate ages for eon-, era- and period-level subdivisions as soon as practicable. We also outline the geological basis behind the current timescale and outline where immediate changes to the present scheme could be formalised, as a framework for future GSSP development. We agree with previous workers that the informal four-fold Archean subdivision could be simplified to a tripartite scheme pending more detailed analysis. Although the ages of period boundaries would inevitably change in a more closely rock-based or chronostratigraphic scheme, we support retention of all currently ratified period names. Existing period names, borrowed from the Greek, were chosen to delimit natural phenomena of global reach. Any new global nomenclature ought to follow this lead for consistency (e.g., *Scourian, Kratian, Kleisian, Syndian*), and so we discourage the use of both supercontinent names (e.g., Rodinian, Columbian) and regional phenomena, however exceptional they may be. Here we propose that a new period could precede the Tonian as the first period of the Neoproterozoic Era and concur with previous authors that the existing Siderian Period (named for iron formations) would fit better as a chronostratigraphically defined period of the terminal Archean rather than the basal Proterozoic. Indeed, all pre-Cryogenian subdivisions will need better conceptual grounding in any future chronostratigraphic scheme. We conclude that an improved rock-based Proterozoic Eon could potentially comprise a three-fold, period-level subdivision of the Paleoproterozoic Era (*early Paleoproterozoic or Scourian,* Rhyacian, Orosirian), a four-fold subdivision of the Mesoproterozoic Era (Statherian, Calymmian, Ectasian, Stenian) and potentially four-fold subdivision of the Neoproterozoic Era (pre-Tonian or *Kleisian*, Tonian, Cryogenian and Ediacaran). Refinements towards an improved rock-based pre-Cryogenian time scale could potentially use the proposed framework for further development by international bodies with remits over the 1) pre-Ediacaran Neoproterozoic, 2) Mesoproterozoic, 3) Paleoproterozoic and 4) Archean (plus Hadean) as few experts and disciplines can speak to the entire pre-Cryogenian rock record.

1. Introduction

The term 'Precambrian', or more traditionally 'pre-Cambrian' (Glaessner, 1962), is an informal geological term that refers to the time before the beginning of the Cambrian Period at c. 0.54 Ga (Peng et al., 2020). The two pre-Cambrian eonothems (Archean and Proterozoic) have long pedigrees (Sedgwick, 1845; Logan, 1857; Dana, 1872), but, were introduced formally only after extensive discussion among members of the Subcommission on Precambrian Stratigraphy (SPS), which was tasked in 1966, with Kalervo Rankama as chair, with standardizing Precambrian nomenclature (Trendall, 1966). James (1978), summarising discussions within the subcommission, outlined five categories of proposals: 1) subdivision by intervals of equal duration (Goldich, 1968; see also Hofmann, 1990; 1992; Trendall, 1991); 2) subdivision by major magmatic-tectonic cycles (Stockwell, 1961; 1982); 3) subdivision by stratotypes (Dunn et al., 1966; see also Crook, 1989); 4) subdivision by breaks in the geological record defined by radiometric ages (James, 1972); and 5) subdivision based on Earth evolution concepts (Cloud, 1976). One result of those early discussions was that an approximate chronological age of 2500 Ma was assigned to a somewhat transitional Archean-Proterozoic boundary (James, 1978). However, further subdivision of the Precambrian in a comparable manner to that achieved for younger rocks, although favoured by some (Hedberg, 1974), proved unworkable (James, 1978) due to 1) the relatively fragmentary nature of the Precambrian rock record, much of which is strongly deformed and metamorphosed, and 2) a scarcity of age-diagnostic fossils. For this reason, a mixed approach was applied: Global Standard Stratigraphic Ages (GSSAs) were introduced to subdivide Precambrian time but the absolute ages of periods were chosen to bracket major magmatic-tectonic episodes (Plumb and James, 1986; Plumb, 1991). Since that decision was ratified, all of pre-Cryogenian Earth history and its geological record has been subdivided using geochronology rather than chronostratigraphy.

The principal Precambrian subdivisions now comprise the informal Hadean and formal Archean and Proterozoic eons (Fig. 1A), which, following the GSSA concept, are defined as units of time rather than stratigraphic packages. The Hadean Eon refers to the interval with no preserved crustal fragments that followed formation of the Earth at c. 4.54 Ga (Patterson, 1956; Manhes et al., 1980). Because the Hadean Eon left no rock record on Earth (other than reworked mineral grains or meteorites), it cannot be regarded as a stratigraphic entity (eonothem) and has never been formally defined or subdivided. It is succeeded by the Archean Eon, which is usually taken to begin at 4.0 Ga and is itself succeeded at precisely 2.5 Ga by the Proterozoic Eon. The Archean Eon is informally divided into four eras (Eoarchean, Paleoarchean, Mesoarchean and Neoarchean; e.g., Bleeker, 2004a), although a three-fold subdivision is widely favoured (van Kranendonk et al., 2012; Strachan et al., 2020). The Proterozoic Eon is currently subdivided into three eras (Paleoproterozoic, Mesoproterozoic and Neoproterozoic) and ten periods (Siderian, Rhyacian, Orosirian, Statherian, Calymmian, Ectasian, Stenian, Tonian, Cryogenian and Ediacaran). The era names were conceived after a proposal from Hans

Hofmann in 1987 (Hofmann, 1992; Plumb, 1992), while the period names derive from discussions within the SPS (Plumb 1991). The three Proterozoic eras were originally proposed to begin at 2.5 Ga (Proterozoic I), 1.6 Ga (Proterozoic II) and 0.9 Ga (Proterozoic III), respectively (Plumb and James, 1986). However, the beginning of the Neoproterozoic Era was subsequently moved to 1.0 Ga in the final proposal (Plumb, 1991).

The ages of Precambrian boundaries were selected to delimit major cycles of sedimentation, orogeny and magmatism (Plumb, 1991; Fig. 1A). However, knowledge has improved considerably over the past thirty years due to 1) increasingly precise and accurate U-Pb zircon dating, 2) improved isotopic and geochemical proxy records of tectonic, environmental and biological evolution, and 3) new rock and fossil discoveries. As a result, some of these numerical boundaries no longer bracket the events for which they were named. The International Commission on Stratigraphy (ICS) began to address the GSSA immobility problem in 2004 when they ratified the basal Ediacaran GSSP (Global Stratotype Section and Point) on the basis of the stratigraphic expression of a global chemo-oceanographic (and climatic) event in a post-glacial dolostone unit in South Australia (Knoll et al., 2004). Latest geochronology and chronostratigraphy confirms that all typical Marinoan 'cap dolostone' units were deposited contemporaneously at c. 635.5 Ma (Xiao and Narbonne, GTS 2020). The Ediacaran GSSP is thus one of the most highly resolved system-level divisions of the entire geological record.

The chronostratigraphic (re)definition of the Ediacaran Period (and System) replaced the provisional GSSA (650 Ma) that had been used to mark the end of the Cryogenian Period. This allowed the Marinoan 'snowball' glaciation (c. 645 – c. 635.5 Ma) to be included within the geological period that owed its name to that glaciation. The 850 Ma age marking the beginning of the Cryogenian was subsequently found to be much older than consensus estimates for the onset of widespread Sturtian 'snowball' glaciation at c. 717 Ma (Macdonald et al., 2010; Halverson et al., 2020) and so it was also removed, following a proposal from the Cryogenian Subcommission (Shields-Zhou et al., 2016). A globally correlative stratigraphic horizon at or beneath this level has not yet been proposed by the Cryogenian Subcommission, although an approximate age of c. 720 Ma for the boundary, pending a ratified GSSP, has been written into the international geological time scale. Despite the lack of a GSSP, the age revision of the Cryogenian Period by 130 million years has been quickly accepted by the geological community worldwide, presumably because it now matches the natural phenomena for which it was named. International geological bodies have yet to tackle other issues of non-alignment between names and ages for any other Proterozoic period despite occasional challenges, e.g., Bleeker (2004a,b), van Kranendonk et al. (2012).

In both cases (Cryogenian and Ediacaran GSSPs), and in the case of the earlier ratification of the Precambrian-Cambrian boundary GSSP (Brasier et al., 1994), establishment of a rock-based or chronostratigraphic concept permitted relatively easy consensus around an approximate, stratigraphically calibrated age, before more prolonged and detailed discussions could take place towards eventual GSSP proposal and ratification. In the light of rapidly expanding knowledge about

158 Precambrian Earth history, these three precedents serve to illustrate how the GSSA approach has
159 become outdated and how it is now evident that all Precambrian subdivisions will require revision to a
160 more natural, chronostratigraphic framework (e.g., Bleeker 2004a,b; Van Kranendonk et al., 2012;
161 Ernst et al., 2020). Identified shortcomings with the inflexible GSSA approach include: a) a lack of ties
162 to the rock record and broader Earth and planetary history, b) the diachronous nature of the tectonic
163 events on which the current scheme (Fig. 1A) is based, and c) the lack of any major sedimentological,
164 geochemical and biological criteria that can be used to correlate subdivision boundaries in stratigraphic
165 records. As a result, Proterozoic period nomenclature, although increasingly used in the scientific
166 literature, is commonly out of step with the concepts or phenomena for which they were named, while
167 the underlying basis for both era and period nomenclature is neither universally accepted nor widely
168 understood.
169 An alternative stratigraphic scheme for the Precambrian was therefore revisited for discussion
170 based on potential Global Boundary Stratotype Sections and Points (GSSPs) (Fig. 1B) (Van
171 Kranendonk et al., 2012). Following the rationale of Cloud (1972), the approach taken was to base a
172 revised Precambrian time scale as closely as possible around geobiological events, such as changes to
173 oceans, atmosphere, climate or the carbon cycle that would be near instantaneous compared to changes
174 in geotectonic processes. We agree with the rationale pursued in Van Kranendonk et al. (2012), which
175 followed an earlier proposal of Bleeker (2004a), while noting that some newly proposed subdivisions
176 represent a radical departure from standard practice. This is illustrated by the proposal of a new and
177 exceptionally long 'Rodinian' Period between 1800 Ma and 850 Ma Van Kranendonk et al. (2012),
178 which replaced five of the pre-existing Proterozoic periods. The principle of naming a geological period
179 after a hypothetical supercontinent set a further precedent that is not widely accepted.
180 Recent progress towards, and widespread acceptance of, chronostratigraphic definitions for two
181 Precambrian periods suggests that the international community can act expeditiously to address
182 inadequacies of the chronometric scheme, while overcoming the confusion generated by the informal
183 erection of new periods and unsupported concepts. This contribution outlines current understanding of
184 Earth history in order to encourage broader consultation on new recommendations around 1) a time
185 frame for GSSA removal, 2) rock-based concepts and approximate ages for eon-, era- and possible
186 period-level subdivision of pre-Cryogenian time, and 3) new international expert bodies to propose
187 concepts, criteria and candidates for future GSSPs. Our aim is to outline the geological basis behind
188 current chronometric divisions, explore how boundaries might differ in any future chronostratigraphic
189 scheme, identify where major issues might arise during the transition to that scheme, and identify where
190 some immediate changes to the present scheme could be easily updated/formalised, as a framework for
191 future GSSP development. We note that this is not simply a matter of academic interest for geologists.
192 Establishing a robust, coherent and intuitive stratigraphic nomenclature is of great importance for
193 improving understanding of Earth's history for schools, universities and the wider community alike.

Transitioning from a purely chronometric to a chronostratigraphic scheme will inevitably place more emphasis on the rock record and on precise stratigraphic levels within key successions and their global equivalents. In this regard, we accept the arguments made by Zalasiewicz et al. (2004) that units of time and strata are, following the introduction of boundary stratotypes and points or GSSPs, interchangeable and largely superfluous. Specifically, we agree that chronostratigraphic units such as eonothem, erathem or system are confusing and argue that they are particularly inappropriate for subdividing the enormously long time intervals and relatively incomplete rock records of the pre-Cryogenian archive. As a result, we mainly use time subdivisions below (eons, eras, periods), while recalling that their precise definitions and stratigraphically calibrated ages would eventually need to be defined using a level within a global boundary stratotype section.

2. Eon- and Era-level subdivisions of Precambrian time

2.1 Hadean Eon (> c.4.0 Ga)

Spanning the interval between the formation of the Solar System (c. 4.567 Ga) and the first rock-based evidence for crust on Earth (c. 4.0 Ga), the Hadean Eon was a time of planetary accretion and differentiation. Defining an absolute time scale for the eon is challenging due to the criterion on which it is typically defined: the lack of a preserved rock record on Earth (Cloud, 1976; Strachan et al., 2020). Nevertheless, our understanding of the geological processes that shaped our planet during the Hadean continues to improve. Neither the beginning nor the end of the Hadean are yet formally defined by the International Commission on Stratigraphy (ICS) but the end is usually taken as 4.0 Ga (Fig. 1A). It has been proposed that the Hadean-Archaean boundary be defined as the age of the oldest preserved crustal rock (van Kranendonk et al., 2012). The oldest unambiguously dated rocks are 4.031 ± 0.003 Ga orthogneisses from the Acasta gneiss of the Slave Craton, Canada (Stern and Bleeker, 1998; Bowring and Williams, 1999), which led van Kranendonk et al. (2012) to propose that the boundary be placed at c. 4.03 Ga (Fig. 1B). However, other authorities have preferred a younger boundary at c. 3.85 Ga to represent the time when crustal preservation on multiple cratonic fragments increased sharply (Bleeker, 2004a,b; Kamber, 2015). A definition based around the ages of the oldest unambiguous supracrustal rocks matches closely the ideas of Cloud (1972) and may facilitate more robust linkages with wider solar system evolution

Controversially, older model ages of up to ~4.4 Ga have been inferred for mafic gneisses in the Nuvvuagittuq Supracrustal Belt in the Superior Province, Canada (O'Neil et al., 2008, 2012), based on contested interpretations of the short-lived ^{146}Sm-^{142}Nd systematics in these highly metamorphosed rocks (e.g., see Caro et al., 2017). Zircon U-Pb ages from felsic orthogneisses in the Nuvvuagittuq Belt suggest a formation age of >3.8 Ga (e.g., Darling et al., 2014), and coupled Lu-Hf and Sm-Nd model ages of ~3.9 Ga for the mafic gneisses have been taken as evidence for an Archean, rather than Hadean

origin (e.g., Guitreau et al., 2013). However, O'Neil et al. (2012) report a ^{147}Sm-^{143}Nd isochron from intrusive gabbro in the Nuvvuagittuq Belt of 4.115 ± 0.1 Ga. Taken together, these studies highlight the difficulty in unambiguously dating highly deformed and metamorphosed ancient crustal rocks from very small preserved fragments (Kamber, 2015), while confirming that c. 4.0 Ga (or later) still represents a suitable approximate age for the Hadean-Archean boundary if defined on the basis of potentially correlative rock and mineral assemblages. To debate this boundary further, however, lies beyond the scope and intent of the current paper, as the defining concept of the Hadean remains largely unchallenged.

2.2 Archean Eon (c. 4.0 to 2.45/2.5 Ga)

The Archean Eon spans the period of early crustal formation and thickening, leading to the formation of the first cratons and platform sedimentation. It is characterised by granite-greenstone terranes and the extrusion of ultramafic lavas (komatiites), which are very rare in post-Archean rocks. Away from the recognised granite-greenstone terranes or younger platform covers, the Archean is characterised by high-grade, polymetamorphic granite-gneiss complexes, of various ages.

Subdivision of the chronometric Archean Eon was not formalised, pending collection of more data and analysis (Plumb, 1991). Nevertheless, the Subcommission on Precambrian Stratigraphy (SPS) voted in 1991 and again in 1995 to pursue formal subdivision into four eras: Eoarchean (>3.6 Ga), Paleoarchean (3.6 to 3.2 Ga), Mesoarchean (3.2 to 2.8 Ga), and Neoarchean (2.8 to 2.5 Ga) (Fig. 1A); no reasons for the choice of these boundaries were given. Since these subdivisions have not been formally ratified (Robb et al., 2004), they are considered to be recommendations only (Bleeker, 2004a). An alternative subdivision scheme was proposed by van Kranendonk et al. (2012), which simplified these to three: the Paleoarchean (4.03 to 3.49 Ga), Mesoarchean (3.49 to 2.78 Ga), and Neoarchean (2.78 to 2.42 Ga), each composed of a number of periods (Fig. 1B). The base of the Paleoarchean in the 2012 proposal was defined by the age of the oldest extant rocks, the Acasta Gneiss, Canada, while the base of the overlying Mesoarchean was defined at the oldest microbially-influenced textures or structures in stromatolites of the North Pole Dome in western Australia, thus representing the oldest potential "golden spike" (Fig. 1B). The Paleoarchean contained an 'Acastan Period', the lower limit of which was defined by the oldest preserved rocks (Acasta Gneiss, Canada) and an 'Isuan Period', the lower limit of which was defined at 3.81 Ga (the age of the Earth's oldest supracrustal rocks, the Isua Supracrustal Belt in Greenland).

The problem with this approach is that the oldest occurrence of a particular rock type may identify chance preservation rather than any fundamental change in geological process, and older terranes may be identified in the future. It also runs counter to the concept of the international geological time scale as a correlative 'stratigraphic' framework, leading us to support leaving the base of the Archean at ~4.0 Ga, pending formal definition of the Hadean-Archean boundary. This argument also invalidates the Eoarchean as a fundamental unit of geological time. A similar problem arises with the placement of the

base of the Mesoarchean at c. 3.49 Ga for the North Pole Dome stromatolites; not only the problem of these being the "oldest" stromatolites, but the occurrence of stromatolites is controlled by the particular environment, rather than being a definable moment in evolution. A less ambiguous boundary for the base of the Mesoarchean could be the near-coeval base of the first preserved Barberton and Pilbara granite-greenstone terranes. This is currently considered to be ~3.5 Ga, or perhaps a little older. High-grade metamorphic-plutonic complexes, with little internal stratigraphic structure (e.g., Limpopo Belt; Western Gneiss Terranes, Western Australia) become more common toward the top of the interval.

Van Kranendonk et al. (2012) also proposed changing the end of the Archean to c. 2.42 Ga, based on the first widespread appearance of 'Huronian' glacial deposits in the rock record (Young, 2019) and the approximately contemporaneous change to an oxygenated atmosphere (Great Oxidation Event or GOE), which followed the end of the world's greatest development of banded iron formation (BIF). This approach seems reasonable based on the rock record, which constrains globally significant climatic and atmospheric changes to before this time (Gumsley et al., 2017). Although the GOE is sometimes taken to refer to a more prolonged interval of the early Paleoproterozoic, we restrict our usage here to this shorter interval between c. 2.45 to c. 2.32 Ga, with a preference for the earlier age (e.g., Warke et al., 2020b). The GOE has been defined in various ways but in recent years has been presumed to begin when atmospheric oxygen had accumulated sufficiently to prevent the formation and/or preservation of mass independent S-isotope fractionation in sedimentary rocks (Farquhar et al., 2000; Bekker et al., 2004). However, it is currently unclear whether this was a globally synchronous event, with estimates for MIF-S disappearance varying from 2.45 to 2.32 Ga due to uncertainties over memory effects caused by oxidative weathering of sulphides and recycling of the MIF signature or stratigraphic ambiguities (Reinhard et al., 2013; Philippot et al., 2018; cf. Torres et al., 2018; Warke et al., 2020b). The MIF-S record has also shown structure within the later Archean (oxygen 'whiffs') that could potentially be used as a future stratigraphic marker (Farquhar et al., 2007; Domagal-Goldman et al., 2008; Halevy et al., 2010; Kurzweil et al., 2013) if the structure is confirmed as a global phenomenon rather than superimposed local signals (see e.g., Gallagher et al., 2017).

While the precise ages and correlation of the GOE with MIF-S events and Paleoproterozoic tillites remain uncertain (Young, 2019), an equally significant event in the transition is the end of the major late Archean BIF deposition. The Archean-Proterozoic boundary might be best constrained/defined by accurately dated tuffs (~2.45 Ga) at the top of the Hamersley Group BIF (Trendall et al, 2004); BIFs in the Transvaal Basin of South Africa have similar ages. This would imply redefining the Siderian Period, named for the global peak in iron formations, and moving it into the Neoarchean (van Kranendonk et al., 2012); a simple solution also to the criticism that 2.5 Ga splits this important rock unit. A 2.45 Ga date also prevents splitting some younger classic "Archean" terranes which overlap the chronometric 2.5 Ga boundary. We concur with this reasoning and propose that the terminal Archean Siderian Period end at c. 2.45 Ga, to be followed by a new *Scourian* Period (named after the Greek term for rust (skouria), as a nod to rock-based evidence for widespread oxidative weathering since the GOE.

Signal reworking should not affect other geochemical or isotopic markers of upper ocean oxygenation, e.g., redox-sensitive elemental and isotopic enrichments. Geochemical signs of oxidation are recorded intermittently from the Mesoarchean (Ossa Ossa et al., 2019), becoming more expansive during the Neoarchean (Ostrander et al., 2019) and are attributed to transient pulses of oxygen prior to the GOE (the so-called 'whiffs of oxygen') (Anbar et al., 2007; Kendall et al., 2015; Stueeken et al., 2015) or more persistent oxygenation of shallow marine platform environments (Riding et al., 2014). Therefore, the Archean-Proterozoic transition interval is characterised as much by the decline of anoxic shallow marine environments as by the onset of sustained atmospheric oxygenation. The Neoarchean is also remarkable for the highly negative carbon isotope composition of deposited organic carbon during the interval between c. 2.8 Ga and c. 2.6 Ga (Hayes, 1994) as well as a number of other uniquely extreme stable isotope signatures, possibly related to nascent stages of local environmental oxidation (Thomazo et al., 2009).

Complementary records of Archean change, which can potentially be divided into three chapters, are provided by geochemical and isotopic studies of magmatic rocks that appear to indicate major secular changes in tectonic processes (Kamber and Tomlinson, 2019). On this basis, Griffin et al. (2014) concurred that the Archean Eon is best divided into three: 'Paleoarchean' (4.0-3.6 Ga), 'Mesoarchean' (3.6-3.0 Ga) and 'Neoarchean' (3.0-2.4 Ga) eras. In this interpretation, during the 'Paleoarchean' Era, Earth's dominantly mafic crust acted as a stagnant-to-sluggish lid. Towards the close of the era, zircon grains reveal subtle geochemical signs of a change in tectonic regime interpreted as a move away from granitoid production from oceanic plateaus to some form of arc-like settings (Ranjan et al., 2020). It has been suggested that the subsequent 'Mesoarchean' was dominated by major episodes of mantle overturn and plume activity (Van Kranendonk, 2011) that led to development of the subcontinental lithospheric mantle and a steady increase between c. 3.3 and c. 3.0 Ga in the K_2O/Na_2O ratios of TTG (tonalite-trondhjemite-granodiorite) rock suites (Johnson et al., 2019). However, early evidence of subduction is also interpreted at this time, along with diapiric doming, in adjoining terranes of the Pilbara Craton (Hickman, 2004; Van Kranendonk et al., 2004).

The Neoarchean witnessed the onset of some form of plate tectonics, and the development of significant volumes of continental crust, characterised by the first K-rich granitoids (Bédard, 2018). However, gravity-driven doming and plume activity was still an active process in the formation of granite-greenstone terranes ~2720-2600 Ga (Jones et al, 2020). Progressive cratonization is reflected by the development of the first true platform covers – the Witwatersrand and Ventersdorp Supergroups from ~2.95 Ga on the Barberton Craton, the Mount Bruce Supergroup from ~2770 Ga on the Pilbara Craton and the c. 2.93 Ga to c. 2.80 Ga successions of Canada, e.g., the Steep Rock Lake Group (Riding et al., 2014; Fralick and Riding, 2015) or the Central Slave Cover Group (Bleeker et al., 1999; Sircombe et al., 2001. The Pongola Group (~2980 Ga) probably represents an earlier platform, but is intruded by late-tectonic granites. Emergence of this more buoyant crust may have led to these early carbonate platforms, although pre-3.0 Ga fluvial sediments imply at least some earlier regional emergence

(Heubeck and Lowe, 1994). The first development of platform covers on stable cratons provides a logical interim boundary within the Archean and the base of the Neoarchean at ~3.1-3.0 Ga. Increasing lithospheric stability is also represented by the oldest extensive mafic dyke swarms between ~2.8 and 2.7 Ga (Evans et al., 2017; Gumsley et al., 2020).

It seems significant that the youngest widespread granite-greenstone terranes (e.g., Yilgarn, southern Superior craton, Bulawayan) are coeval with the basalt-rich Fortescue and Ventersdorp platform covers. This could form a basis for future 3-fold subdivision of the Neoarchean, into three periods based on the rock records of a newly defined Siderian Period (see above), the coeval Fortescue–Ventersdorp groups, and the Witwatersrand-Pongola groups, respectively. To address period-level Archean subdivision any further lies beyond the scope of the present study, although we note that one of these periods could be named *Kratian* for the cratonization that typifies the later Archean.

Clear evidence for the transport of surface crustal material to the deep mantle is found in diamonds within kimberlites. Their stable isotope compositions, geochronology and mineral inclusions imply deep transport to the lower mantle of eclogitized basaltic protoliths that had interacted with seawater as long ago as 3.0 Ga (Shirey and Richardson, 2011; Schulze et al, 2013). Cratonization culminated in a globally stable "supercraton" regime around the Archean-Proterozoic boundary (Bleeker, 2003; Cawood et al., 2018). This configuration set up the lithospheric conditions, due to secular cooling of the mantle, for a switch to a full mode of plate tectonics, which arguably began with rift and drift of these Archean cratons and led eventually to prolonged amalgamation after c. 1.9 Ga of Nuna (Columbia), which is widely considered to have been a true supercontinent as opposed to a megacontinent comprising <50% of all continental area.

2.3 Proterozoic Eon (2.45/2.5 to c. 0.539 Ga)

The Archean and Proterozoic eons represent fundamentally different Earth systems, and the boundary between the two is currently placed at precisely 2.5 Ga. This boundary approximates the change from an early Earth that, although still characteristically Archean (e.g., rare K-rich granitoids but widespread komatiite magmatism, granite-greenstone terranes), had gradually developed many aspects of modern tectonics, to a plate tectonic regime that was characterised by stabilized, emergent continental (super)cratons and the onset of a supercontinent cycle as well as a notable paucity of the high-MgO lavas that are characteristically occur throughout the Archean. The Archean-Proterozoic boundary precedes quite closely, but does not correspond precisely to a change in surface environments from a reducing to an oxygenated atmosphere, and from wholly anoxic oceans to a more complex ocean redox structure characterised by oxic, anoxic-ferruginous and anoxic-euxinic portions. Consequently, the boundary must represent a planetary step change that significantly transformed, within 100 to 150 Myr, the Earth's biogeochemical cycles, presumably accompanied by the development of novel microbial pathways and metabolisms, leading eventually to larger and more complex (eukaryotic) forms. The Proterozoic marine sedimentary rock record is also marked by a greater diversity of authigenic minerals

(Hazen, 2010; Hazen et al., 2011) and carbonate rock textures (James et al., 1998; Shields, 2002; Hodgskiss et al., 2018). The Proterozoic Eon is divided into three eras, namely the Paleo-, Meso-, and Neo-Proterozoic eras.

i. Paleoproterozoic Era (2.45/2.5 to 1.8/1.6 Ga)

The Paleoproterozoic Era witnessed the transition from an Archean tectonic regime of scattered, small supercratons (Bleeker, 2003) to a more conventional form of plate tectonics, which resulted in formation of Earth's earliest widely accepted supercontinent, Nuna (Hoffman, 1989, 1997; Rogers and Santosh, 2002; Zhao et al., 2002; Payne et al., 2009; Evans and Mitchell, 2011; Zhang et al., 2012; Yang et al., 2019), as evidenced by ~2.0-1.6 Ga orogenic belts on all present-day continents. Redefining the Siderian to contain within it the BIFs at the top of the Neoarchean requires a new period to be defined and named for the earliest Paleoproterozoic. Van Kranendonk et al. (2012) refer to this period as the Oxygenian Period, although we consider *Scourian* (Skourian), after the Greek word for rust, to be a suitable, rock-based alternative.

The Paleoproterozoic sedimentary record provides clues to significant events, some of which are likely to have been global in scale and can probably be related to the large-scale tectonic processes outlined above. Abundances of molybdenum, uranium, selenium, sulfate and iodate increased in marine sedimentary rocks in multiple Paleoproterozoic basins, indicating increasing ocean reservoirs of those redox-sensitive species (Scott et al., 2008; Partin et al., 2013; Kipp et al., 2017; Hardisty et al., 2017; Blättler et al., 2018). This trend has been interpreted as evidence of oxidative weathering caused by atmospheric oxygenation after the GOE together with expansion of oxic conditions in the marine realm, which stabilised these elements as oxyanions in solution, while titrating redox-sensitive iron, manganese and cerium out of solution (Tsikos et al., 2010; Warke et al., 2020a). Accumulation of iron formations (IFs) peaked around the Archean-Proterozoic boundary, but continued until c. 1.8 Ga (Klein, 2005), after which major BIF deposits are scarce but not entirely absent (Bekker et al., 2010; 2014; Canfield et al., 2018). The initial decline in the abundance of BIF is widely attributed to the widespread development of euxinic waters on productive continental shelves at ~1.84 Ga, which titrated ferrous iron in the form of pyrite (Canfield, 1998; Poulton et al., 2010; Poulton and Canfield, 2011). However, ferriginous deeper oceans persisted throughout most of the mid-Proterozoic (Poulton et al., 2010; Planavsky et al., 2011), and the paucity of BIF through this period is likely also related to diminished hydrothermal sources of iron after c. 1.8 Ga (Cawood and Hawkesworth, 2014). The disappearance of redox-sensitive detrital minerals, such as pyrite, uraninite and siderite, has long been attributed to the GOE (Holland, 1984, 2006; Frimmel, 2005; van Kranendonk et al., 2012), although the onset and duration of the GOE is still inadequately constrained (e.g., Luo et al., 2016) and may not have been synchronous everywhere (Phillipot et al., 2018; Hodgskiss et al., 2019). The onset of the GOE is generally considered to have been approximately contemporaneous with what some have interpreted as

the Earth's first global scale glaciations (Bekker and Kaufman, 2007; Brasier et al., 2013; Tang and Chen, 2013; Bekker, 2014; Young, 2019). The strongest evidence for a Paleoproterozoic Snowball Earth comes from South Africa, with evidence of low-latitude glaciation in the Makganyene Formation at ~2.43 Ga (Evans et al., 1997). This glaciation is considered to have occurred shortly after the initial disappearance of MIF-S isotope fractionation, as recorded in pre-glacial sediments in Karelia (Warke et al. 2020b).

Paleoproterozoic glacial episodes were followed by the Earth's largest known positive $\delta^{13}C$ excursion (or excursions, see Martin et al., 2015), the Lomagundi-Jatuli Event (LJE) between c. 2.31-2.22 and c. 2.11-2.06 Ga (Martin et al., 2013), which accompanied the first major evaporite sulfate deposits (Melezhik et al., 2005; Schröder et al., 2008; Brasier et al., 2011; Blättler et al., 2018). The LJE is followed by the c. 2.06 Ga Shunga Event that is characterised by a major accumulation of C_{org}-rich sedimentary rocks, the generation of giant petroleum deposits (Melezhik et al. 2004) and pyrite-rich black shale (Sheen et al., 2019) as well as the first sedimentary phosphorite deposits (Kipp et al., 2020). The c. 2.06 Ga Shunga Event interestingly coincides with the emplacement of two Large Igneous Provinces (LIPs), the Bushveld LIP (Kaapvaal craton) and the Kevitsa LIP on the Karelian craton (e.g., Ernst et al. 2020), which inspired the name of the chronometric Rhyacian Period (2.3 – 2.05 Ga) after the Greek word Rhyax (meaning streams of lava) (Plumb, 1991). One potentially distinctive feature of the middle Paleoproterozoic is a disputed tectono-magmatic lull between c. 2.3 to 2.2 Ga (Spencer et al., 2018), during which evidence of continental magmatism and orogenesis is scarce, but not entirely absent (Partin et al., 2014; Moreira et al., 2018). Juvenile magmatism reinitiated after c. 2.2 Ga (Condie et al., 2009; Spencer et al., 2018). The chronometric Rhyacian-Orosirian boundary (2050 Ma) possibly correlates also with an abrupt increase in magnitude of a mass-independent O-isotope anomaly of photochemical origin that is carried in sedimentary sulfate minerals (gypsum/anhydrite and barite). The observed box-like secular shift to a large (negative) $\Delta^{17}O$ anomaly is tentatively ascribed to a collapse without parallel in global gross primary productivity (Hodgskiss et al., 2019; Crockford et al., 2019) and ushering in a period of muted isotopic variability and low oxygen levels.

The first macroscopic organic-walled fossils, coiled forms similar to *Grypania spiralis*, appear within Paleoproterozoic strata by c. 1.89 Ga (Han and Runnegar, 1992; Javaux and Lepot, 2018) to be joined by large, more convincingly eukaryote-grade fossils by the end of the era (Zhu et al., 2016). The Paleoproterozoic fossil record contains the c. 1.88 Ga Gunflint fossil microbes, which are taken to be the oldest unambiguous evidence of iron-oxidising bacteria and oxygenic cyanobacteria (Planavsky et al., 2009; Crosby et al., 2014; Lepot et al., 2017), although cyanobacterial fossils are known also from the c. 2.0 Ga Belcher Group in eastern Hudson Bay (Hofmann, 1975; Hodgskiss et al., 2019).

A period of worldwide orogeny and major crustal growth from c. 2.06 to 1.78 Ga, and reaching maximum intensity between 1.90-1.85 Ga, (Condie, 1998, 2004; Puetz and Condie, 2019; Condie and Puetz, 2019) culminated in the formation of the supercontinent Nuna or Columbia (Zhao et al., 2002),

speculated to have been Earth's first "true" supercontinent (Hoffman, 1989; Bleeker, 2003; Mitchell, 2014). For example, Nuna assembly is largely constrained to between ca. 2.0-1.8 Ga, from the 1970 Ma Thelon orogen (Bowring and Grotzinger, 1992), with the Rae craton serving as the upper plate of the growing Laurentia (Hoffman, 2014) that was central to Nuna (Evans and Mitchell, 2011). Local orogeny continued through the Statherian, culminating with final suturing events in Australia continuing into the Calymmian (ca. 1.6-1.4 Ga) (Pourteau et al., 2018; Yang et al., 2019; Gibson et al., 2020), which were peripheral in Nuna (Kirscher et al., 2019), which were peripheral in Nuna.

The end of the Paleoproterozoic Era, as currently defined, is characterised by the widespread formation of unmetamorphosed, shallow-marine sedimentary basins with expansive carbonate platforms over increasingly stable cratons, following amalgamation of Nuna. Some such as the c.1.7–c. 1.4 Ga Changcheng-Jixian groups of the Sino-Korean or North China craton, are traditionally considered and mapped as Mesoproterozoic successions (Zhao and Cawood, 2012), despite their slightly earlier origin prior to 1.6 Ga. Many other classic mid-Proterozoic sequences also fall into this category, having begun their depositional history similarly during the chronometric Statherian Period (1.8-1.6 Ga). For example, pre-1.6 Ga units originally envisaged to fall within the chronometric Proterozoic II (Plumb and James, 1986: Figure 1) include the lower McArthur Basin of Australia (Rawlings, 1999); the lower Riphean Burzyan Group of Russia (Semikhatov et al., 2015); the Espinhaço Supergroup and Araí Group of Brazil and coeval Chela Group of central Africa (Chemale et al., 2012; Guadagnin et al., 2015; Pedreira and de Waele, 2008); the Vindhyan and Cuddupah supergroups of India (Ray, 2006; Collins et al., 2015; Chakraborty et al., 2020) and the Uncompahgre Group of SW Colorado, USA, which formed during the late stages of the Yavapai orogeny (1.71-1.68 Ga) (Whitmeyer and Karlstrom, 2007).

The difficulty in assigning a precise age for the Paleoproterozoic - Mesoproterozoic boundary due to the prolonged nature of late Paleoproterozoic orogenies, now interpreted to relate to the amalgamation of Nuna, was recognized early on by the Precambrian Subcommission who expressed "*individual preferences … from 1400 Ma to 1800 Ma*" (Plumb and James, 1986). In this contribution, we recommend that the end of the Paleoproterozoic be provisionally redefined as ~1.8 Ga, with the Statherian placed in the Mesoproterozoic, pending future definition of GSSPs. This age is constrained by the latest Orosirian magmatic activity dated at ~1.82 Ga and the base of first platform covers ~1.8 Ga.

ii. Mesoproterozoic Era (1.8/1.6 to c. 1.0 Ga)

The Mesoproterozoic Era represents a period of seeming overall stability in Earth history, during which there were long thought to be few changes in the sedimentary record, biogeochemical cycling, climate and biological evolution (Buick et al., 1995; Brasier and Lindsay, 1998). New platform covers, soon after Orosirian orogeny, developed across most cratons. For example, the McArthur Basin of North

Australia saw up to 10 km of sediments deposited throughout the period from 1.8-1.6 Ga: the Tawallah Group of sandstone and volcanics from ~1.8-1.7 Ga, succeeded by stromatolitic and evaporitic carbonates of the McArthur Group (1.7-1.6 Ga), Nathan Group (~1.6-1.55 Ga) and the Roper Group (~1.55-1.31 Ga). The near basal mafic volcanics and intrusives across the coeval Tawallah and Kimberley Groups represent the major extensional Carson LIP (Ernst et al., 2020). Detailed studies show significant breaks throughout which correlate with changes in direction in a polar wander curve from the same sections, illustrating active plate tectonic control of basins near craton margins (Idnurm et al., 1995, Page et al, 2000). Relatively thin sandstone-volcanic sequences were initiated about the same time in Brazil and central Africa, but did not continue up into carbonates (Pedreira et al., 2008). The arenitic Changcheng Group of China began later, after ~1.7 Ga, and continued through the carbonate-rich Jixian Group until after ~1.44 Ga (Qu et al., 2014), as did the Lower Riphean of Russia (Semikhatov et al, 2015).

The final assembly of Nuna was probably completed by ~1.6 Ga (Pourteau et al., 2018; Gibson et al., 2020) and followed soon after by thick terrigenous deposition in the Roper (North Australia) and Belt-Purcell (western North America) Basins. However, some studies suggest that the West Australian Craton did not combine with North and South Australia until ~1.4 Ga (Yang et al., 2019). The period 1.4–1.25 Ga saw few short-lived basins worldwide, and was dominated by the breakup of the core of supercontinent Nuna (Evans and Mitchell, 2011; Pisarevsky et al., 2014), although the breakup may have been relatively incomplete (Ernst et al., 2016; Li et al., 2019) as it was likely followed by re-amalgamation into a different configuration by around 1.0 Ga to form the supercontinent Rodinia (Li et al., 2008). This partial breakup could be reflected in the 1.33-1.30 Ga Derim Derim-Yanliao LIP of northern Australia and the North China craton (Bodorkos et al., 2020; Yang et al. 2020).

The final period of the Mesoproterozoic was named Stenian for the “Grenvillian” worldwide linear orogenic belts (Plumb, 1991). The type Grenvillian is specifically defined by two events: Boundary, ~1090 – 1020 Ma and Rigolet, ~1000 – 980 Ma (Rivers, 2015). The Boundary event was probably the time of collision and is defined by high-grade metamorphic rocks from deep in the crust. The Rigolet boundary was a higher-level event with less movement. An extensional event separated the two, and magmatic emplacement of anorthosites, charnockites and metagranites occurred throughout. Earlier events, integral to the belt, extend back to c. 1200 Ma. The Sunsás and Natal-Namaqua belts display similar deep-seated metamorphism and magmatism between c. 1200 – 1000 Ma (Cornell et al., 2006; Teixeira et al., 2010). The continuity and contemporaneity of these orogens was challenged by Fitzsimons (2000) who demonstrated that the apparent linear, linked, nature of these belts encircling Antarctica was an artifact of imprecise dating and lack of outcrop. For example, in Central Australia, the high-grade 1240-1120 Ma Musgrave Orogeny is followed by the Warkuma LIP. The mafic-ultramafic Giles Complex was emplaced at various levels into the metamorphic rocks, coeval with high-level post-tectonic granites and the bimodal Bentley Supergroup (Howard et al, 2014).

Increasingly convincing discoveries of fossil eukaryotes, in the form of large, multicellular organic-walled fossil fronds and ornamented acritarchs (Zhu et al., 2016; Miao et al. 2019), first occur in rocks that straddle the chronometric Paleoproterozoic–Mesoproterozoic boundary at 1.6 Ga, and suggest that much of the Mesoproterozoic fossil record remains undiscovered. Current fossil and molecular evidence agree that crown group Archaeplastida (a group that includes the red, green and glaucophyte algae) emerged during the Mesoproterozoic Era (Butterfield, 2000; Eme et al. 2014), or possibly even earlier in non-marine environments (Sánchez-Baracaldo et al., 2017). Multicellular eukaryotic algae appear before 1.0 Ga in the form of isolated examples of red algae (*Bangiomorpha pubescens* at c. 1.05 Ga) and green algae (*Proterocladus antiquus* at c. 1.0 Ga) (Butterfield et al., 1994; Tang et al., 2020), with possibly earlier examples of red algae from India (*Rafatazmia chitrakootensis* and *Ramathallus lobatus)* at c. 1.6 Ga (Bengtson et al., 2017). Ornamented acritarchs are more common eukaryote-grade fossils and some may prove useful for biostratigraphy, e.g., *Tappania plana* is a widely reported Mesoproterozoic fossil taxon, which has been found in the Ruyang Group of China (Yin, 1997; Yin et al., 2018), Roper Group of Australia (Javaux et al., 2001; Javaux and Knoll, 2017); Siberia (Nagovitsin, 2009), USA (Adam et al., 2017) and Singhora Group, India (Singh et al., 2019). Therefore, the Mesoproterozoic Era, although often given the epithet 'boring', marks the point in geological time when biostratigraphy begins to seem possible.

As summarised by Cawood and Hawkesworth (2014), the period from 1.7 to 0.75 Ga is characterised by a paucity of passive margins (Bradley, 2008), anoxic-ferruginous and regionally euxinic marine environments, an absence of significant Sr isotope deviations in the seawater record, few highly evolved $\varepsilon_{Hf(t)}$ values in zircon grains, limited orogenic gold and VHMS (but major sedimentary exhalative Pb-Zn) deposits, an absence of glacial deposits and a paucity of massive BIF. Although thought to be Paleoproterozoic in age (Bekker et al., 2003; Papineau, 2010), some of the oldest significant phosphorite deposits may instead have formed around the 1.6 Ga mark in India and Australia (McKenzie et al., 2013; Crosby et al., 2014; Chakraborty et al., 2020; Fareeduddin and Banerjee, 2020). Anorthosites and related intrusive rocks are characteristic of the middle Mesoproterozoic (c. 1.5 – 1.2 Ga) and are in places spatially and temporally linked to convergent plate margins (Whitmeyer and Karlstrom, 2007; McLelland et al., 2010; Ashwal and Bybee, 2017). Their development during the Mesoproterozoic was attributed by Cawood and Hawkesworth (2014) to secular cooling of the mantle to a temperature at which continental lithosphere was strong enough to be thickened, but still warm enough to result in melting of the lower thickened crust.

A lack of stratigraphically useful new life forms, major climatic changes, and demonstrably global C isotope excursions throughout the Mesoproterozoic makes it particularly difficult to subdivide. However, the Mesoproterozoic C-isotope record may have been less invariant than has been appreciated until now as exceptions to the apparent monotony are emerging (e.g., Zhang, K. et al., 2018; Shang et al., 2019). Regional scale magmatic events such as the c. 1320 Ma and c. 1230 Ma dyke swarms of North China (Zhai et al., 2015; Peng et al., 2015; Wang et al., 2016), the 1320 Ma swarm also found

558 throughout northern Australia (Yang et al. 2020; Bodorkos et al. 2020), the Mackenzie dyke swarm in
559 Canada (c. 1.27 Ga) and the approximately contemporaneous Ghanzi-Chobe-Umkondo and
560 Midcontinent Rift Systems (c. 1.12-1.08 Ga) have not been linked to any global-scale isotopic
561 excursions that could be used for correlation, although the coincidence of widespread ca. 1385 Ma LIPs
562 and black shales has been proposed as potential rock-based markers of Mesoproterozoic subdivision,
563 e.g., at the Calymmian-Ectasian boundary (Zhang, S. et al., 2018).
564 The final period of the Mesoproterozoic was named 'Stenian' for a series of orogenies (Plumb,
565 1991) that led eventually to formation of the supercontinent Rodinia, which completed its final
566 amalgamation phase by c. 950 Ma (Li et al., 1999; Evans et al., 2016; Merdith et al. 2017a). The first
567 period of the Neoproterozoic was named 'Tonian', due to the lithospheric stretching now known to be
568 related to the break-up of Rodinia, and originally placed at 0.9 Ga (Plumb and James, 1986).
569
570 **iii. Neoproterozoic Era (c.1.0 – c.0.54 Ga)**

571 The subdivision of Neoproterozoic time has largely been informed by 1) the occurrence of widespread
572 glacial units now known to be of late Precambrian age (Thomson, 1871; 1877; Reusch, 1891; Kulling,
573 1934; Lee, 1936; Howchin, 1901; Mawson, 1949) and 2) fossils of metazoan affinity that postdate those
574 glaciogenic deposits but predate Cambrian strata (Glaessner, 1962). Harland (1964) first proposed the
575 term "infra-Cambrian" or "Varangian" for the late Precambrian system (Fig. 2) based on two discrete
576 diamictite units, the Smalfjord (Bigganjargga) and Mortensnes, although these are now known to be of
577 late Cryogenian (Marinoan) and Ediacaran age, respectively. Harland proposed that the start of this new
578 period should correspond to the base of the lower of these two glacial horizons on the Varanger
579 Peninsula, NE Norway, first described by Reusch (1891). Dunn et al. (1971) subsequently introduced
580 the terms "Sturtian" and "Marinoan" (named after Sturt Gorge and Marino Rocks near Adelaide) for
581 the two glacial epochs recorded in the late Proterozoic strata of the Adelaide Geosyncline of South
582 Australia, emphasizing their utility as chronostratigraphic markers. Cloud and Glaessner (1982)
583 proposed the term "Ediacarian" for the interval spanning from the upper limit of the last late
584 Precambrian glacial deposit to the base of the Cambrian. This term also originates from South Australia
585 (the Ediacaran Hills) where Ediacara-type fossils were recognized (Sprigg, 1947). Plumb (1991) penned
586 the name "Cryogenian" for the period that included the more widespread of the late Neoproterozoic ice
587 ages and the term "Tonian" (meaning stretching in Greek and in reference to the onset of rifting, now
588 related to the break-up of Rodinia) for the preceding period, setting the chronological boundary between
589 them at precisely 850 Ma. These terms and GSSA boundaries were revised from previously suggested
590 period-rank subdivisions on the geological time scale by the Subcommission on Precambrian
591 Stratigraphy (Plumb and James, 1986).
592 The number, duration, and intensity of the glaciations have been intensely debated (e.g.,
593 Kaufman et al., 1997; Kennedy et al., 1998; Halverson et al., 2005), particularly in the light of the

Snowball Earth hypothesis (Hoffman et al., 1998; Hoffman and Schrag, 2002; Fairchild and Kennedy, 2007; Etienne et al., 2007). Notwithstanding these debates, the base of the Ediacaran System (Period) was formally ratified in 2004 in the Adelaide Geosyncline (Knoll et al., 2004; 2006) at the same stratigraphic level as originally proposed by Cloud and Glaessner (1982) for their "Ediacarian" period. The terms Cryogenian and Tonian are now widely accepted for the two preceding periods (Shields-Zhou et al., 2012, 2016). Recent proliferation of radioisotopic ages spanning Neoproterozoic glacial deposits has largely resolved the question of the number and timing of late Precambrian glacial intervals. It is now well established that two discrete glaciations of global extent occurred during the Cryogenian Period (i.e., between c. 717 Ma and c. 635 Ma). Despite initial reservations, the international community generally uses the terms *Sturtian* and *Marinoan* to refer to these two glacial events ("cryochrons", cf. Hoffman et al., 2017) of the Cryogenian Period. This subdivision, though still informal, appears justifiable in light of the geochronological evidence that 1) the Sturtian glaciation is now thought to have begun at c. 717 Ma (Macdonald et al., 2010, 2018; McLennan et al., 2018) and ended at c. 660 Ma (Rooney et al., 2015; 2020; Cox et al., 2018; Wang et al., 2019) synchronously worldwide, within the uncertainty of available ages, and that 2) the Marinoan glaciation, though shorter-lived and of uncertain duration (between about 4 and 17 Myr; Hoffmann et al., 2004; Condon et al., 2005; Prave et al., 2016; Nelson et al., 2020) also ended synchronously at c. 635.5 Ma (Crockford et al., 2018; Zhou et al., 2019). The start of the Cryogenian Period has now been changed to c. 720 Ma so as to encompass only the glacigenic sequences, pending proposal and ratification of a GSSP.

The preceding Tonian Period now lasts 280 million years. Having originally been envisaged to encapsulate a period of lithospheric thinning (supercontinent break-up), the Tonian now covers the final amalgamation of Rodinia (Evans et al., 2016; Merdith et al. 2017) and a prolonged interval of relative stability prior to the onset of major break-up after 0.85 Ga, and perhaps as late as 0.75 Ga (Jing et al., 2020; Merdith et al 2017b).

A proliferation of sedimentary basins in Rodinia between c. 850 and c. 800 Ma (e.g., the Centralian Superbasin of Australia, the East-Svalbard-East Greenland basin, the Mackenzie Mountains-Amundsen and associated basins of northern-northwestern Canada, the Nanhua rift basin of South China and the Central Africa Copperbelt (Lindsay, 2002, Hoffman et al., 2012; Rainbird et al., 1996; Wang et al., 2011; Bull et al., 2011; Li et al., 2013) were originally interpreted to record an initial phase of Rodinia break-up (Li et al., 1999; Macdonald et al., 2012), perhaps related to insulation of the underlying mantle (Lindsay, 2002) and/or the influence of a series of similarly aged mantle plumes and associated LIP events that impinged on Rodinia at this time (Li et al., 1999, 2003). The existence of widespread basin-scale evaporite deposits with ages ranging from c. 830 to c. 730 Ma (Prince et al., 2019) is consistent with rifting around this time. However, aside from the western margin of North America (e.g., Macdonald et al., 2012; Timmons et al., 2001; Jefferson et al., 1998) evidence of extension leading to continental separation is lacking and true break-up probably began in earnest only around the start of the Cryogenian (e.g., Merdith et al., 2017a,b), followed by a peak in passive margin

abundance at c. 600 Ma (Bradley, 2008). Therefore, Rodinia's tenure as a supercontinent coincided with the Tonian Period, as currently defined, which was named for the tectonic stretching that led to its break-up. Division of the long Tonian into two periods is therefore desirable, although at present most c. 850-800 Ma basins lack adequate geochronological control.

3. Tracers of crustal evolution: cornerstone of the geological time scale

Recent research has focused on understanding episodicity and secular trends in the Precambrian geological record, recognising that the supercontinent cycle and mantle dynamics exert a fundamental control on the evolution of not only the Earth's lithosphere, but also the atmosphere and biosphere, including the spatial distribution of elements and therefore the evolution of mineral deposits (e.g., Huston et al., 2016; Frimmel, 2018), via a series of complex, incompletely understood feedbacks (e.g., Worsley et al., 1985; Lindsay and Brasier, 2002; Cawood et al., 2013; Young 2013; Grenholm and Schersten, 2015; O'Neill et al., 2015; Hawkesworth et al. 2016; van Kranendonk and Kirkland 2016; Gumsley et al., 2017; Nance and Murphy 2018; Alcott et al., 2019).

Various workers have proposed that the Precambrian can be divided into a number of major intervals based on the dominant tectonic process at any one time. Hawkesworth et al. (2016) suggested five intervals: 1) initial accretion, core/mantle differentiation, development of magma ocean and an undifferentiated mafic crust; 2) plume-dominated tectonics (pre-subduction) at c. 4.5–3.0 Ga; 3) stabilisation of cratons and onset of "hot subduction" between c. 3.0 and c. 1.7 Ga; 4) the "boring billion" at 1.7–0.75 Ga; and 5) Rodinia breakup and development of "cold subduction" from 0.75 Ga onwards. Similarly, van Kranendonk and Kirkland (2016) suggested five intervals, each of which starts with a pulse of mafic-ultramafic magmatism, includes the formation of a supercontinent, and ends with an often protracted period of relative quiescence as the previously formed supercontinent drifts and breaks apart. Following c. 4.03–3.20 Ga – the period from the start of the preserved rock record to the onset of modern-style plate tectonics – these stages are: 1) 3.20–2.82 Ga – the onset of modern-style plate tectonics and the oldest recognised Wilson cycle; 2) 2.82–2.25 Ga – commencing with major crustal growth, emergence of the continents and formation of Superior-type BIFs, and closing with magmatic slowdown and stagnant-lid behaviour; 3) 2.25–1.60 Ga – global mafic/ultramafic magmatism followed by global terrane accretion and the formation of Nuna; 4) 1.60–0.75 Ga – the "Boring Billion" but included partial break-up of Nuna and subsequent formation of Rodinia during the Grenvillian and other orogenies; 5) 0.75 Ga to present – breakup of Rodinia, the Pangean supercontinent cycle and present transition to Amasia (Safonova and Maruyama 2014; Mitchell et al., 2012; Merdith et al. 2019).

Worsley et al. (1985) and Nance et al. (1986) pointed out that processes associated with the supercontinent cycle can be tracked by several isotopic proxies. For example, the distribution of U-Pb zircon ages for the past 4.0 Ga (Fig. 3) in orogenic granitoids and detrital sedimentary rocks record

667 similar peaks at 2.7 Ga (and 2.5 Ga), 1.87 Ga, 1.0 Ga, 0.6 Ga and 0.3 Ga, which correspond to the times
668 of global-scale collisional orogenesis and magmatism associated with the amalgamations of Kenora
669 (Kenorland), Nuna (Columbia), Rodinia, Gondwana and Pangea, respectively. A more recent
670 compilation (Condie and Puetz, 2019) interprets these peaks to be pulses of crustal growth and revises
671 the timing of later peaks to 1875 Ma, 1045 Ma, 625 Ma, 265 Ma and 90 Ma. A kernel density estimation
672 analysis (Vermeesch et al., 2016) of almost 600,000 detrital zircons (Spencer et al., 2020) confirms
673 similar peaks at 2.69 Ga, 2.50 Ga, 1.86 Ga, 1.02 Ga, 0.61 Ga, 0.25 Ga and 0.1 Ga, and troughs at 2.27
674 Ga, 1.55-1.28 Ga, 0.88-0.73 Ga, 0.38 Ga and 0.20 Ga. Variations in the mean initial εHf and $\delta^{18}O$ values
675 from detrital zircon grains in recent sediments show negative troughs and positive peaks, respectively,
676 that correspond to times of supercontinent assembly (Fig. 3). Both proxies are consistent with extensive
677 crustal re-working at the time of assembly with more juvenile contributions representing times of
678 supercontinent breakup and dispersal. Most importantly, all current major subdivisions of geological
679 time, 2.5 Ga, 1.6 Ga, 1.0 Ga, c.539 Ma, c.252 Ma and c.66 Ma, sit within the downslope of troughs that
680 follow peaks in zircon abundance. Note, however, that the time between the 'Nuna' peak at 1.87 Ga
681 and the currently defined Paleoproterozoic-Mesoproterozoic boundary, which precedes a long-lived
682 abundance trough, is anomalously long, and reflects protracted assembly of the Nuna supercontinent.
683 The effect of crustal processes on seawater composition is recorded by the $^{87}Sr/^{86}Sr$ ratios of
684 marine carbonates. High $^{87}Sr/^{86}Sr$ values are attributed to times of increased exhumation of old
685 radiogenic crystalline rocks that would accompany supercontinent amalgamation and disaggregation,
686 while low $^{87}Sr/^{86}Sr$ values signify reduced exhumation of old crustal domains that occur when
687 supercontinent breakup is accompanied by enhanced ocean ridge hydrothermal activity, rift-related
688 magmatism and sea level rise (Veizer, 1989). Although commonly used seawater $^{87}Sr/^{86}Sr$ curves
689 (Veizer et al., 1999; Shields and Veizer, 2002; Shields 2007) imply that continental weathering had
690 little influence before the end of the Archean, recent studies (e.g., Satkoski et al., 2016) suggest that
691 continental weathering and low-temperature surface alteration were more important than previously
692 suspected during the Archean. Two prolonged peaks in the Sr isotope composition of seawater
693 correspond with the Paleoproterozoic-Mesoproterozoic and Neoproterozoic-Phanerozoic transitions
694 (Shields, 2007; Kuznetsov et al., 2018). These intervals of enhanced continental weathering of more
695 radiogenic rocks coincide with the amalgamation of Nuna and Gondwana, respectively (e.g., Cawood
696 et al., 2013; Nance and Murphy, 2018). The widespread orogenesis that accompanied amalgamation of
697 Rodinia (Namaqua-Natal (Africa), Grenville-Sveconorwegian (North America-Europe) and Sunsás
698 (South America) does not feature prominently in the seawater Sr isotope curve or zircon εHf
699 compilations, likely because these orogens primarily involved juvenile arcs in external orogens (e.g.,
700 Spencer et al, 2013) rather than old radiogenic crustal domains. The dominant influence of lithology
701 over weathering rates on the $^{87}Sr/^{86}Sr$ record is consistent with the observed negative covariation
702 between $^{87}Sr/^{86}Sr$ and zircon εHf records (Hawkesworth et al., 2016).

703 Supercontinent amalgamation has been proposed to increase nutrient availability (including
704 important bio-limiting nutrients such as iron and phosphorus, e.g., Tyrell, 1999) and organic production
705 via higher rates of chemical weathering, leading to pulses of oxygenation (Campbell and Allen, 2008).
706 However, the concept of greatly increased weathering rates would appear to be in conflict with the
707 silicate weathering feedback, which regulates the long-term carbon cycle (Walker et al., 1981).
708 Moreover, carbon isotope trends, which are commonly used to mirror changes in organic burial and
709 therefore oxygenation (e.g., Des Marais et al., 1992; Lyons et al., 2014), may relate instead to tectonic
710 forcing of carbonate weathering, resulting in an inverse (or no) covariation between $\delta^{13}C$ and carbon
711 burial (Shields and Mills, 2017). The relationship between $\delta^{13}C$ excursions and oxygenation is made
712 more complex when we consider that oxidative weathering of organic carbon could have been limited
713 by low atmospheric oxygen (Bekker and Holland, 2012; Daines et al., 2017). As a consequence,
714 negative as well as positive carbon isotope excursions could indicate Proterozoic oxygenation events,
715 driven instead by pyrite burial, particularly at times of enhanced evaporite sulfate weathering since
716 about 2.0 Ga (Shields et al., 2019). Despite the widespread acceptance of a two-step rise in atmospheric
717 oxygen during the Proterozoic Eon (Lyons et al., 2014), sophisticated biogeochemical models have
718 seldom been applied to the Precambrian Earth system and few proxies exist to constrain absolute
719 atmospheric oxygen levels (Planavsky et al., 2014).
720 Geochemical evidence indicates that during much of the Proterozoic Eon, upper oceans were
721 oxygenated due to mixing with the atmosphere, but the deep ocean in contrast still tended towards
722 anoxia with local euxinia (Canfield, 1998; Shen et al., 2002; Arnold et al., 2004; Poulton et al., 2004;
723 Farquhar et al., 2010). However, the extent of surface oxygenation is still highly disputed (Slack et al.,
724 2007; Planavsky et al., 2014; Tang et al., 2016; Zhang et al., 2016; Daines et al., 2017). Deep ocean
725 anoxia suggests that atmospheric oxygen levels were low enough that oxygen became easily exhausted
726 at productive margins where organic remineralisation scavenged first oxygen then sulphate. After the
727 assembly of Rodinia, euxinia became less common, leading to mostly ferruginous conditions (Guilbaud
728 et al., 2015). Under such conditions efficient phosphorus removal may have helped to sustain low
729 atmospheric oxygen levels (Guilbaud et al., 2020). A two-step oxygenation history (first surface oceans
730 and atmosphere and then deep oceans) has also been supported by Fe speciation studies, which show
731 increased amounts of Fe (III) relative to Fe (II) in subaerial volcanic rocks after the GOE, but no change
732 in submarine volcanics until after the NOE (Stolper and Brenhin-Keller, 2018).
733 How environmental parameters, such as climate and redox conditions, were modulated by the
734 supercontinent cycle remains uncertain but tectonic and environmental changes track the same
735 episodicity, providing optimism that natural subdivision of the Proterozoic Eon would be geologically
736 meaningful. Plume generated LIP magmatism could also help define natural Precambrian (and
737 Phanerozoic) boundaries through their likely effects on the wider environment (Horton, 2015; Ernst
738 and Youbi 2017; Ernst et al. 2020). Examples include the Archean-Siderian boundary LIPs (2460-2450

739 Ma Matachewan and coeval events in Karelia-Kola and Pilbara cratons), Rhyacian-Orosirian boundary
740 LIPs (2058 Ma Bushveld and Kevitsa events), Orosirian-Statherian boundary (1790 Ma LIPs on many
741 blocks), Statherian-Calymmian boundary (1590 Ma LIPs), Calymmian-Ectasian boundary (1385 Ma
742 LIPs on many cratons), Ectasian-Stenian boundary (c. 1205 Ma Marnda Moorn LIP), Stenian-Tonian
743 boundary (c. 1005 Ma Sette Daban event or c. 925 Ma Dashigou event), and Tonian-Cryogenian (720
744 Ma Franklin LIP and other related LIPs (Ernst and Youbi 2017). Despite the difficulty of matching the
745 isotopic record with LIP emplacement and weathering, the 720 Ma Tonian-Cryogenian boundary, now
746 defined by the start of the Sturtian glaciation, has been linked to the Franklin Large Igneous Province
747 (LIP) of northern Laurentia (Macdonald et al., 2010; Macdonald and Wordsworth, 2017; Ernst and
748 Youbi, 2017) and potentially other LIP fragments (Ernst et al., 2020) either through an increase in
749 planetary albedo associated with the release of aerosols or an increase in global weatherability
750 associated with the tropical emplacement of soluble Ca- and Mg-rich flood basalts. This discovery
751 builds on the recognition that LIPs are coeval with many Phanerozoic chronostratigraphic boundaries
752 and that, although regional in scale, LIPs can have global environmental effects and leave global
753 sedimentary records. Thus, while LIPs are not "golden spikes" in themselves, they can represent proxies
754 for golden spikes in the sedimentary record, which bodes well for Proterozoic stratigraphic correlation
755 along Phanerozoic lines.

756 There is a clear consensus that the Earth's surface environment evolved in a series of events
757 that were controlled ultimately by magmatism and tectonics. In this, there appears to be no essential
758 difference between major geological transitions of the Phanerozoic and Proterozoic, all of which reflect
759 complex interactions and feedbacks between the lithosphere, atmosphere and biosphere. Despite
760 significant gaps in understanding, various isotopic and geochemical proxies track tectonic
761 (supercontinent) cyclicity and offer prospects for a more robust, rock-based pre-Cryogenian time scale.
762

763 ## 4. Nascent potential of Proterozoic biostratigraphy and chemostratigraphy

764 Stromatolite textures (and structures) were once thought to be age-diagnostic, although this is now more
765 frequently interpreted to reflect a general tendency towards greater biological control over calcium
766 carbonate precipitation through time (Grotzinger, 1990; Arp et al., 2001; Riding, 2008). Coarse sparry
767 texture (botryoidal fans and microdigitate stromatolites, dendrites, isopachous laminites, and
768 herringbone calcite) is common in Late Archean-Mesoproterozoic carbonate systems. Although such
769 textures have commonly been referred to as seafloor cement, they formed at the open sediment-water
770 interface rather than as void-fills, unlike later calcite microspar cements, which peaked in the early
771 Neoproterozoic (James et al., 1998), just as cyanobacterial sheaths began to be calcified, forming
772 clotted, 'thrombolite' mounds of calcimicrobial fabric (Arp et al., 2001). Despite evident trends, few if
773 any sharp temporal divisions can be identified in stromatolite type or microbially induced sedimentary
774 structures (MISS). For example, abiotically controlled seafloor carbonate precipitation did not entirely

775 disappear at the end of the Archean, while the first occurrence of fossilised bacteria (or stromatolites)
776 cannot be used to date the evolutionary origins of cyanobacteria (Blank, 2013; Sánchez-Baracaldo et
777 al., 2017; although see Ward et al., 2016), which from geochemical data ought to predate Neoarchean
778 evidence of oxygenation (Farquhar et al., 2011; Riding et al., 2014). Supposedly age-diagnostic
779 sedimentary textures, like stromatolite fabrics, have lost favour, while discoveries of new fossils each
780 year continually resurrect the hope that Precambrian biostratigraphy will be a genuine possibility.
781 Although Precambrian paleontology is a relatively young field, with only belated acceptance
782 of Ediacaran body fossils (Glaessner, 1962), tremendous advances have been made in recent years.
783 Nevertheless, Precambrian biostratigraphy is still in its infancy with respect to fossil discovery and
784 systematic description. It is not unusual, for example, for a new discovery to extend the stratigraphic
785 range of fossil species by tens or even hundreds of millions of years. Macroscopic forms are too rare or
786 simple to be of stratigraphic use, and while organic-walled microfossils are common in both fine-
787 grained siliciclastic sedimentary rocks or concretions, assemblages are typically dominated by simple,
788 smooth-walled vesicles known as *Leiosphaeridia*, a biologically uninformative acritarch taxon.
789 Nonetheless, with a growing number of taxonomic studies linked to new paleoenvironmental,
790 chemostratigraphic and geochronologic constraints (e.g., Sergeev et al., 2012; Tang et al., 2013, 2015;
791 Baludikay et al., 2016; Porter and Riedman 2016; Riedman and Porter, 2016; Beghin et al. 2017a, b;
792 Loron and Moczydłowska, 2017; Loron et al., 2019a; Cohen et al. 2017a,b; Javaux and Knoll, 2017;
793 Miao et al., 2019), a nascent Proterozoic biostratigraphic record is beginning to take shape.
794

795

796 **4.1 Biostratigraphy of the Proterozoic Eon (Eonothem)**

797 The oldest macroscopic organic-walled fossils are known from Paleoproterozoic rocks (Han and
798 Runnegar, 1992; Javaux and Lepot, 2018), now dated to <1891 ± 3 Ma (Pietrzak-Renaud and Davis,
799 2014). However, these simple coils and spirals, similar in appearance to *Grypania spiralis* (e.g., Walter
800 et al., 1976; Sharma and Shukla, 2009), are not diagnostically eukaryotic in affinity. Decimeter-sized
801 seaweed-like compressions (Zhu et al., 2016) and ornamented acritarchs occur in rocks at c. 1.6 Ga
802 (e.g., Miao et al., 2019) and are widely considered to be the first convincing fossilised eukaryotes
803 (Javaux and Lepot, 2018).
804 Molecular clock analyses place the origin of crown-group eukaryotes sometime in the
805 Mesoproterozoic or late Paleoproterozoic (e.g., Berney and Pawlowski, 2006; Parfrey et al., 2011; Eme
806 et al., 2014; Betts et al., 2018). Some phylogenetic data suggest that the first photosynthetic eukaryotes
807 may have emerged in freshwater habitats (Blank, 2013; Sanchez-Baracaldo et al., 2017), which may
808 lower their preservation potential in the rock record. The Stenian-Tonian transition interval is
809 increasingly being viewed as a time of crown group eukaryote diversification (e.g., Knoll et al., 2006;
810 Cohen and Macdonald, 2015; Butterfield, 2015; Xiao and Tang, 2018). Latest Mesoproterozoic and

811 earliest Neoproterozoic rocks are the first to preserve fossils with clear similarities to particular modern
812 eukaryotic clades, including red and green algae, fungi, amoebozoans, and stramenopiles (Butterfield
813 et al., 1994; Butterfield, 2004; Porter et al., 2003; Nagovitsin, 2009; Loron et al., 2019b; Tang et al.,
814 2020), though the affinities of most early Neoproterozoic fossils remain enigmatic. A number of
815 eukaryotic innovations also appear in the record during this time, including scales, tests,
816 biomineralization, and eukaryovory (Porter and Knoll, 2000; Cohen and Knoll, 2012; Cohen et al.,
817 2017a,b; Porter, 2016). In addition, eukaryote-derived sterane biomarkers appear for the first time c.
818 810 Ma (Brocks, 2018; Zumberge et al., 2019).
819 Given these evolutionary changes, it is not surprising that late Mesoproterozoic/early
820 Neoproterozoic fossil assemblages are largely distinct from those of early Mesoproterozoic age
821 (Sergeev et al., 2017), and that several organic-walled microfossils have been proposed as index fossils
822 for this interval. These include the acritarch *Trachyhystrichosphaera aimika* (spheroidal vesicles with
823 sparse, irregularly distributed, hollow processes), which is found in more than 20 sections worldwide
824 in Stenian and Tonian strata, aged c. 1100 to c. 800 Ma (Butterfield et al., 1994; Tang et al., 2013;
825 Riedman and Sadler, 2018) or c. 1150 to c. 720 Ma (Pang et al., 2020) and *Cerebrosphaera globosa*
826 (=*C. buickii*), robust spheroidal vesicles with distinctive wrinkles, common in late Tonian units c. 800–
827 740 Ma (Hill et al., 2000; Grey et al., 2011; Riedman and Sadler, 2018) (Fig. 4).
828 Several other distinctive fossils from rocks c. 780–740 Ma have potential in subdividing the
829 Tonian, but there are too few occurrences known at present to have confidence in their ranges (Riedman
830 and Sadler, 2018). Vorob'eva et al. (2009) noted that many long-ranging early Neoproterozoic and late
831 Mesoproterozoic taxa may be biostratigraphically useful with respect to their last appearances, and in
832 this regard it is worth noting that Riedman and Sadler (2018) found that the disappearance of many
833 ornamented taxa in the later Tonian occurred just before or around the time that distinctive vase-shaped
834 microfossils appear. The vase-shaped microfossils, constrained to range from c. 790-730 Ma (Riedman
835 and Sadler, 2018; Riedman et al., 2018), provide the most promising biostratigraphic marker for
836 subdividing Tonian time, and may be useful in defining the Cryogenian GSSP (Strauss et al., 2014),
837 although the extent to which the range is controlled by taphonomic factors is not clear.
838
839 **4.2 Chemostratigraphy of the Proterozoic Eon (Eonothem)**
840 With the possible exception of the Neoarchean, chemostratigraphy of the Precambrian is restricted to
841 the Proterozoic Eon. The GOE can be traced using a number of redox-sensitive geochemical proxies,
842 e.g., mass-independent fractionation of sulfur isotopes, trace metal concentrations and isotopes, while
843 related changes to microbial metabolisms and biogeochemical cycles may be apparent in nitrogen, iron
844 and other isotope records.
845 For later portions of the sedimentary archive, the carbon isotope record has most potential for
846 identifying chemo-oceanographic events during the Proterozoic, beginning with the widespread
847 positive anomaly (anomalies), referred to the Lomagund-Jatuli Event (LJE), which started before c.

2.22 Ga and ended by 2.06 Ga (Karhu and Holland, 1996; Melezhik et al., 2007; Martin et al., 2013). Later negative anomalies have been reported at about 2.0 Ga (Kump et al., 2011; Ouyang et al., 2020), 1.6 Ga (Zhang, K. et al., 2018; Kunzmann et al., 2019) and 0.93 Ga (Park et al., 2016). Carbon and strontium isotope stratigraphy (mainly on marine carbonates) are the most widely applied chemostratigraphic tools in the Neoproterozoic, and notwithstanding challenges to their general robustness to diagenetic alteration (e.g., Knauth and Kennedy, 2009; Derry, 2010) and reliability as global seawater proxies (Ahm et al., 2019), consistently reveal similar secular trends at both basinal and global scales.

The early Neoproterozoic carbon isotope record is identified by its sustained intervals of high $\delta^{13}C_{carb} \geq +5‰$ (Fig. 4; Kaufman et al., 1997; Halverson et al., 2005). The shift towards the high $\delta^{13}C_{carb}$ values appears to be transitional, with moderate fluctuations ($\leq 4‰$) in $\delta^{13}C_{carb}$ beginning in the late Mesoproterozoic (Knoll et al., 1995; Bartley et al., 2001; Kah et al., 2012) and continuing into the early Neoproterozoic (Kuznetsov et al., 2006). However, due to a paucity of earliest Neoproterozoic marine carbonate successions globally and poor age control on those successions that do exist, the $\delta^{13}C_{carb}$ record for the interval c. 1100–850 Ma is still poorly constrained. Available data indicate that significant $\delta^{13}C_{carb}$ excursions could have taken place during this interval but values remained between -5‰ and 5‰, while $^{87}Sr/^{86}Sr$ fluctuated between 0.7052 and 0.7063 (Fig. 5; Cox et al., 2016; Kuznetsov et al., 2017; Zhou et al., 2020).

The shift towards higher sustained $\delta^{13}C_{carb}$ ($\geq 5‰$) values occurred at c. 850 Ma (though not directly dated), as recorded in the Little Dal Group and equivalent strata of northwestern Canada (Fig. 5; Halverson, 2006; Macdonald et al., 2012; Thomson et al., 2015). However, this trend to high $\delta^{13}C_{carb}$ values is punctuated by a discrete and long-lived interval of near zero to negative $\delta^{13}C_{carb}$ values, referred to as the Bitter Springs Anomaly (BSA) (Halverson et al., 2005) after the Bitter Springs Formation in the Amadeus Basin of central Australia where it was first documented (Hill and Walter, 2000). The BSA is well documented in central Australia, Svalbard, northwestern Canada, Ethiopia (Swanson-Hysell et al., 2012, 2015; and references therein) and possibly India (George et al., 2018). It is constrained by U-Pb zircon CA-TIMS ages to have initiated after 811.5 Ma (Macdonald et al., 2010) and terminated prior to 788.7 Ma (MacLennan et al., 2018). Using a thermal subsidence-type age model applied to Svalbard, Halverson et al. (2018) estimated the BSA to have begun c. 810 Ma and ended c. 802 Ma, for a duration of 8 million years.

Available strontium isotope data show a plateau near 0.7070 following recovery from the Bitter Springs anomaly that is punctuated by a few minor downturns. A larger decline to 0.7064–0.7065 broadly coincides with the recovery from the c. 738–735 Ma Russøya negative $\delta^{13}C_{carb}$ excursion (Halverson et al., 2018; MacLennan et al., 2018). Cox et al. (2016) suggested that these late Tonian declines in $^{87}Sr/^{86}Sr$ were driven by preferential silicate weathering of continental flood basalt associated with the breakup of Rodinia, with the larger late Tonian drop to 0.7064 corresponding to weathering of juvenile arcs in the Arabian-Nubian Shield (Park et al., 2019). Furthermore, the early

885 Neoproterozoic $^{87}Sr/^{86}Sr$ record is strongly biased by data from a small handful of successions (mainly
886 Svalbard and NW Canada) and suffers from poor age control. Additional high-quality Sr isotope data
887 are necessary to fill in the secular record of Neoproterozoic seawater $^{87}Sr/^{86}Sr$, and have been
888 forthcoming from Russia (Kuznetsov et al., 2017) and the North China craton (Zhou et al., 2020).
889 The broad contours of the secular trend in Tonian–Cryogenian seawater $^{87}Sr/^{86}Sr$ are now well
890 established, dominated by a long-term rise in $^{87}Sr/^{86}Sr$ (from ~0.7052 to ~0.7073; Fig. 5). However,
891 strontium isotope chemostratigraphy in the Neoproterozoic is severely limited by the small number of
892 stratigraphic intervals containing limestones that are sufficiently well preserved (i.e., with high Sr/Ca
893 and low Mn/Sr) to record reliably the $^{87}Sr/^{86}Sr$ of contemporaneous seawater. Therefore, the record is
894 constructed typically from small numbers of data points from discrete intervals in different successions.
895 When combined with limited age control on most samples, the result is an irregular record with a large
896 number of temporal gaps and limited verification of trends among coeval successions (Fig. 5).
897 Moreover, due to the near absence of syn-glacial carbonate strata, no proxy data for seawater exist for
898 the Cryogenian glacial intervals (i.e. c.717–660 and c.≥640–635.5 Ma). Nevertheless, due to the
899 prominent rise in $^{87}Sr/^{86}Sr$ through the Neoproterozoic, the strontium isotopic record can potentially
900 distinguish between the early Tonian (i.e., 1000–810 Ma), late Tonian (810–720 Ma) and Cryogenian
901 non-glacial interval (c. 660–650 Ma).
902
903 ## 5. Discussion

904 The embryonic nature of Proterozoic bio- and chemostratigraphy outlined above illustrates how
905 ratification of pre-Cryogenian GSSPs lies far in the future and beyond the scope of the current review,
906 which is focussed on a template for agreed rock-based criteria to permit the removal of current GSSAs,
907 to be replaced by interim chronostratigraphic units, bounded by approximate ages. Development of a
908 natural Precambrian time scale, especially for periods (systems), is still a 'work in progress' but we
909 consider nevertheless that improved rock-based subdivision is already possible, desirable and overdue.
910 In working towards this aim, it is however important not to lose sight of the merits of the established
911 chronometric scheme, which has served geologists well over the last 30 years. Indeed, it would appear
912 that most boundaries would change by only small degrees. In order for future units of time (and strata)
913 to be both widely acceptable and scientifically meaningful, they need to be fully defined conceptually,
914 as has been done for the Cryogenian, Ediacaran and Cambrian periods, before they can be pinned down
915 numerically.
916 As detailed above, the boundary definitions for the Hadean, Archean, Proterozoic and
917 Phanerozoic eons help to broadly delimit four distinct parts of Earth history that are characterised by
918 particular tectonic and biogeochemical regimes. Similarly, the eras of the Proterozoic Eon are
919 recognised to be distinct intervals of tectonic, environmental and biological significance. The goal of
920 any revision to the Precambrian geological time scale should therefore be to minimise disruption to

921 both the current international time scale and existing regional and national stratigraphic norms. In this
922 vein, it may be pertinent to recall the advice given by James (1978), following Trendall (1966), that:
923 (1) "the classification should be the simplest possible that will meet immediate needs [as] every
924 additional complexity provides a basis for disagreement or rejection; (2) The subdivision of time
925 embodied in the classification should reflect major events in Earth's history, yet not be in such a form
926 as to inhibit critical review of that history; (3) The classification must be acceptable to most students of
927 the Precambrian; (4) The nomenclature should not be identified closely with one particular region; and
928 (5) The subdivision scheme should be accompanied by operational criteria, so that assignment to the
929 classification will be guided by objective rather than theoretical considerations". It is in this spirit that
930 we explore below how an improved rock-based geological time scale might depart from the existing
931 chronometric time scale.
932
933 **5.1 Tripartite rock-based subdivision of Archean time**
934 The current geological time scale divides the Archean into four eras, although none of these eras (or the
935 preceding Hadean Eon) has been formally defined or ratified. Successive studies of crustal evolution
936 have tended to favour a simpler three-fold subdivision of the Archean even if the precise numerical
937 boundaries of those eras differ in each study. We support a tripartite subdivision because the rationale
938 for the Eoarchean is conceptually unsound as it seems to be based on the chance preservation of crustal
939 fragments rather than on any fundamental change in Earth history. Although a rock-based onset for the
940 Archean Eon at c. 3.85 Ga is supported by some (Bleeker, 2004b; Kamber, 2015), proposing a specific
941 age for the Hadean-Archean boundary lies outside the scope of the current discussion. Moreover it is
942 also too difficult at present to propose a robust subdivision of Archean time based on diagnostic rock
943 assemblages with the possible exception of the Neoarchean Era. We consider that three rock-based
944 Archean eras of equal duration would constitute a robust subdivision to be characterised by the
945 following rock types and geological processes, while acknowledging that future advances in knowledge
946 may amend these preferences in the future:
947
948 **Paleoarchean** (c. 4.0 Ga – c. 3.5 Ga) Oldest crustal fragments of largely mafic composition, widespread
949 TTG (Tonalite-Trondhjemite-Granodiorite) granitization; remnants of metamorphosed supracrustals.
950
951 **Mesoarchean** (c. 3.5 Ga – c. 3.0 Ga) Development of the subcontinental lithospheric mantle.
952 Appearance of granite-greenstone terranes (coeval Pilbara and Barberton cratons) with high-grade,
953 polymetamorphic granite-gneiss complexes elsewhere. Widespread uncontroversial stromatolite and
954 other microbial fabrics, largely submerged continents, pulses in TTG magmatism that become
955 progressively more potassium-rich. The base of the Mesoarchean could potentially be chosen for the
956 base of a granite-greenstone terrane
957

Neoarchean (c. 3.0 Ga – c. 2.45/2.5 Ga) The Neoarchean witnessed a major pulse of (more felsic) crustal growth and the first platform covers on stable Archean cratons (Witwatersrand, Transvaal, Pongola Supergroups, South Africa; Mount Bruce Supergroup, Western Australia). Coeval "youngest" widespread granite-greenstone terranes (Kenoran, North America; Eastern Goldfields, Western Australia; Bulawayan, Zimbabwe); largest Superior-type BIFs in Earth history (Hamersley and Transvaal groups); initiation of a nascent form of plate tectonics; first passive margins; oldest large carbonate platforms; oldest mafic dyke swarms; methanogenic C-isotope signatures in kerogen; and traces of free oxygen from c. 3.0 Ga. We propose that the Neoarchean should include a redefined c. 2.63-2.45 Ga Siderian Period**,** encompassing BIF deposition of the Hamersley Group and coeval Transvaal. There is also potential for additional, as yet unnamed periods from c. 2.78-2.63 Ga, encompassing the basalt-rich Fortescue and Ventersdorp groups and coeval youngest widespread granite-greenstone terranes as well as prominent cratonization events; and c. 3.0-2.78 Ga encompassing the first platform covers (Witwatersrand and Pongola Groups). The base of the Neoarchean could potentially be chosen for the first appearance of carbonate platform covers. Depending on the outcome of further research on the global distribution of cratonization events, the term *Kratian*, after the Greek root 'kratos' or strength, could be reserved as a possible name for one of these older periods.

5.2 Tripartite rock-based subdivision of Proterozoic time

The current three-fold subdivision of the Proterozoic Eon is broadly accepted with each era following prolonged orogenesis, interpreted to represent supercontinent amalgamation and marked by zircon abundance peaks at around 2.7-2.5 Ga, 1.90-1.85 Ga and 1.05-1.00 Ga, respectively. The Archean-Proterozoic boundary follows two major zircon abundance peaks associated with the amalgamation of the putative megacontinent Kenora (Kenorland). Rock-based characteristics of the three Proterozoic eras might include:

Paleoproterozoic (≤2.5 Ga to ≤1.8 Ga) Plate tectonic regime switch; new platform covers accompanied by onset of widespread (global?) glaciation, oxygenation of the atmosphere (crossing the threshold of disappearance of mass-independent S-isotope fractionation), first widespread sulfate evaporites, putative rise in continental freeboard (rising seawater $^{87}Sr/^{86}Sr$), positive $\delta^{13}C$ excursions (LJE). Era ends with widespread orogenesis, interpreted to mark major stages in Nuna assembly.

Mesoproterozoic (≤ 1.8 Ga to ≤1.0 Ga) Widespread stable cratons and major platform covers, coeval with orogenesis, interpreted to represent final stages in the amalgamation of Nuna. Incorporates thick stromatolitic carbonate systems, with megascopic organic-walled fronds, beads, discs and coils, first ornamented microscopic acritarchs, appearance of multicellular red and green algae; rare negative

994 $\delta^{13}C$ excursions, widespread euxinia. Era ends with widespread orogenesis, interpreted to mark the
995 assembly of Rodinia.
996
997 **Neoproterozoic** (≤1.0 Ga to c. 0.539 Ga) New platform covers, interpreted to coincide with final
998 amalgamation, tenure and break-up of Rodinia. Diversification of eukaryotic algae and metazoans,
999 rising but unstable seawater $^{87}Sr/^{86}Sr$, high-amplitude $\delta^{13}C$ excursions (>8‰) and climate
1000 perturbations, episodic ocean oxygenation. Following a prolonged interval of worldwide glaciation
1001 (Snowball Earth), the era ends with evolution of the unique Ediacaran multicellular biota, as well as
1002 widespread orogenesis, uplift and erosion throughout the late Ediacaran to early Cambrian interval.
1003

1004 ## 5.3 Rock-based period subdivisions of the Proterozoic Eon

1005 Existing period-level GSSAs could be replaced by approximate chronostratigraphic ages as has been
1006 done for the Cryogenian Period. The Proterozoic period names of Plumb (1991) are retained below,
1007 with the addition of the *Scourian* Period, cf. Oxygenian Period of van Kranendonk et al. (2012):

1008 **Paleoproterozoic Era** (currently from 2.5 Ga, but interim boundary proposed at c. 2.45 Ga)

1009 ***Scourian* Period** (after *Skouria*, the Greek word for rust) replaces the Siderian Period (currently 2500
1010 Ma – 2300 Ma) after *Sideros* (= iron), named for the voluminous "Banded Iron Formations" (BIFs)
1011 deposited between c. 2.6 and c. 2.4 Ga, and peaking at c. 2.45 Ga. The *Scourian* Period was marked
1012 by widespread glaciation and oxygenation as evidenced from a range of redox-sensitive elemental and
1013 isotopic proxies, the decline of redox-sensitive detrital minerals such as pyrite and the eventual
1014 apperance of red beds, oxidised paleosols and evaporite sulfate minerals.

1015 **Rhyacian Period** (currently 2300 Ma – 2050 Ma) after *Rhyax* (= stream of lava), named for the
1016 "injection of layered complexes". The name 'Rhyacian' was coined specifically for the exceptional c.
1017 2.054 Ga Bushveld Igneous Complex of South Africa. The period is a generally quiet interval in terms
1018 of basin formation and orogeny. 2.2 Ga marks the onset of increased magmatism globally (Spencer,
1019 2018) with the major Bushveld LIP emplaced near the end of the period. The most characteristic
1020 feature of this period is arguably the widespread occurrence of very high $\delta^{13}C$ values in marine
1021 carbonate rocks (the Lomagundi-Jatuli Event) and the approximately contemporaneous appearance of
1022 major evaporite sulfate deposits.

1023 **Orosirian Period** (currently 2050 Ma – 1800 Ma) after *Orosira* (= mountain range), named for a
1024 "global orogenic period". This period is characterised by widespread orogenic events, reflected in an
1025 exceptional zircon abundance peak (Fig. 3), and interpreted to mark the main assembly of Nuna. The
1026 period incorporates the appearance of the first macroscopic fossils.

Mesoproterozoic Era (to begin at or after c. 1.8 Ga)

Statherian Period (c. 1800 Ma – c. 1600 Ma) after *Statheros* (= stable), named for "stabilization of cratons". This period is characterized on most continents by new platforms and by coeval orogeny marginal to Nuna (e.g., North America; Kimban Orogeny, South Australia). The McArthur Basin of northern Australia represents a suitable candidate 'stratotype'. The sandstone-volcanic Tawallah Group and Carson LIP, pass up into stromatolitic carbonates of the McArthur Group, encompassing the full interval from 1800 -1600 Ma with several age-constrained sequence breaks. Coeval sandstone-volcanic sequences in Brazil (Diamantina Group), central Africa (Chela Group), Russia (Lower Riphean), and north China (Changcheng Group) (north China). Macroscopic and microscopic fossils with diagnostically indicative eukaryote features appear in rocks towards the end of this period.

Calymmian Period (c. 1600 Ma – c. 1400 Ma) after *Calymma* (= cover), named for "platform covers". This period is characterized by the expansion of existing platform covers. Microbially influenced carbonates of the Jixian Group (North China) could provide a suitable 'stratotype', although there are similar carbonate successions in coeval Lower Riphean (Russia). Suturing events, interpreted to represent final stages of Nuna amalgamation, were followed by thick terrigenous basins that emerged during this period; e.g, Roper Group (North Australia), Belt-Purcell Supergroups (North America), Paraguacu-Chapada Diamantina Groups (Brazil). The Statherian- Calymmian boundary is represented by a regional unconformity between the McArthur and Nathan Groups (McArthur Basin) in northern Australia.

Ectasian Period (c.1400 Ma – c. 1200 Ma) after *Ectasis* (= extension), named for "continued expansion of platform covers". A tectonically quiet period, with little basin development or orogeny; e.g., upper Roper Group (Australia), Xiamaling Group (North China), Yurmatau Group (Russia), Kibaran Supergroup (central Africa). Derim Derim-Yanliao and 1230 Ga Maojiagou LIPs. Although there is currently little to distinguish it from the Calymmian Period, it is retained in Figure 6B. No suitable "stratotype" exists for now, although some authors have proposed a level close to the Jixian-Xiamaling group boundary on the North China craton, inferred to be c. 1400 Ma (between 1380 and 1440 Ma).

Stenian Period (c. 1200 Ma – c. 1000 Ma) after *Stenos* (= narrow), named for "narrow belts of intense metamorphism and deformation", e.g., Grenville, Musgrave, Sunsás, Namaqua orogenies. Conselheiro Mata Group (Brazil) and Keweenawan mafic rift (North America) elsewhere. Defining a chronostratigraphy from high-grade, deep crustal metamorphic rocks is problematic and specifically discouraged by ICS. An interim arbitrary base at c. 1200 Ma is assigned to encompass all the events across the "Grenvillian" belts, and coeval Conselheiro Mata Group. The end of the period marks the appearance of stem group multicellular red and green algae in the fossil record.

Neoproterozoic Era (to begin at or after c. 1.0 Ga).

Tonian Period (currently 1000 Ma – c. 720 Ma) after *Tonas* (= stretch), named for the lithospheric stretching that we now associate with the breaking apart of the supercontinent Rodinia, now thought to have occurred largely after c. 800 Ma based on estimated rift lengths, evaporite deposits and flood basalts (Merdith et al., 2019). Although not currently essential, a new period might conceivably cover the preceding interval of cratonization from the final amalgamation to initial rupture of Rodinia, i.e. approximately ≤ 1.0 Ga to ≥0.8 Ga, with a revised Tonian Period from ≥0.8 Ga to c. 0.72 Ga. We tentatively propose either of the terms *Kleisian* or *Syndian* in Figure 6B, following the Greek words respectively for the 'closure' or 'connection' that naturally followed the narrowing of Grenvillian-closing oceans in the final assembly phase of Rodinia. TheTonian Period saw the first appearance of mineralised scales and vase-shaped tests in the fossil record, suggesting nascent stages of biomineralization and heterotrophic protistan evolution.

6. Concluding remarks and recommendations

1) The four major divisions of Earth history are the Hadean, Archean, Proterozoic and Phanerozoic eons, whereby the Hadean-Archean boundary is taken to represent the start of the terrestrial rock record at c. 4.0 Ga.

2) Two first-order (*Archean and Proterozoic eon*) and six second-order (*Palaeoarchean, Mesoarchean, Neoarchean, Palaeoproterozoic, Mesoproterozoic, Neoproterozoic era*) stratigraphic intervals provide intuitive subdivision of post-Hadean / pre-Phanerozoic time. We consider that the Archean Eon would be more parsimoniously subdivided into three informal units of equal duration (Fig. 6B) instead of the current four eras, to be defined further after detailed discussions by a commission of international experts.

3) Major transitions in Earth's tectonic, biological and environmental history occurred at approximately 2.5-2.3, 1.8-1.6 and 1.0-0.8 Ga. We consider, therefore, that current GSSAs at 2.5, 1.6 and 1.0 Ga could be replaced expeditiously by rock-based Proterozoic eras beginning at or after c. 2.5 Ga, c. 1.8 Ga and c. 1.0 Ga, respectively, based around these major transitions, all of which occurred following orogenic peaks and during times of waning zircon abundance (post-acme, but not yet zenith) in line with Phanerozoic boundaries.

4) We suggest that current period-level GSSAs be replaced by improved rock-based concepts and interim chronostratigraphic units as soon as practicable, continuing recent progress towards that

goal, illustrated, for example, by the establishment of an Ediacaran GSSP in 2004 and chronostratigraphic definition of the base of the Cryogenian at c. 720 Ma in 2012. Although all existing period names could be retained in a future chronostratigraphic scheme, some will need more conceptual underpinning, which would likely result in movement of the Siderian Period into the Archean Eon.

5) We recommend that a future Paleoproterozoic Era contain only three periods beginning at or after c. 2.45 Ga, c. 2.3 Ga and c. 2.05 Ga, respectively, so that the era begins near the end of major Archean BIF deposition, the onset of widespread glaciation and the Great Oxidation Event, but ends close to the onset of a prolonged period of cratonic, climatic and isotopic stability. Future attention will likely focus on ensuring that rock-based Paleoproterozoic periods (currently Siderian, Rhyacian and Orosirian) bracket the natural phenomena for which they were named (iron formation, magmatism and orogenies, respectively). We propose therefore that the Siderian Period be moved into the Neoarchean, in which case a new period, potentially the *Scourian* Period (Fig. 6B), would become the first period of the Paleoproterozoic Era.

6) We recommend that a future Mesoproterozoic Era contain four periods (Statherian at, or more likely, after 1.8 Ga, Calymmian at c. 1.6 Ga, Ectasian at c. 1.4 Ga and Stenian at c. 1.2 Ga) so that it begins after major orogenic climax but before putative eukaryote-grade fossil assemblages, in the form of ornamented acritarchs and megascopic fronds, and ends after the Grenville orogeny near the time of final stages of supercontinent amalgamation.

7) We recommend that a future Neoproterozoic Era contain four periods (a pre-Tonian period at or after c. 1.0 Ga, Tonian at c. 0.85 Ga, Cryogenian at c. 0.72 Ga and Ediacaran, which has a ratified GSSP dated at c. 0.635 Ga) so that it begins around the final amalgamation of Rodinia and ends traditionally at the Ediacaran-Cambrian boundary. We tentatively propose that the pre-Tonian period could be named the *Kleisian* Period (Fig. 6B), although *Syndian* might also be considered.

8) These and further refinements of pre-Cryogenian time and strata could be developed by new expert subcommissions to cover the 1) pre-Ediacaran Neoproterozoic (currently, the Cryogenian Subcommission), 2) Mesoproterozoic, 3) Paleoproterozoic and 4) Archean (+ Hadean).

Acknowledgements

The authors represent the core of a working group of the International Commission on Stratigraphy for pre-Cryogenian chronostratigraphic subdivision. We are greatly indebted to many people who have provided comments and helpful advice on various drafts of this article from its early green paper stage, including David Harper, Brian Huber, Phil Gibbard, Stan Finney, Phil Donoghue, A.K. Jain, Vivek Kale, Mihir Deb, M. Jayananda, Jyotiranjan Ray, Aivo Lepland, Peter Haines, Martin Whitehouse. New period names were suggested by A. Bekker (*Scourian*), D. Evans (*Kleisian, Syndian*) and G. Shields (*Kratian*).

References

Adam, Z.R., Skidmore, M.L., Mogk, D.W., Butterfield, N.J., 2017. A Laurentian record of the earliest fossil eukaryotes. Geology 45, 387-390.

Ahm, A.-S. C., Maloof, A. C., Macdonald, F. A., Hoffman, P. F., Bjerrum, C. J., Bold, U., Rose, C. V., Strauss, J. V., Higgins, J. A., 2019. An early diagenetic deglacial origin for basal Ediacaran "cap dolostones". Earth and Planetary Science Letters 506, 292–307.

Alcott, L.J., Mills, B.J.W., Poulton, S.W., 2019. Stepwise Earth oxygenation is an inherent property of global biogeochemical cycling. Science, 6471, 1333-1337 doi: 10.1126/science.aax6459.

Anbar, A.D., Duan, Y., Lyons, T.W., Arnold, G.L., Kendall, B., Creaser, R.A., Kaufman, A.J., Gordon, G.W., Scott, C., Garvin, J., Buick, R., 2007. A whiff of oxygen before the Great Oxidation Event. Science, 317, 1903-1906.

Arnold, G. L., Anbar, A. D., Barling, J. and Lyons, T. W. 2004. Molybdenum isotope evidence for widespread anoxia in mid-Proterozoic oceans. Science, 304, 87–90.

Arp, G., Reimer, A., Reitner, J., 2001. Photosynthesis-induced biofilm calcification and calcium concentrations in Phanerozoic oceans. Science, 292, 1701-1074.

Ashwal, L.D., Bybee, G.M., 2017. Crustal Evolution and the temporality of anorthosites. Earth Science Reviews 173: 307-330.

Baludikay, B.K., Storme, J.Y., François, C., Baudet, D., Javaux, E.J., 2016. A diverse and exquisitely preserved organic-walled microfossil assemblage from the Meso–Neoproterozoic Mbuji-Mayi Supergroup (Democratic Republic of Congo) and implications for Proterozoic biostratigraphy. Precambrian Research 281, 166–184.

Bartley, J.K., Semikhatov, M.A., Kaufman, A.J., Knoll, A.H., Pope, M.C., Jacobsen, S.B., 2001. Global events across the Mesoproterozoic–Neoproterozoic boundary: C and Sr isotopic evidence from Siberia. Precambrian Research 111, 165–202.

1164 Bédard, J.H., 2018. Stagnant lids and mantle overturns: Implications for Archean tectonics,
1165 magmagenesis, crustal growth, mantle evolution, and the start of plate tectonics. Geoscience Frontiers,
1166 9, 19-49.
1167 Beghin, J., Guilbaud, R., Poulton, S.W., Gueneli, N., Brocks, J.J., Storme, J.-Y., Blanpied, C., Javaux,
1168 E.J., 2017a. A palaeoecological model for the late Mesoproterozoic – early Neoproterozoic Atar/El
1169 Mreïti Group, Taoudeni Basin, Mauritania, northwesternAfric. Precambrian Research 299, 1–14.
1170 Beghin, J., Storme, J.-Y., Blanpied, C., Gueneli, N., Brocks, J.J., Poulton, S.W., Javaux, E.J., 2017b.
1171 Microfossils from the late Mesoproterozoic – early Neoproterozoic Atar/El Mreïti Group, Taoudeni
1172 Basin, Mauritania, northwesternAfric. Precambrian Research 291, 63–82.
1173 Bekker, A., 2014. Great Oxygenation Event. In: Encyclopedia of Astrobiology (eds: R. Amils et al.),
1174 Springer-Verlag, Berlin, Heidelberg, pp. 1-9.
1175 Bekker, A., Holland, H.D., 2012. Oxygen overshoot and recovery during the early Paleoproterozoic.
1176 Earth and Planetary Science Letters, 317, 295-304.
1177 Bekker, A, Holland, H.D, Wang, P.L., Ruble, D., Stein, H.J., Hannah, J.L., Coetzee, L.L., Beukes, N.J.,
1178 2004. Dating the rise of atmospheric oxygen. Nature, 427, 117-120.
1179 Bekker, A., Karhu, J.A., Eriksson, K.A., Kaufman, A.J., 2003. Chemostratigraphy of Paleoproterozoic
1180 carbonate successions of the Wyoming Craton: tectonic forcing of biogeochemical change?
1181 Precambrian Research, 120: 279-325.
1182 Bekker, A., Kaufman, A.J., 2007. Oxidative forcing of global climate change: a biogeochemical record
1183 across the oldest Paleoproterozoic ice age in North America. Earth and Planetary Science Letters, 258,
1184 486-499.
1185 Bekker, A., Planavsky, N., Rasmussen, B., Krapez, B., Hofmann, A., Slack, J.F., Rouxel, O.J.,
1186 Konhauser, K.O., Iron formations: Their origins and implications for ancient seawater chemistry.
1187 Treatise on Geochemistry, 12, 561-628.
1188 Bekker, A., Slack, J.F., Planavsky, N., Krapez, B., Hofmann, A., Konhauser, K.O., Rouxel, O.J., 2010.
1189 Iron formation: the sedimentary product of a complex interplay among mantle, tectonic, oceanic, and
1190 biospheric processes. Economic Geology, 105, 467-508.
1191 Bengtson, S., Sallstedt T., Belivanova V., Whitehouse M., 2017. Three-dimensional preservation of
1192 cellular and subcellular structures suggests 1.6 billion-year-old crown-group red algae. PLoS Biol
1193 15(3):e2000735.doi:10.1371/ journal.pbio.2000735.
1194 Berney, C., Pawlowski, J., 2006. A molecular time-scale for eukaryote evolution recalibrated with the
1195 continuous microfossil record. Proceedings of the Royal Society B 273, 1867–1872.
1196 Betts, H.C., Puttick, M.N., Clark, J.W., Williams, T.A., Donoghue, P.C.J., Pisani, D., 2018. Integrated
1197 genomic and fossil evidence illuminates life's early evolution and eukaryote origin. Nature Ecology
1198 & Evolution 2, 1556–1562.

1199 Blank, C.E., 2013. Origin and early evolution of photosynthetic eukaryotes in freshwater environments:
1200 reinterpreting Proterozoic paleobiology and biogeochemical processes in light of trait evolution.
1201 Journal of Phycology, 49(6), 1040-1055.
1202 Blättler, C.L., Claire, M.W., Prave, A.R., Kirsimäe, K., Higgins, J.A., Medvedev, P.V., 2018. Two-
1203 billion-year-old evaporites capture Earth's great oxidation. Science, 360: 320-323.
1204 Bleeker, W., 2003. The late Archean record: a puzzle in c. 35 pieces. Lithos, 71: 99-134.
1205 Bleeker, W., 2004a. Towards a "natural" Precambrian time scale. In: Gradstein, F.M., Ogg, J.G., Smith,
1206 A.G. (Eds.), A Geologic Time Scale 2004. Cambridge University Press, Cambridge, pp. 141-146.
1207 Bleeker, W., 2004b. Towards a 'natural' time scale for the Precambrian – A proposal. Lethaia, 219-
1208 222.
1209 Bleeker, W., Ketchum, J.W.F., Jackson, V.A., Villeneuve, M.E., 1999. The Central Slave Basement
1210 Complex, Part 1: Its structural topology and autochthonous cover. Canadian Journal of Earth Sciences
1211 36 (7), 1083-1109.
1212 Bodorkos, S., Crowley, J.L., Claoue-Long, J.C., Anderson, J.R., Magee, C.W. Jr., 2020. Precise U-Pb
1213 baddelyite dating of the Derim Derim dolerite, McArthur Basin, Northern Territory: old and new
1214 SHRIMP and ID-TIMS constraints. Australian Journal of Earth Sciences,
1215 doi:10.1080/08120099.2020.1749929.
1216 Bowring, S. A., Grotzinger, J. P., 1992. Implications of new chronostratigraphy for tectonic evolution
1217 of Wopmay orogen, northwest Canadian Shield. American Journal of Science, 292, 1-20.
1218 Bowring, S.A., Williams, I.S., 1999. Priscoan (4.00–4.03 Ga) orthogneisses from northwestern,
1219 Canada. Contributions Mineralogy and Petrology, 134, 3–16.
1220 Bradley, D. C., 2008. Passive margins through earth history. Earth-Science Reviews, 91, 1–26.
1221 Brasier, M., Cowie, J., Taylor, M., 1994. Decision on the Precambrian-Cambrian boundary stratotype.
1222 Episodes, 17, 3-8.
1223 Brasier, A.T., Fallick, A.E., Prave, A.R., Melezhik, V.A., Lepland, A., FAR-DEEP scientists, 2011.
1224 Coastal sabkha dolomites and calcitised sulphates preserving the Lomagundi-Jatuli carbon isotope
1225 signal. Precambrian Research, 189, 193-211.
1226 Brasier, A.T., Martin, A.P., Melezhik, V.A., Prave, A.R., Condon, D.J., Fallick, A.E., 2013. Earth's
1227 earliest global glaciation? Carbonate geochemistry and geochronology of the Polisarka Sedimentary
1228 Formation, Kola Peninsula, Russia. Precambrian Research, 235, 278-294.
1229 Brocks, J.J., 2018. The transition from a cyanobacterial to algal world and the emergence of animals.
1230 Emerging Topics in Life Sciences 2, 181–190.
1231 Bull, S., Selley, D., Broughton, D., Hitzman, M., Cailteux, J., Large, R., McGoldrick, P., 2011.
1232 Sequence and carbon isotopic stratigraphy of the Neoproterozoic Roan Group strata of the Zambian
1233 copperbelt. Precambrian Research 190, 70–89.
1234 Butterfield, N.J., 2000. Bangiomorphapubescens n. gen., n. sp.: implications for the evolution of sex,
1235 multicellularity, and the Mesoproterozoic radiation of eukaryotes. Paleobiology, 26, 386-404.

1236 Butterfield, N.J., 2004. A vaucheriacean alga from the middle Neoproterozoic of Spitsbergen:
1237 implications for the evolution of Proterozoic eukaryotes and the Cambrian explosion. Paleobiology,
1238 30, 231–252.
1239 Butterfield, N.J., 2015. Early evolution of the Eukaryota. Palaeontology, 58, 5–17.
1240 Butterfield, N.J., Knoll, A.H., Swett, K., 1994. Paleobiology of the Neoproterozoic Svanbergfjellet
1241 Formation, Spitsbergen. Fossils and Strata, 34, 1–84.
1242 Campbell, I.H., Allen, C.A., 2008. Formation of supercontinents linked to increases in atmospheric
1243 oxygen. Nature Geoscience, 1, 554-558.
1244 Canfield, D.E., 1998. A new model for Proterozoic ocean chemistry. Nature, 396, 450–453.
1245 Canfield, D.E., Zhang, S., Wang, H., Wang, X., Zhao, W., Su, J., Bjerrum, C.J., Haxen, E.R.,
1246 Hammarlund, E.U., 2018. A Mesoproterozoic iron formation. PNAS, doi:10.1073/pnas.1720529115.
1247 Caro, G., Morino, P., Mojzsis, S.J., Cates, N.L. and Bleeker, W., 2017. Sluggish Hadean
1248 geodynamics: Evidence from coupled 146,147 Sm–142,143 Nd systematics in Eoarchean
1249 supracrustal rocks of the Inukjuak domain (Québec). Earth and Planetary Science Letters,
1250 457, 23-37.
1251 Cawood, P.A., Hawkesworth, C.J., 2014. Earth's middle age. Geology, 42, 503-506.
1252 Cawood, P.A., Hawkesworth, C.J., Dhuime, B. 2013. The continental record and the generation of
1253 continental crust. Geological Society of America Bulletin 125: 14-32.
1254 Cawood, P.A., Hawkesworth, C.J., Pisarevsky, S.A., Dhuime, B., Capitanio, F.A., Nebel, O., 2018.
1255 Geological archive of the Onset of Plate Tectonics. Philosophical Transactions of the Royal Society
1256 A, 376, 20170405.
1257 Chakraborty, P.P., Mukhopadhyay, J., Paul, P., Banerjee, D.M., Bera, M.K., 2020. Early atmosphere
1258 and hydrosphere oxygenation: Clues from Precambrian paleosols and chemical sedimentary records
1259 of India. Episodes, 43, 175-186.
1260 Chemale, F., Dussin, I.A., Alkmim, F.F., Martins, M.S., Queiroga, G., Armstrong, R., Santos, M.N.,
1261 2012. Unravelling a Proterozoic basin history through detrital zircon geochronology: The case of the
1262 Espinhaço Supergroup, Minas Gerais, Brazil. Gondwana Research 22, 200-206.
1263 Cloud, P., 1972. A working model of the primitive Earth. American Journal of Science, 272: 537-548.
1264 Cloud, P., 1976. Major features of crustal evolution. Geol. Soc. South Africa, Alex L. Du Toit Mem.
1265 Lect. Ser., 14, 33pp.
1266 Cloud, P., Glaessner, M.F., 1982. The Ediacarian Period and System: Metazoa inherit the Earth. Science
1267 217, 783–792.
1268 Cohen, P.A., Knoll, A.H., 2012. Scale Microfossils from the Mid-Neoproterozoic Fifteenmile Group,
1269 Yukon Territory. Journal of Paleontology 86, 775–800.
1270 Cohen, P.A., Macdonald, F.A., 2015. The Proterozoic record of eukaryotes. Paleobiology 41, 610-632.

1271 Cohen, P.A., Irvine, S.W., Strauss, J.V., 2017a. Vase-shaped microfossils from the TonianCallison
1272 Lake Formation of Yukon, Canada: taxonomy, taphonomy and stratigraphic palaeobiology.
1273 Palaeontology 60, 683–701.
1274 Cohen, P. A., Strauss, J. V., Rooney, A. D., Sharma, M., Tosca, N., 2017b. Controlled hydroxyapatite
1275 biomineralization in an 810 million-year-old unicellular eukaryote. Science Advances 3, e1700095.
1276 Collins, A.S., Patranabis-Deb, S., Alexander, E., Bertram, C., Falster, G., Gore, R., Mackintosh, J.,
1277 Dhang, P.C., Saha, D., Payne, J., Jourdan, F., Backé, G., Halverson, G.P., Wade, B.P., 2015. Detrital
1278 Mineral Age, Radiogenic Isotopic Stratigraphy and Tectonic Significance of the Cuddapah Basin,
1279 India. Gondwana Research, 28, 1294-1309.
1280 Condie, K. C., 1998. Episodic continental growth and supercontinents: a mantle avalanche connection?
1281 Earth and Planetary Science Letters 163, 97–108.
1282 Condie, K.C., 2004. Supercontinents and superplume events: distinguishing signals in the geologic
1283 record. Physics of the Earth and Planetary Interiors, 146, 319–332.
1284 Condie, K.C., 2014. Growth of continental crust: a balance between preservation and recycling.
1285 Mineralogical Magazine 78, 623–637.
1286 Condie, K.C., Aster, R.C., 2010. Episodic zircon age spectra of orogenic granitoids: the supercontinent
1287 connection and continental growth. Precambrian Research, 180: 227-236.
1288 Condie, K.C., O'Neill, C. Aster, R.C., 2009. Evidence and implications for a widespread magmatic
1289 shutdown for 250 Myr on Earth. Earth and Planetary Science Letters, 282, 294-298.
1290 Condie, K.C., Puetz, S.J., 2019. Time series analysis of mantle cycles II: The geologic record in zircons,
1291 large igneous provinces and mantle lithosphere. Geoscience Frontiers, 10, 1327-1336.
1292 Condon, D., Zhu, M., Bowring, S., Jin, Y., Wang, W., Yang, A., 2005. From the Marinoan glaciation
1293 to the oldest bilaterians: U-Pb ages from the Doushantuo Formation, China. Science 308, 95–98.
1294 Cornell, D.H., Thomas, R.J., Gibson, R., Moen, H.F.G., Moore, J.M., Reid, D.L., 2006. Namaqua-Natal
1295 Province. In: Johnson, M.R., Anhauesser, C.R., Thomas, R.J. (Eds.), The Geology of South Africa.
1296 Geol. Soc. S. Afr, Johannesburg/Council for Geoscience, Pretoria, pp. 325–379.
1297 Cox, G. M., Halverson, G. P., Stevenson, R. K., Vokaty, M., Poirier, A., Kunzmann, M., Li, Z.-X.,
1298 Denyszyn, S. W., Strauss, J. V., Macdonald, F. A., 2016. Continental flood basalt weathering as a
1299 trigger for Neoproterozoic Snowball Earth. Earth and Planetary Science Letters 446, 89–99.
1300 Cox, G.M., Isakson, V., Hoffman, P.F., Gernon, T.M., Schmitz, M.D., Shahin, S., Collins, A.S., Preiss,
1301 W., Blades, M.L., Mitchell, R.N., Nordsvan, A., 2018. South Australian U-Pb zircon (CA-ID-TIMS)
1302 age supports globally synchronous Sturtian deglaciation. Precambrian Research 315, 257–263.
1303 Crockford, P.W., Hodgskiss, M.S.W., Uhlein, G.J., Caxito, F., Hayles, J.A., Halverson, G.P., 2018.
1304 Linking paleocontinents through $\Delta^{17}O$ anomalies. Geology 46, 179–182.
1305 Crockford, P.W, Kunzmann, M., Bekker, A., Hayles, J., Bao, H., Halverson G.P., Peng, Y., Bui,
1306 T.H., Cox, G., Gibson T.M., Worndle, S., Rainbird, R., Lepland, A., Swanson-Hysell, N., Master,

S., Sreevanis, B., Kuznetsov, A., Krupenik, V., Wing, B.A., 2019. Claypool Continued: Extending the isotopic record of sedimentary sulfate. *Chemical Geology*, 514, 200-225

Crosby, C.H., Bailey, J.V., Sharma, M., 2014. Fossil evidence of iron-oxidizing chemolithotrophy linked to phosphogenesis in the wake of the Great Oxidation Event. Geology 42, 1015-1018.

Crook, K.A.W., 1989. Why the Precambrian time-scale should be chronostratigraphic: A response to recommendations by the Subcommission on Precambrian stratigraphy. Precambrian Research, 43, 143-150.

Darling, J. R., Moser, D. E., Heaman, L. M., Davis, W. J., O'Neil, J., Carlson, R. (2014). Eoarchean to Neoarchean evolution of the Nuvvuagittuq Supracrustal belt: New insights from U-Pb zircon geochronology. American Journal of Science, 313(9), 844–876.

Daines, S.J., Mills, B.J.W., Lenton, T.M., 2017. Atmospheric oxygen regulation at low Proterozoic levels by incomplete oxidative weathering of sedimentary organic carbon. Nature Communications, 8, 14379, doi: 10.1038/ncomms14379.

Dana, J.D. (1872) American Journal of Science and Arts. 3rd series, **3**, 16, 250–257.

Derry, L.A., 2010. A burial diagenesis origin for the Ediacaran Shuram-Wonoka carbon isotope anomaly, Earth and Planetary Science Letters 292, 152–172.

Des Marais, D.J., Strauss, H., Summons, R.E., Hayes, J.M., 1992. Carbon isotope evidence for the stepwise oxygenation of the Proterozoic environment. Nature, 359, 605-609.

Domagal-Goldman, S.D., Kasting, J.F., Johnston, D.T., Farquhar, J., 2008. Organic haze, glaciations and multiple sulfur isotopes in the Mid-Archean Era. Earth and Planetary Science Letters, 269(1-2), pp.29-40.

Dunn, P.R., Plumb, K.A., Roberts, H.G., 1966. A proposal for time-stratigraphic classification of the Australian Precambrian. Geol. Soc. Aust. J., 13, 593-608.

Dunn, P., Thomson, B., Rankama, K., 1971. Late Pre-Cambrian glaciation in Australia as a stratigraphic boundary. Nature 231, 498–502.

Eme, L., Sharpe, S.C., Brown, M.W., Roger, A.J., 2014. On the age of eukaryotes: evaluating evidence from fossils and molecular clocks. Cold Spring Harbor Perspectives in Biology 6, a016139.

Ernst, R.E. and Youbi, N., 2017. How large igneous provinces affect global climate, sometimes cause mass extinctions, and represent natural markers in the geological record. Palaeogeography, Palaeoclimatology, Palaeoecology, 478, 30-52.

Ernst, R.E., Wingate, M.T.D., Buchan, K.L., Li, Z.-X. 2008. Global record of 1600–700 Ma Large Igneous Provinces (LIPs): Implications for the reconstruction of the proposed Nuna (Columbia) and Rodinia supercontinents. Precambrian Research 160, 159–178.

Ernst, R.E., Bond, D.P.G., Zhang, S.H., 2020. Influence of Large Igneous Provinces. From: F.M. Gradstein, J.G. Ogg, M.D. Schmitz, G.M. Ogg. (Eds). The Geologic Time Scale 2020 volume 2, Elsevier Science Limited, pp. 345-356.

1343 Etienne, J.L., Allen, P.A., Rieu, R., Le Guerroué, E., 2007. Neoproterozoic glaciated basins: a critical
1344 review of the Snowball Earth hypothesis by comparison with Phanerozoic basins, in: Hambrey, M.J.,
1345 Christoffersen, P., Glasser, N.F., Hubbard, B. (Eds.), Glacial Sedimentary Processes and Products.
1346 Volume 39 of International Association of Sedimentologists Special Publication, pp. 343–399.
1347 Evans, D.A.D., Beukes, N.J., Kirschvink, J.L., 1997. A Paleoproterozoic Snowball Earth. Nature, 386,
1348 262-266.
1349 Evans, D.A.D., Mitchell, R.N., 2011. Assembly and breakup of the core of Paleoproterozoic-
1350 Mesoproterozoic supercontinent Nuna. Geology, 39, 443-446.
1351 Evans, D.A.D., Smirnov, A.N., Gumsley, A.P., 2017. Paleomagnetism and U–Pb geochronology of
1352 the Black Range dykes, Pilbara Craton, Western Australia: a Neoarchean crossing of the polar circle.
1353 Australian Journal of Earth Sciences, v. 64, p. 225–237, doi:10.1080/08120099.2017.1289981.
1354 Evans, D.A.D., Trindade, R.I.F., Catelani, E.L., D-Agrella-Filho, M.S., Heaman, L.M., Oliveira, E.P.,
1355 Soderlund, U., Ernst, R.E., Smirnov, A.V., Salminen, J.M., 2016. Return to Rodinia? Moderate to
1356 high palaeolatitude of the São Francisco / Congo craton at 920 Ma. From: Z. Li, D.A.D. Evans, J.B.
1357 Murphy (eds) Supercontinent Cycles Through Earth History, Geological Society, London, Special
1358 Publications, 424, 167-190.
1359 Fairchild, I.J., Kennedy, M.J., 2007. Neoproterozoic glaciation in the Earth system. Journal of the
1360 Geological Society, London 164, 895–921.
1361 Fareeduddin, Banerjee, D.M., 2020. Aravalli craton and its mobile belts: An update. Episodes, 43, 88-
1362 108.
1363 Farquhar, J., Bao, H., Thiemens, M., 2000. Atmospheric influence of Earth's earliest sulphur cycle.
1364 Science, 289, 756-758.
1365 Farquhar, J., Nanping, W., Canfield, D.E., Oduro, H., 2010. Connections between Sulfur Cycle
1366 Evolution, Sulfur Isotopes, Sediments, and Base Metal Sulfide Deposits. Economic Geology 105:
1367 509-533.
1368 Farquhar, J., Peters, M., Johnston, D.T., Strauss, H., Masterson, A., Wiechert, U. and Kaufman, A.J.,
1369 2007. Isotopic evidence for Mesoarchaean anoxia and changing atmospheric sulphur chemistry.
1370 Nature, 449, 706-709.
1371 Farquhar, J., Zerkle, A.L., Bekker, A., 2011. Geological constraints on the origin of oxygenic
1372 photosynthesis. Photosynthesis Research, 107, 11-36.
1373 Fitzsimons, I.C.W., 2010. Grenville-age basement provinces in East Antarctica: evidence for three
1374 separate collisional orogens. Geology, 28 (10), 879-882.
1375 Fralick, P. and Riding, R. 2015. Steep Rock Lake: Sedimentology and geochemistry of an Archean
1376 carbonate platform. Earth-Science Reviews, 151, 132-175.
1377 Frimmel, H.E., 2005. Archaean atmospheric evolution: evidence from the Witwatersrand gold fields,
1378 South Africa. Earth Science Reviews 70, 1-46.

Frimmel, H.E., 2018. Episodic concentration of gold to ore grade through Earth's history. Earth Science Reviews 180, 148-158.

Gallagher, M., Whitehouse, M.J., Kamber, B.S., 2017. The Neoarchaean surficial sulphur cycle: An alternative hypothesis based on analogies with 20th-century atmospheric lead. Geobiology, 15, 385-400.

George, B.G., Ray, J.S., Shukla, A.D., Chatterjee, A., Awasthi, N. Laskar, A.H., 2018. Stratigraphy and geochemistry of the Balwan Limestone, Vindhyan Supergroup, India: Evidence for the Bitter Springs $\delta^{13}C$ anomaly. Precambrian Research, 313, 18-30.

Gibson, T.M., Wörndle, S., Crockford, P.W., Bui, T.H., Creaser, R.A., Halverson, G.P., 2019. Radiogenic isotope chemostratigraphy reveals marine and nonmarine depositional environments in the late Mesoproterozoic Borden Basin, Arctic Canada. Geological Society of America Bulletin, 131(11-12), 1965-1978, doi: 10.1130/B35060.1.

Gibson, G.M., Champion, D.C., Huston, D.L., Withnall, I.W., 2020. Orogenesis in Paleo-Mesoproterozoic Eastern Australia: A response to arc-continent and continent-continent collision during assembly of the Nuna supercontinent. Tectonics, doi: 10.1029/2019TC005717

Glaessner, M.F., 1962. Pre-Cambrian fossils. Biological Reviews, 37, 467-494.

Goldich, S.S., 1968. Geochronology in the Lake Superior region. Canadian Journal of Earth Science, 5, 715-724.

Grenholm, M., Schersten, A., 2015. A hypothesis for Proterozoic-Phanerozoic supercontinent cyclicity, with implications for mantle convection, plate tectonics and Earth system evolution. Tectonophysics, 662, 434-453.

Grey, K., Hill, A.C., Calver, C., 2011. Biostratigraphy and stratigraphic subdivision of Cryogenian successions of Australia in a global context. In: E. Arnaud, G.P. Halverson and G. Shields-Zhou (Editors), The Geological Record of Neoproterozoic Glaciations. Geological Society, London, Memoirs, 36, pp. 113–134.

Griffin, W.L., Belousova, E.A., O'Neill, C., O'Reilly, S.Y., Malkovets, V., Pearson, N.J., Spetsius, S., Wilde, S.A., 2014. The world turns over: Hadean-Archean crust-mantle evolution. Lithos, 189, 2-15.

Grotzinger, J.P., 1990. Geochemical model for Proterozoic stromatolite decline. Am. J. Sci., 290-A, 80–103.

Guadagnin, F., Chemale Jr., F., Magalhães, J., Santana, A., Dussin, I., Takehara, L., 2015. Age constraints on crystal-tuff from the Espinhaço Supergroup - insight into the Paleoproterozoic to Mesoproterozoic intracratonic basin cycles of the Congo-São Francisco Craton. Gondwana Research 27, 363-376.

Guilbaud, R., Poulton, S.W., Butterfield, N.J., Zhu, M., Shields, G.A., 2015. A global transition into ferruginous conditions in the early Neoproterozoic oceans. Nature Geoscience, 8(6), 466-470 doi:10.1038/NGEO2434.

1415 Gumsley, A., Stamsnijder, J., Larsson, E., Söderlund, U., Naeraa, T., de Kock, M., Salacinska, A.,
1416 Gaweda, A., Humbert, F., Ernst, R., 2020. Neoarchean large igneous provinces on the Kaapvaal
1417 Craton in southern Africa re-define the formation of the Ventersdorp Supergroup and its temporal
1418 equivalents. Geological Society of America Bulletin, v. 132; no. 9/10; p. 1829–1844;
1419 https://doi.org/10.1130/B35237.1.
1420 Guitreau, M., Blichert-Toft, J., Mojzsis, S. J., Roth, A. S. G., & Bourdon, B., 2013. A legacy of Hadean
1421 silicate differentiation inferred from Hf isotopes in Eoarchean rocks of the Nuvvuagittuq supracrustal
1422 belt (Québec, Canada). Earth and Planetary Science Letters, 362, 171–181.
1423 Gumsley, A.P., Chamberlain, K.R., Bleeker, W., Söderlund, U., de Kock, M.O., Larsson, E.R., Bekker,
1424 A., 2017. Timing and tempo of the Great Oxidation Event. PNAS, 114: 1811-1816,
1425 Halevy, I., Johnston, D.T., Schrag, D.P., 2010. Explaining the structure of the Archean mass-
1426 independent sulfur isotope record. Science 329, 204-207.
1427 Halverson, G.P., 2006. A Neoproterozoic chronology. In: Xiao, S., Kaufman, A. (Eds.), Neoproterozoic
1428 Geobiology and Paleobiology. Vol. 27 of Topics in Geobiology. Springer, Dordrecht, the Netherlands,
1429 pp. 231–271.
1430 Halverson, G.P., Hoffman, P.F., Schrag, D.P., Maloof, A.C., Rice, A.H., 2005. Towards a
1431 Neoproterozoic composite carbon isotope record. Geological Society of America Bulletin 117, 1181–
1432 1207.
1433 Halverson, G. P., Kunzmann, M., Strauss, J. V., Maloof, A. C., 2018. The Tonian-Cryogenian transition
1434 in Svalbard. Precambrian Research 319, 79–95.
1435 Halverson, G.P., Porter, S.M., Shields, G.A. (2020) The Tonian and Cryogenian periods. From: F.M.
1436 Gradstein, J.G. Ogg, M.D. Schmitz, G.M. Ogg (Eds.). The Geologic Time Scale 2020 volume 1.
1437 Elsevier Science Limited 495-519pp.
1438 Han, T., Runnegar, B., 1992. Megascopic eukaryotic algae from the 2.1-billion-year-old Negaunee
1439 Iron-Formation, Michigan. Science 257:232–235.
1440 Hardisty, D.S., Lu, Z., Bekker, A., Diamond, C.W., Gill, B.C., Jiang, G., Kah, L.C., Knoll, A.H., Loyd,
1441 S.J., Osburn, M.R. and Planavsky, N.J., 2017. Perspectives on Proterozoic surface ocean redox from
1442 iodine contents in ancient and recent carbonate. Earth and Planetary Science Letters, 463, pp.159-170.
1443 Harland, W., 1964. Critical evidence for a great infra-Cambrian glaciation. Geologische Rundschau 54,
1444 45–61.
1445 Hawkesworth, C.J., Cawood, P.A., Dhuime, B., 2016.Tectonics and crustal evolution. GSA Today,
1446 26(9), 4-11, doi: 10.1130/GSATG272A.1.
1447 Hayes, J.M., 1994. Global methanotrophy at the Archean-Proterozoic transition, in: S. Bengtson (Ed.),
1448 Early life on Earth, Columbia University Press, New York, 1994, pp. 220–236.
1449 Hazen, R.M., 2010. The evolution of minerals. Scientific American 303(3), 58-65.

1450 Hazen, R.M., Bekker, A., Bish, D.L., Bleeker, W., Downs, R.T., Farquhar, J., Ferry, J.M., Grew, E.S.,
1451 Knoll, A.H., Papoineau, D., Ralph, J.P., Sverjensky, D.A., Valley, J.W., 2011. Needs and
1452 opportunitires in mineral evolution research. American Mineralogist, 96, 953-963.
1453 Hedberg, H., 1974. Basis for chronostratigraphic classification of the Precambrian. Precambrian
1454 Research, 1, 165-177.
1455 Heubeck, C., Lowe, D.R., 1994. Depositional and tectonic setting of the Archean Moodies Group,
1456 Barberton greenstone belt, South Africa. Precambrian Research, 68(3-4), 257-290.
1457 Hill, A.C., Cotter, K.L., Grey, K., 2000. Mid-Neoproterozoic biostratigraphy and isotope stratigraphy
1458 in Australia. Precambrian Research 100, 28–298.
1459 Hill, A. C., Walter, M. R., 2000. Mid-Neoproterozoic (~830-750 Ma) isotope stratigraphy of Australia
1460 and global correlation. Precambrian Research 100, 181–211.
1461 Hodgskiss, M.S.W., Crockford, P.W., Peng, Y., Wing, B.A., Horner, T.J., 2019. A productivity collapse
1462 to end Earth's Great Oxidation. PNAS, 116, 17207-17212, doi: 10.1073/pnas.1900325116.
1463 Hodgkiss, M.S.W., Kunzmann, M., Poirier, A.,, Halverson, G.P., 2018. The role of microbial iron
1464 reduction in the formation of Proterozoic molar tooth structures. Earth and Planetary Science Letters,
1465 482, 1-11.
1466 Hofmann, H.J., 1975. Precambrian microflora, Belcher Islands, Canada: significance and systematics.
1467 Journal of Paleontology 50, 1040-1071.
1468 Hofmann, H.J., 1990. Precambrian time units and nomenclature – the geon concept. Geology, 18, 340-
1469 341.
1470 Hofmann, H.J., 1992. New Precambrian time scale: Comments. Epsiodes, 15(2), 122-123.
1471 Hoffman, P. F., 1989. Speculations on Laurentia's first gigayear (2.0 to 1.0 Ga): Geology, 17, 135-138.
1472 Hoffman, P.F. 1997, Tectonic genealogy of North America, *in* van der Pluijm, B.A., and Marshak, S.,
1473 eds., Earth Structure: An Introduction to Structural Geology and Tectonics: New York, McGraw-Hill,
1474 p. 459–464.
1475 Hoffman, P.F., 2014. The origin of Laurentia: Rae craton as the backstop for proto-Laurentian
1476 amalgamation by slab suction: Geoscience Canada, 41, 313-320.
1477 Hoffman, P.F., Abbott, D.S., Ashkenay, Y., Benn, D. I., Brocks, J.J., Cohen, P.A., Cox, G.M.,
1478 Creveling, J.R., Donnadieu, Y., Erwin, D.H., Fairchild, I.J., Ferreira, D., Goodman, J.C., Halverson,
1479 G.P., Jansen, M.F., Le Hir, G., Love, G.D., Macdonald, F.A., Maloof, A.C., Partin, C.A., Ramstein,
1480 G., Rose, B.E.J., Rose, C.V., Sadler, P.M., Tziperman, E., Voigt, A., and Warren, S.G. (2017)
1481 Snowball Earth climate dynamics and Cryogenian geology and geobiology. Science Advances 3,
1482 e1600983.
1483 Hoffman, P.F., Halverson, G. P., Domack, E. W., Maloof, A. C., Swanson-Hysell, N. L., Cox, G. M.,
1484 2012. Cryogenian glaciations on the southern tropical paleomargin of Laurentia (NE Svalbard and
1485 East Greenland), and a primary origin for the upper Russøya (Islay) carbon isotope excursion.
1486 Precambrian Research 206-207, 137–158.

1487 Hoffman, P., Kaufman, A., Halverson, G., 1998. Comings and goings of global glaciations on a
1488 Neoproterozoic tropical platform in Namibia. GSA Today 8, 1–9.
1489 Hoffman, P.F., Schrag, D.P., 2002. The snowball Earth hypothesis: testing the limits of global change.
1490 Terra Nova, 14, 129-155.
1491 Hoffmann, K.H., Condon, D.J., Bowring, S.A., Crowley, J.L., 2004. A U-Pb zircon date from the
1492 Neoproterozoic Ghaub Formation, Namibia: Constraints on Marinoan glaciation. Geology 32, 817–
1493 820.
1494 Holland, H.D., 1984. The Chemical Evolution of the Atmosphere and Oceans. Princeton University
1495 Press, Princeton, pp. 582.
1496 Holland, H.D., 2006. The oxygenation of the atmosphere and oceans. Philosophical Transactions of the
1497 Royal Society B, 361: 903-915.
1498 Horton, F., 2015. Did phosphorus derived from the weathering of large igneous provinces fertilize the
1499 Neoproterozoic ocean? Geochemistry, Geophysics, Geosystems 16, 1723–1738.
1500 Howard, H.M., Smithies, R.H., Kirkland, C.L., Kelsey, D.E., Aitken, A., Wingate, M.T.D., Quentin de
1501 Gromard, R., Spaggiari, C.V., Maier, W.D., 2014. The burning heart: The Proterozoic geology and
1502 geological evolution of the west Musgrave region, central Australia. Gondwana Research 27, 64-94.
1503 Howchin, W., 1901. Preliminary note on the evidence of glacial beds of Cambrian age in South
1504 Australia. Transactions of the Royal Society of South Australia, 25, 10-13.
1505 Huston, D.L., Mernagh, T.P., Hagemann, S.G., Doublier, M.P., Fiorentini, M.L., Champion, D.C.,
1506 Jaques, A.L., Czarnota, K., Cayley, R., Skirrow, R., Bastrakov, E. (2016) Tectono-metallogenic
1507 systems — The place of mineral systems within tectonic evolution, with an emphasis on Australian
1508 examples. Ore Geology Reviews 76, 168-210.
1509 Idurnum et al., 1995.
1510 James, H.L., 1972. Note 40 – Subdivision of Precambrian: an interim scheme to be used by U.S.
1511 Geological Survey. Amer. Assoc. Petrol. Geol. Bull., 56, 1128-1133.
1512 James, H.L., 1978. Subdivision of the Precambrian - a brief review and a report on recent decisions by
1513 the Subcommissionon Precambrian Stratigraphy. Precambrian Research, 7, 193--204.
1514 James, N.P., Narbonne, G.M., Sherman, A.G., 1998. Molar-tooth carbonates: shallow subtidal facies of
1515 the mid- to late Proterozoic. Journal of Sedimentary Research, 68, 716-722.
1516 Javaux, E.J., Knoll, A.H., 2017. Micropaleontology of the lower Mesoproterozoic Roper Group,
1517 Australia, and implications for early eukaryotic evolution. Journal of Paleontology 91, 199–229.
1518 Javaux, E.J., Knoll, A.H., Walter, M.R. 2001. Morphological and ecological complexity in early
1519 eukaryotic ecosystems. Nature, 412, 66-69.
1520 Javaux, E.J., Lepot, K., 2018. The Paleoproterozoic fossil record: Implications for the evolution of the
1521 biosphere during Earth's middle-age. Earth Science Reviews, 176, 68-86.

1522 Jing, X., Yang, Z., Evans, D.A.D., Tong, Y., Xi, Y., Wang, H., 2020. A pan-latitudinal Rodinia in the
1523 Tonian true polar wander frame. Earth and Planetary Science Letters, 530, 115880.
1524 Johnson, T.E., Kirkland, C.L., Gardiner, N.J., Brown, M., Smithies, R.H., Santosh, M., 2019. Secular
1525 change in TTG compositions: Implications for the evolution of Archaean geodynamics. Earth and
1526 Planetary Science Letters, 505: 66-75.
1527 Jones et al (2020)
1528 Kah, L.C., Bartley, J.K., Teal, D. A., 2012. Chemostratigraphy of the Late Mesoproterozoic Atar Group,
1529 Taoudeni Basin, Mauritania: Muted isotopic variability, facies correlation, and global isotopic trends.
1530 Precambrian Research 200-203, 82–103.
1531 Kamber, B.S., 2015. The evolving nature of terrestrial crust from the Hadean, through the Archean, into
1532 the Proterozoic. Precambrian Research, 258, 48-82.
1533 Kamber, B.S., Tomlinson, E.L., 2019. Petrological, mineralogical and geochemical peculiarities of
1534 Archean cratons. Chemical Geology, 511, 123-151.
1535 Karhu, J., Holland, H.D., 1996. Carbon isotopes and the rise of atmospheric oxygen. Geology, 24, 867-
1536 870.
1537 Kaufman, A.J., Knoll, A.H., Narbonne, G.M., 1997. Isotopes, ice ages, and terminal Proterozoic Earth
1538 history. Proceedings of the National Academy of Sciences 95, 6600–6605.
1539 Kendall, B., Creaser, R.A., Reinhard, C.Y., Lyons, T.W., Anbar, A.D., 2015. Transient episodes of mild
1540 environmental oxygenation and oxidative weathering during the late Archean. Science Advances,
1541 1(10), 1500777 doi: 10.1126/sciadv.1500777.
1542 Kennedy, M.J., Runnegar, B., Prave, A.R., Hoffmann, K.H., Arthur, M., 1998. Two or four
1543 Neoproterozoic glaciations? Geology 26, 1059–1063.
1544 Kipp, M.A., Lepland, A., Buick, R., 2020. Redox fluctuations, trace metal enrichment and
1545 phosphogenesis in the ~2.0 Ga Zaonega Formation. Precambrian Research, 343, 105716.
1546 Kipp, M.A., Stüeken, E.E., Bekker, A., Buick, R., 2017. Selenium isotopes record extensive marine
1547 suboxia during the Great Oxidation Event. Proceedings of the National Academy of Sciences, 114(5),
1548 pp.875-880.
1549 Kirscher, U., Liu, Y., Li, Z. X., Mitchell, R. N., Pisarevsky, S., Denyszyn, S. W., Nordsvan, A., 2019.
1550 Paleomagnetism of the Hart Dolerite (Kimberley, Western Australia) - A two-stage assembly of the
1551 supercontinent Nuna?: Precambrian Research, 329, 170-181.
1552 Klein, C., 2005. Some Precambrian banded iron-formations (BIFs) from around the world: Their age,
1553 geologic setting, mineralogy, metamorphism, geochemistry, and origin. American Mineralogist, 90:
1554 1473-1499.
1555 Knauth, P., Kennedy, M.J., 2009. The late Precambrian greening of the Earth. Nature 460, 728–732.
1556 Knoll, A.H., Javaux, E.J., Hewitt, D., Cohen, P., 2006. Eukaryotic organisms in Proterozoic oceans.
1557 Philosophical Transactions of the Royal Society B 361, 1023–1038.

1558 Knoll, A., Kaufman, A., Semikhatov, M., 1995. The carbon-isotopic composition of Proterozoic
1559 carbonates: Riphean successions from northwestern Siberia (Anabar Massif, Turukhansk Uplift).
1560 American Journal of Science 295, 823–850.
1561 Knoll, A., Walter, M., Christie-Blick, N., 2004. A new period for the geological time scale. Science
1562 305, 621–622.
1563 Knoll, A.H., Walter, M.R., Narbonne, G.M., Christie-Blick, N., 2006. The Ediacaran Period: a new
1564 addition to the geologic time scale. Lethaia 39, 13–30.
1565 Kulling, O., 1934. The Hecla Hoek Formation around Hinlopenstredet. Geografiska Annaler 14, 161–
1566 253.
1567 Kump, L.R., Junium, C., Arthur, M.A., Brasier, A., Fallick, V., Lepland, A., Crne, A.E., Luo, G., 2011.
1568 Isotopic evidence for massive oxidation of organic matter following the great oxidation event. Science
1569 334, 1694-1696.
1570 Kunzmann, M., Schmid, S., Blaikie, T.N., Halverson, G.P., 2019. Facies analysis, sequence
1571 stratigraphy, and carbon isotope chemostratigraphy of a classic Zn-Pb host succession: The
1572 Proterozoic middle McArthur Group, McArthur Basin, Australia. Ore Geology Reviews, 106, 150-
1573 175.
1574 Kurzweil, F., Claire, M., Thomazo, C., Peters, M., Hannington, M. and Strauss, H., 2013. Atmospheric
1575 sulfur rearrangement 2.7 billion years ago: Evidence for oxygenic photosynthesis. Earth and Planetary
1576 Science Letters, 366, 17-26.
1577 Kuznetsov, A.B., Semikhatov, M.A., Maslov, A.V., Gorokhov, I.M., Prasolov, E.M., Krupenin, M.T.,
1578 Kislova, I.V., 2006. New data on Sr- and C-isotopic chemostratigraphy of the Upper Riphean type
1579 section (southern Urals). Stratigraphy and Geological Correlation 14, 602–628.
1580 Kuznetsov, A.B., Bekker, A., Ovchinnikova, G.V., Gorokhov, I.M., Vasilyeva, I.M., 2017.
1581 Unradiogenic strontium and moderate-amplitude carbon isotope variations in early Tonian seawater
1582 after the assembly of Rodinia and before the Bitter Springs Excursion. Precambrian Research 298,
1583 157–173.
1584 Kuznetsov, A.B., Semikhatov, M.A., Gorokhov, I.M., 2018. Strontium isotope stratigraphy: principles
1585 and state-of-the-art. Stratigraphy and Geological Correlation 26, 367-386.
1586 Lee, C.T.A., Yeung, L.Y., McKenzie, N.R., Yokoyama, Y., Ozaki, K., Lenardic, A., 2016. Two-step
1587 rise of atmospheric oxygen linked to the growth of continents. Nature Geoscience, 9: 417–424
1588 Lee, Y.Y., 1936. The Sinian glaciation in the lower Yangtze Valley. Bulletin of the Geoogical Society
1589 of China 15, 131–134.
1590 Li, Z.X., Bogdanova, S.V., Collins, A.S., Davidson, A., DeWaele, B., Ernst, R.E., Fitsimmons, C.W.,
1591 Fuck, R.A., Gladkochub, D.P., Jacons, J., Karlstrom, K.E., Lu, S., Natapov, L.M., Pease, V.,
1592 Pisarevsky, S.A., Thrane, K., Vernikovsky, V., 2008. Assembly, configuration and break-up history
1593 of Rodinia: a synthesis. Precambrian Research, 160: 179-210.

1594 Li, Z.X., Evans, D.A.D., Zhang, S., 2004. A 90° spin on Rodinia: possible causal links between the
1595 Neoproterozoic supercontinent, superplume, true polar wander and low-latitude glaciation. Earth and
1596 Planetary Science Letters 220, 409–421.
1597 Li, Z.X., Evans, D.A.D., Halverson, G. P., 2013. Neoproterozoic glaciations in a revised global
1598 palaeogeography from the breakup of Rodinia to the assembly of Gondwanaland. Sedimentary
1599 Geology 294, 219–232.
1600 Li, Z.X., Li, X.H., Kinny, P.D., Wang, J., 1999. The breakup of Rodinia: did it start with a mantle plume
1601 beneath South China? Earth and Planetary Science Letters 173, 171–181.
1602 Li, Z.X., Mitchell, R.N., Spencer, C.J., Ernst, R., Pisarevsky, S., Kirscher, K., Murphy, J.B., 2019.
1603 Decoding Earth's rhythms: modulation of supercontinent cycles by longer superocean episodes.
1604 Precambrian Research, 323, 1-5 doi: 10.1016/j.precamres.2019.01.009.
1605 Lindsay, J.F., 1987. Upper Proterozoic evaporites in the Amadeus basin, central Australia, and their
1606 role in basin tectonics. Geological Society of America Bulletin, 99, 852–865.
1607 Lindsay, J.F., 2002. Supersequences, superbasins, supercontinents–evidence from the Neoproterozoic-
1608 Early Palaeozoic basins of central Australia. Basin Research 14, 207–223.
1609 Lindsay, J.F., Brasier, M.D., 2002. Did global tectonics drive early biosphere evolution? Carbon isotope
1610 record from 2.6 to 1.9 Ga carbonates of Western Australian basins. Precambrian Research, 114, 1-34.
1611 Logan, W.E., 1857. On the division of Azoic rocks of Canada into Huronian and Laurentian. Proc. Am.
1612 Assoc. Adv. Sci., 1857, 44-47.
1613 Loron, C., Moczydłowska, M., 2017. Tonian (Neoproterozoic) eukaryotic and prokaryotic organic-
1614 walled microfossils from the upper Visingsö Group, Sweden. Palynology, 42, 220-254, doi:
1615 10.1080/01916122.2017.1335656.
1616 Loron, C.C., François, C., Rainbird, R.H., Turner, E.C., Borensztajn, S., Javaux, E.J., 2019b. Early
1617 fungi from the Proterozoic Era in Arctic Canada. Nature 270, 232–235.
1618 Loron, C.C., Rainbird, R.H., Turner, E.C., Greenman, J.W., Javaux, E.J., 2019a. Organic-walled
1619 microfossils from the late Mesoproterozoic to early Neoproterozoic lower Shaler Supergroup (Arctic
1620 Canada): diversity and biostratigraphic significance. Precambrian Research 321, 349–374.
1621 Luo, G., Ono, S., Beukes, N.J., Wang, D.T., Xie, S., Summons, R.E., 2016. Rapid oxygenation of
1622 Earth's atmosphere 2.33 billion years ago. Scientific Advances, 2: e1600134.
1623 Lyons, T.W., Reinhard, C.T., Planavsky, N.J., 2014. The rise of oxygen in Earth's early ocean and
1624 atmosphere. Nature, 506: 307–315.
1625 Macdonald, F.A., Halverson, G.P., Strauss, J., Smith, E., Cox, G., Sperling, E., 2012. Early
1626 Neoproterozoic basin formation in Yukon, Canada: Implications for the make-up and break-up of
1627 Rodinia. Geoscience Canada, 39, 77-100.

1628 Macdonald, F.A., Schmitz, M.D., Crowley, J.L., Roots, C.F., Jones, D.S., Maloof, A.C., Strauss, J.V.,
1629 Cohen, P.A., Johnston, D.T., Schrag, D.P., 2010. Calibrating the Cryogenian. Science 327, 1241–
1630 1243.
1631 Macdonald, F.A., Schmitz, M.D., Strauss, J.V., Halverson, G.P., Gibson, T.M., Eyster, A., Cox, G.,
1632 Mamrol, P., Crowley, J.L., 2018. Cryogenian of Yukon. Precambrian Research 319, 114–143.
1633 Macdonald, F.A., Wordwsorth, R., 2017. Initiation of Snowball Earth with volcanic sulfur aerosol
1634 emissions. Geophysical Research Letters, 44, 1938-1946.
1635 MacLennan, S., Park, Y., Swanson-Hysell, N., Maloof, A., Schoene, B., Gebreslassie, M., Antilla, E.,
1636 Tesema, T., Alene, M., Haileab, B., 2018. The arc of the Snowball: U-Pb dates constrain the Islay
1637 anomaly and the initiation of the Sturtian glaciation. Geology 46, 539–542.
1638 Manhes, G., Allègre, C., Dupré, C., Hamelin, B., 1980. Lead isotope study of basic-ultrabasic layered
1639 complexes: Speculations about the age of the earth and primitive mantle characteristics. Earth and
1640 Planetary Science Letters, 47, 370-382.
1641 Martin, A.P., Condon, D.J., Prave, A.R., Lepland, A., 2013. A review of temporal constraints for the
1642 Palaeoproterozoic large, positive carbonate carbon isotope excursion (the Lomagundi-Jatuli Event.
1643 Earth Science Reviews, 127, 242-261.
1644 Martin, A.P., Prave, A.R., Condon, D.J., Lepland, A., Fallick, A.E., Romashkin, A.E., Medvedev, P.V.,
1645 Rychanchik, D.V., 2015. Multiple Palaeoproterozoic carbon burial episodes and excursions. Earth
1646 and Planetary Science Letters, 424, 226-236.
1647 Mawson, D., 1949. The Late Precambrian ice age and glacial record of the Bibliando dome. Journal
1648 and Proceedings of the Royal Society of New South Wales 82, 150–174.
1649 McKenzie, R.N., Hughes, N.C., Myrow, P.M, Banerjee, D.M., Deb, M., and Planavasky, N.J., 2013,
1650 New age constraints for the Proterozoic-Delhi successions of India and their implications.
1651 Precambrian Research, 238, 120–128.
1652 McLelland, J.M., Selleck, B.W., Hamilton, M.A., Bickford, M.E., 2010. Late- to post-tectonic setting
1653 of some major Proterozoic anorthosite-mangerite-charnokite-granite (AMCG) suites. Canadian
1654 Mineralogist, 48: 729-750.
1655 Meert, J.G., Santosh, M., 2017. The Columbia supercontinent revisited. Gondwana Research, 50, 67-
1656 83.
1657 Melezhik, V.A., Fallick, A.E., Hanski, E.J., Kump, L.R., Lepland, A., Prave, A.R., Strauss, H., 2005.
1658 Emergence of the aerobic biosphere during the Archean-Proterozoic transition: Challenges of future
1659 research. GSA Today, 15, 11, 4-11.
1660 Melezhik, V.A., Filippov, M.M., Romaskin, A.E., 2004. A giant Palaeoproterozoic deposit of shungite
1661 in NW Russia: Genesis and practical applications. Ore Geology Reviews, 24, 135-154.
1662 Melezhik, V.A., Huhma, H., Condon, D.J., Fallick, A.E., Whitehouse, M.J., 2007. Temporal constraints
1663 on the Paleoproterozoic Lomagundi-Jatuli carbon isotopic event. Geology, 35, 655-658.

1664 Merdith, A. S., Collins, A. S., Williams, S. E., Pisarevsky, S., Foden, J. D., Archibald, D. B., Blades,
1665 M. L., Alessio, B. L., Armistead, S., Plavsa, D., Clark, C., Müller, D., 2017a. A full-plate global
1666 reconstruction of the Neoproterozoic. Gondwana Research 50, 84–134.
1667 Merdith, A.S., Williams, S.E., Müller, R.D., Collins, A.S., 2017b. Kinematic constraints on the Rodinia
1668 to Gondwana transition. Precambrian Research, 299, 132-150.
1669 Merdith, A.S., Williams, S. E., Brune, S., Collins, A.S., Müller, R.D., 2019. Rift and plate boundary
1670 evolution across two supercontinent cycles. Global and Planetary Change, 173, 1-14.
1671 Miao, L., Moczydłowska, M., Zhu, S., Zhu, M., 2019. New record of organic-walled, morphologically
1672 distinct microfossils from the late Paleoproterozoic Changcheng Group in the Yanshan Range, North
1673 China. Precambrian Research 321, 172–198.
1674 Mitchell, R.N., 2014. True polar wander and supercontinent cycles: implications for lithospheric
1675 elasticity an d the triaxial earth. American Journal of Science, 514, 966-979.
1676 Mitchell, R.N., Kilian, T.M., Evans, D.A.D., 2012. Supercontinent cycles and the calculation of
1677 absolute palaeolongitude in deep time: Nature, 482, 208-211
1678 Mitchell, R.N., Spencer, C.J., Kirscher, U., He, X.-F., Murphy, J.B., Li, Z.X., Collins, W.J., 2019.
1679 Harmonic hierarchy of mantle and lithospheric convective cycles: Time series analysis of hafnium
1680 isotopes of zircon. Gondwana Research, 75, 239-248.
1681 Moreira, H., Seixas, L., Storey, C., Fowler, M., Lasalle, S., Stevenson, R., Lana, C., 2018. Evolution of
1682 Siderian juvenile crust to Rhyacian high Ba-Sr magmatism in the Mineiro Belt, southern São
1683 Francisco Craton. Geoscience Frontiers, 9, 977-995, doi: 10.1016/j.gsf.2018.01.009.
1684 Nagovitsin, K., 2009. *Tappania*-bearing association of the Siberian platform: Biodiversity, stratigraphic
1685 position and geochronological constraints. Precambrian Research, 173, 137-145.
1686 Nance, R.D., Murphy, J.B., 2018. Supercontinents and the case for Pannotia. In: Wilson, R.W.,
1687 Houseman, G.A., McCaffrey, K.J.W., Doré, A.G., Buiter, S.J.H. (Eds.), Fifty Years of the Wilson
1688 Cycle Concept in Plate Tectonics 470, Geological Society, London, Special Publications, 470, 65-86.
1689 Nance, R.D., Worsley, T.R., Moody, J.B., 1986. Post-Archean biogeochemical cycles and long-term
1690 episodicity in tectonic processes. Geology, 14, 514-518.
1691 Nelson, L.L., Smith, E.F., Hodgin, E.B., Crowley, J.L., Schmitz, M.D., Macdonald, F.A., 2020.
1692 Geochronological constraints on Neoproterozoic rifting and onset of the Marinoan glaciation from the
1693 Kingston Peak Formation in Death Valley, California (USA). Geology, 48, doi:10.1130/G47668.1.
1694 O'Neil, J., Carlson, R. W., Francis, D., Stevenson, R. K. (2008). Neodymium-142 Evidence for Hadean
1695 Mafic Crust. Science, 321, 1828–1832.
1696 O'Neil, J., Carlson, R. W., Paquette, J. L., & Francis, D. (2012). Formation age and metamorphic history
1697 of the Nuvvuagittuq Greenstone Belt. Precambrian Research, 220–221, 23–44.
1698 O'Neill, C., Lenardic, A., Condie, K.C., 2015. Earth's punctuated tectonic evolution: cause and effect.
1699 In: Roberts, N.M.W., Ven Kranendonk, M.J., Parman, S., Shirey, S., Clift, P.D. (Eds.), Continental
1700 Formation Through Time 389, Geological Society, London, Special Publications, pp. 17-40.

1701 Ossa Ossa, F., Hofmann, A., Spangenberg, J.E., Poulton, S.W., Stueeken, E.E., Schoenberg, R.,
1702 Eickmann, B., Wille, M., Butler, M., Bekker, A., 2019. Limited oxygen production in the
1703 Mesoarchean ocean. Proceedings of the National Academy of Sciences, 116, 6647-6652.
1704 Ostrander, C.M., Nielsen, S.G., Owens, J.G., Kendall, B., Gordon, G.W., Romaniello, S.J., Anbar,
1705 A.D., 2019. Fully oxygenated water columns over continental shelves before the Great Oxidation
1706 Event. Nature Geoscience, 12, 186-191.
1707 Ouyang, G. She, Z., Papineau, D., Wang, X., Luo, G., Li, C., 2020. Dynamic carbon and sulfur cycling
1708 in the aftermath of the Lomagundi-Jatuli Event: Evidence from the Paleoproterozoic Hutuo
1709 Supergroup, North China Craton. Precambrian Research 337, 105549.
1710 Page et al., 2000.
1711 Pang, K., Tang, Q., Wan, B., Yuan, X., 2020. New insights on the palaeobiology and biostratigraphy
1712 of the acritarch Trachyhystrychosphaeraaimika: a potential late Mesoproterozoic to Tonian index
1713 fossil. Palaeoworld, doi:10.1016/j.palwor.2020.02.003.
1714 Papineau, D., 2010. Global biogeochemical change at both ends of the Proterozoic: Insights from
1715 phosphorites. Astrobiology, 10: 165-181.
1716 Parfrey, L.W., Lahr, D.J.G., Knoll, A.H., Katz, L.A., 2011. Estimating the timing of early eukaryotic
1717 diversification with multigene molecular clocks. Proceedings of the National Academy of Sciences
1718 108, 13624–13629.
1719 Park, H.U., Zhai, J.H., Peng, P., Kim, J.N., Zhang, Y.B., Kim, M.C., Park, U., Feng, L.J., 2016.
1720 Deposition age of the Sangwon Supergroup in the Pyongnam basin (Korea) and the early Tonian
1721 negative carbon isotope interval. Acta Petrologica Sinica, 32, 2181-2195.
1722 Partin, C.A., Bekker, A., Planavsky, N.J., Scott, C.T., Gill, B.C., Li, C., Podkovyrov, V., Maslov, A.,
1723 Konhauser, K.O., Lalonde, S.V., Love, G.D., 2013. Large-scale fluctuations in Precambrian
1724 atmospheric and oceanic oxygen levels from the record of U in shales. Earth and Planetary Science
1725 Letters, 369, 284-293.
1726 Partin, C.A., Bekker, A., Sylvester, P.J., Wodicka, N., Stern, R.A., Chacko, T., Heaman, L.M., 2014.
1727 Filling the juvenile magmatic gap: Evidence of uninterrupted Paleoproterozoic plate tectonics. Earth
1728 and Planetary Science Letters, 388, 123-124.
1729 Patterson, C., 1956. Age of meteorites and the Earth. Geochimica et Cosmochimica Acta, 10, 230–237,
1730 Payne, J.L., Hand, M., Barovich, K.M., Reid, A., and Evans, D.A.D., 2009, Correlations and
1731 reconstruction models for the 2500-1500 Ma evolution of the Mawson Continent, *in* Reddy, S.M.,
1732 Mazumder, R., Evans, D.A.D., and Collins, A.S., eds., Palaeoproterozoic Supercontinents and Global
1733 Evolution: Geological Society, London, Special Publications, v. 323, p. 319-355.
1734 Peng, P., 2015. Precambrian mafic dyke swarms in the North China Craton and their geological
1735 implications. SCES, doi: 10.1007/s11430-014-5026-x.
1736 Peng, S., Babcock, L., Ahlberg, P., 2020. The Cambrian Period. From: F.M. Gradstein, J.G. Ogg, M.
1737 Schmitz, G. Ogg). The Geologic Time Scale 2020. Elsevier Science Limited, in press.

1738 Philippot, P., Avila, J.N., Killingsworth, B.A., Tessalina, S., Baton, F., Caquineau, T., Muller, E.,
1739 Pecoits, E., Cartigny, P., Lalonde, S.V., Ireland, T.R., Thomazo, C., van Kranendonk, M.J., Busigny,
1740 V., 2018. Globally asynchronous Sulphur isotope signals require re-definition of the Great Oxidation
1741 Event. Nature Communications, 9(1), 1-10 doi: 10.1038/s41467-018-04621.
1742 Pietrzak-Renaud, N., Davis, D., 2014. U-Pb geochronology of baddeleyite from the Belleview
1743 metadiabase: Age and geotectonic implications for the Negaunee Iron Formation, Michigan.
1744 Precambrian Research, 250, 1-5.
1745 Pimentel, M.M., Heaman, L., Fuck, R.A., Marini, O.J. 1991. U-Pb zircon geochronology of
1746 Precambrian tin-bearing continental-type acid magmatism in central Brazil. Precambrian Research
1747 52, 321-335, 1991.
1748 Pisarevsky, S.A., Elming, S.-Å., Pesonen, L.J., Li, Z.-X., 2014. Mesoproterozoic paleogeography:
1749 Supercontinent and beyond. Precambrian Research, 244, 207-225.
1750 Planavsky, N.J., Rouxel, O.J., Bekker, A., Lalonde, S.V., Konhauser, K.O., Reinhard, C.T., Lyons,
1751 T.W., 2010. The evolution of the marine phosphate reservoir. Nature, 467, 1088-1090.
1752 Planavsky, N.J., Reinhard, C.T., Qang, X., Thomson, D., McGoldrick, P., Rainbird, R.H., Johnson, T.,
1753 Fischer, W.W., Lyons, T.W., 2014. Low mid-Proterozoic atmospheric oxygen levels and the delayed
1754 rise of animals. Science, 346, 635-638.
1755 Plumb, K.A., 1991. New Precambrian time scale. Episodes, 14, 139–140.
1756 Plumb, K.A., 1992. New Precambrian time scale – reply. Episodes, 15(2), 124-125.
1757 Plumb, K.A., James, H.L., 1986. Subdivision of Precambrian time: recommendations and suggestions
1758 by Subcommission on Precambrian stratigraphy. Precambrian Research 32, 65–92.
1759 Porter, S.M., 2016. Tiny vampires in ancient seas: evidence for predation via perforation in fossils from
1760 the 780–740 million-year-old Chuar Group, Grand Canyon, USA. Proceedings of the Royal Society
1761 B 283, 20160221.
1762 Poulton, S.W., Canfield, D.E., 2011. Ferruginous conditions: A dominant feature of oceans
1763 throughout Earth's history. Elements, 10.2113/gselements.7.2.107.
1764 Poulton S.W., Fralick, P.W., Canfield, D.E., 2010. Spatial variability in oceanic redox structure 1.8
1765 billion years ago, Nature Geoscience, 3, 486-490.
1766 Porter, S.M., Knoll, A.H., 2000. Testate amoebae in the Neoproterozoic Era: evidence from vase-
1767 shaped microfossils in the Chuar Group, Grand Canyon. Paleobiology 26, 360-385.
1768 Porter, S.M., Meisterfeld, R., Knoll, A.H., 2003. Vase-shaped microfossils from the Neoproterozoic
1769 Chuar Group, Grand Canyon: a classification guided by modern testate amoebae. Journal of
1770 Paleontology 77, 409-429.
1771 Porter, S.M., Riedman, L.A., 2016. Systematics of organic-walled microfossils from the c. 780–740 Ma
1772 Chuar Group, Grand Canyon, Arizona. Journal of Paleontology 90, 815–853.
1773 Poulton, S.W., Fralick, P.W., Canfield, D.E., 2004. The transition to a sulphidic ocean approximately
1774 1.84 billion years ago, Nature, 431,173-177.

1775 Pourteau, A., Smit, M.A., Li, Z.X., Collins, W.J., Nordsvan, A.R., Volante, S., Li, J., 2018. 1.6 Ga
1776 crustal thickening along the final Nuna suture: Geology, 46, 959-962.
1777 Prave, A.R., Condon, D.J., Hoffmann, K.H., Tapster, S., Fallick, A.E., 2016. Duration and nature of the
1778 end-Cryogenian (Marinoan) glaciation. Geology 44, 631–634.
1779 Prince, J.K.G., Rainbird, R. H., Wing, B.A., 2019. Evaporite deposition in the mid-Neoproterozoic as
1780 a driver for changes in seawater chemistry and the biogeochemical cycle of sulfur. Geology, 47(4),
1781 291-294. doi: 10.1130/G45464.1,
1782 Puetz, S.J., Condie, K., 2019. Time series analysis of mantle cycles Part 1: Periodicities and correlations
1783 among seven global isotopic databases. Geoscience Frontiers, 10, 1305-1326.
1784 Qu et al., 2014.
1785 Rainbird, R.H., Jefferson, C.W., Young, G.M., 1996. The early Neoproterozoic sedimentary succession
1786 B of northwestern Laurentia: Correlations and paleogeographic significance. Geological Society of
1787 America Bulletin, 108, 454–470.
1788 Ranjan, S., Upadhyay, D., Pruseth, K.L., Nanda, J.K., 2020. Detrital zircon evidence for change in
1789 geodynamic regime of continental crust formation 3.7-3.6 billion years ago. Earth and Planetary
1790 Science Letters, 538, 116206 doi: 10.1016/j.epsl.2020.116206.
1791 Rasmussen, B., Buick, R., 1999. Redox state of the Archean atmosphere: evidence from detrital heavy
1792 minerals in ca. 3250-2750 Ma sandstones from the Pilbara Craton, Australia. Geology, 27, 115-118.
1793 Rawlings, D.J., 1999. Stratigraphic resolution of a multiphase intracratonic basin system: the McArthur
1794 Basin, northern Australia. Australian Journal of Earth Sciences, 46(5), 703-723. doi: 10.1046/j.1440-
1795 0952.1999.00739.x.
1796 Ray, J.S., 2006. Age of the Vindhyan Supergroup: A review of recent findings. Journal of Earth System
1797 Science 115, 149–160.
1798 Reusch, H., 1891. SkuringmaerkerogmoraenguseftervistiFinnmarkenfraenperiodemegetaeldre end
1799 'istiden' (Glacial striae and boulder-clay in Norwegian Lapponie from a period much older than the
1800 last ice age). Norges Geologiske Undersøkelse 1, 78–85, 97–100.
1801 Riding, R., 2008. Abiogenic, microbial and hybrid authigenic carbonate crusts: components of
1802 Precambrian stromatolites. Geologia Croatia, 61, 73-103.
1803 Riding, R., Fralick, P., Liang, L., 2014. Identification of an Archean marine oxygen oasis. Precambrian
1804 Research 251, 232-237.
1805 Riedman, L.A., Porter, S., 2016. Organic-walled microfossils of the mid-Neoproterozoic Alinya
1806 Formation, Officer Basin, Australia. Journal of Paleontology 90, 854-887.
1807 Riedman, L.A., Porter, S.M., Calver, C.R., 2018. Vase-shaped microfossil biostratigraphy with new
1808 data from Tasmania, Svalbard, Greenland, Sweden and the Yukon. Precambrian Research 319, 19-
1809 36.
1810 Riedman, L.A., Sadler, P.M., 2018. Global species richness record and biostratigraphic potential of
1811 early to middle Neoproterozoic eukaryote fossils. Precambrian Research 319, 6-18.

1812 Rivers, T., 2015. Tectonic Setting and Evolution of the Grenville Orogen: An Assessment of Progress
1813 Over the Last 40 Years. *Geoscience Canada*, *42*(1), 77-124, doi:10.12789/geocanj.2014.41.057
1814 Rogers, J.J.W., Santosh, M., 2002. Configuration of Columbia: a Mesoproterozoic supercontinent.
1815 Gondwana Research, 5: 5-22.
1816 Rooney, A.D., Strauss, J.V., Brandon, A.D., Macdonald, F.A., 2015. A Cryogenian chronology: Two
1817 long-lasting synchronous Neoproterozoic glaciations. Geology 43, 459–462.
1818 Rooney, A.D., Yang, C., Condon, D.J., Zhu, M., Macdonald, F.A., 2020. U-Pb and Re-Os
1819 geochronology tracks stratigraphic condensation in the Sturtian snowball Earth aftermath. Geology,
1820 48(6), 625-629. doi: 10.1130/G47246.1
1821 Roscoe, S.M., 1969. Huronian rocks and uraniferous conglomerates in the Canadian Shield Geological
1822 Survey of Canada Special Paper, 68-40, 217pp.
1823 Safanova, L., Maruyama, S., 2014. Asia: a frontier for a future supercontinent Amasia. International
1824 Geology Reviews, 56: 1051-1071.
1825 Sánchez-Baracaldo, P., Raven, J.A., Pisani, D., Knoll, A.H., 2017. Early photosynthetic eukaryotes
1826 inhabited low-salinity habitats. Proceedings of the National Academy of Sciences, 114(37), pp.E7737-
1827 E7745.
1828 Satkoski, A.M., Lowe, D.R., Beard, B.L., Coleman, M.L., Johnson, C.M., 2016. A high continental
1829 weathering flux into Paleoarchean seawater revealed by strontium isotope analysis of 3.26 Ga barite.
1830 Earth and Planetary Science Letters, 454: 28–35.
1831 Scott, C., Lyons, T.W., Bekker, A., Shen, Y.A., Poulton, S.W., Chu, X.L., Anbar, A.D., 2008. Tracing
1832 the stepwise oxygenation of the Proterozoic ocean. Nature, 452, 456-459.
1833 Schroeder, S., Bekker, A., Beukes, N.J., Strauss, H., van Niekerk, H.S., 2008. Rise in seawater sulphate
1834 concentrations associated with the Paleoproterozoic positive carbon isotope excursion: evidence from
1835 sulphate evaporites in the ~2.2-2.1 Gyr shallow-marine Lucknow Formation, South Africa. Terra
1836 Nova, 20, 108-117.
1837 Schulze, D.J., Harte, B., Edinburgh Ion Microprobe Facility Staff, Page, Z., Valley, J.W., Channer,
1838 D.M., Jaques, A.L., 2013. Anticorrelation between low □^{13}C of eclogitic diamonds and high □^{18}C
1839 of their coesite and garnet inclusions requires a subduction origin. Geology 41, 455-458.
1840 Sedgwick, A., 1845. On the Older Palæozoic (Protozoic) Rocks of North Wales. Quarterly Journal of
1841 the Geological Society, 1, 5-22.
1842 Semikhatov, M.A., Kuznetsov, A.B., Chumakov, N.M., 2015. Isotope age boundaries between the
1843 general stratigraphic subdivisions of the upper Proterozoic (Riphean and Vendian) in Russia: The
1844 evolution of opinions and the current estimate. Stratigraphy and Geological Correlation, 23, 568-579.
1845 Sergeev, V.N., Vorob'eva, N.G., Petrov, P.Y., 2017. The biostratigraphic conundrum of Siberia: do true
1846 Tonian–Cryogenian microfossils occur in Mesoproterozoic rocks? Precambrian Research 299, 282–
1847 302.

1848 Shang, M., Tang, D., Shi, X., Zhou, L., Zhou, X., Song, H., Jiang, G., 2019. A pulse of oxygen increase
1849 in the early Mesoproterozoic ocean at ca. 1.57-1.56 Ga. Earth and Planetary Science Letters, 527,
1850 115797.
1851 Sharma, Mukund, Shukla, Y. 2009. Taxonomy and affinity of Early Mesoproterozoic megascopically
1852 helically coiled and related fossils from the Rohtas Formation, the Vindhyan Supergroup, India.
1853 Precambrian Research, 173, 105–122.
1854 Shen, Y., Canfield, D. E. and Knoll, A. H. 2002. Middle Proterozoic ocean chemistry: evidence from
1855 the McArthur Basin, northern Australia. American Journal of Science, 302, 81-109.
1856 Shields, G.A., 2002. 'Molar-tooth microspar': a chemical explanation for its disappearance ~750 Ma.
1857 Terra Nova, 14, 108-113.
1858 Shields, G.A., 2007. A normalised seawater strontium isotope curve: possible implications for
1859 Neoproterozoic-Cambrian weathering rates and the further oxygenation of the Earth. eEarth, 2: 35-
1860 42.
1861 Shields, G.A., Halverson, G.P., Porter, S.M., 2018. Descent into the Cryogenian. Precambrian Research
1862 319, 1–5.
1863 Shields, G.A., Mills, B.J.W., 2017. Tectonic controls on the long-term carbon isotope mass balance.
1864 PNAS, doi:10.1073/pnas.1614506114.
1865 Shields, G.A., Mills, B.J.W., Zhu, M., Daines, S., Lenton, T.M., 2019. Unique Neoproterozoic carbon
1866 isotope excursions sustained by coupled evaporite dissolution and pyrite burial. Nature Geoscience,
1867 12, 823-827. doi: 10.1038/s41561-019-0434-3.
1868 Shields, G., Veizer, J., 2002, Precambrian marine carbonate isotope database: Version 1.1:
1869 Geochemistry Geophysics Geosystems, 3(6), 1–12, doi: 10.1029/2001GC000266.
1870 Shields-Zhou, G.A., Hill, A.C., Macbabhann, B.A., 2012. The Cryogenian Period. Chapter 17 in F.M.
1871 Gradstein, J. G. Ogg, M. Schmitz, and G. Ogg (Eds.), The Geological Time Scale 2012 (vol. 1).
1872 Elsevier, pp. 393–411.
1873 Shields-Zhou, G., Porter, S.A., Halverson, G.P., 2016. A new rock-based definition for the Cryogenian
1874 Period (circa 720–635 Ma). Episodes 39, 3–9.
1875 Shirey, S.B., Richardson, S.H., 2011. Start of the Wilson Cycles at 3 Ga shown by Diamonds from
1876 Subcontinental Mantle. Science, 333, 434-458.
1877 Singh, V. K., Sharma Mukund, Sergeev V. N. 2019. A New Record of Acanthomorphic Acritarch
1878 *Tappania* Yin from the Early Mesoproterozoic Saraipali Formation, Singhora Group, Chhattisgarh
1879 Supergroup, India and its Biostratigraphic Significance. Journal of the Geological Society of India,
1880 94, 471-479.
1881 Sircombe, K.N., Bleeker, W., Stern, R.A., 2001. Detrital zircon geochronology and grain-size analysis
1882 of a ~2800 Ma Mesoarchean proto-cratonic succession, Slave Province, Canada. Earth and Planetary
1883 Science Letters, 189, 207-220.

1884 Slack, J.F., Grenne, T., Bekker, A., Rouxel, O.J., Lindberg, P.A., 2007. Suboxic deep seawater in the
1885 late Paleoproterozoic: evidence from hematitic chert and Fe formation related to seafloor
1886 hydrothermal sulfide deposits, central Arizona, USA. Earth and Planetary Science Letters, 255, 243-
1887 256.
1888 Spencer, C.J., Hawkesworth, C., Cawood, P.A., Dhuime, B., 2013. Not all supercontinents are created
1889 equal: Gondwana-Rodinia case study. Geology, 41(7), 795–798.
1890 Spencer, C.J., Murphy, J.B., Kirkland, C.L., Liu, Y., Mitchell, R.M., 2018. A Palaeoproterozoic tecton-
1891 magmatic lull as a potential trigger for the supercontinent cycle. Nature Geoscience, 11: 97-101.
1892 Spencer, C.J., 2020. Continuous continental growth as constrained by the sedimentary record. American
1893 Journal of Science, 320, 373-401.
1894 Sprigg, R.C., 1947. Early Cambrian (?) jellyfishes from the Flinders Ranges, South Australia.
1895 Transactions of the Royal Society of South Australia, 71, 212–224.
1896 Stern, R.A., Bleeker, W., 1998. Age of the world's oldest rocks refined using Canada's SHRIMP:
1897 Acasta Gneiss Complex, Northwest Territories. Geoscience Canada, 25, 27-31.
1898 Stockwell, C.H., 1961. Structural provinces, orogenies, and time classification of rocks of the Canadian
1899 Precambrian Shield. Geol. Surv. Canada. Paper, 61-17, 108-118.
1900 Stockwell, C.H., 1982. Proposals for time classification and correlation of Precambrian rocks and
1901 events in Canada and adjacent areas of the Canadian Shield. Part 1: A time classification of
1902 Precambrian rocks and events. Geol. Surv. Can. Pap. 80-19.
1903 Stolper, D.A.., Brenhin-Keller, C., 2018. A record of deep-ocean dissolved O_2 from the oxidation
1904 state of iron in submarine basalts. Nature, doi:10.1038/nature/25009.
1905 Strachan, R., Murphy, J.B., Darling, J., Storey, C., Shields, G.A., 2020. Precambrian (4.56–1.0 Ga).
1906 From: F.M. Gradstein, J.G. Ogg, M.D. Schmitz, G.M. Ogg (Eds.). The Geologic Time Scale 2020
1907 volume 1. Elsevier Science Limited, 481-493pp.
1908 Strauss, J.V., Rooney, A.D., Macdonald, F.A., Brandon, A.D., Knoll, A.H., 2014. 740 Ma vase-shaped
1909 microfossils from Yukon, Canada: implications for Neoproterozoic chronology and biostratigraphy:
1910 Geology, 42, 659–662.
1911 Swanson-Hysell, N. L., Maloof, A. C., Condon, D. J., Jenkin, G. R. T., Alene, M., Tremblay, M. M.,
1912 Tesema, T., Rooney, A. D., Haileab, B., 2015. Stratigraphy and geochronology of the Tambien Group,
1913 Ethiopia: Evidence for globally synchronous carbon isotope change in the Neoproterozoic. Geology
1914 43, 323–326.
1915 Swanson-Hysell, N. L., Maloof, A. C., Kirschvink, J. L., Evans, D. A. D., Halverson, G. P., Hurtgen,
1916 M. T., 2012. Constraints on Neoproterozoic paleogeography and Paleozoic orogenesis from
1917 paleomagnetic records of the Bitter Springs Formation, central Australia. American Journal of Science
1918 312, 817–884.
1919 Tang, H., Chen, Y., 2013. Global glaciations and atmospheric change at c. 2.3 Ga. Geoscience Frontiers,
1920 4: 583-596.

1921 Tang, Q., Pang, K., Xiao, S., Yuan, X., Ou, Z., Wan, B., 2013. Organic-walled microfossils from the
1922 early Neoproterozoic Liulaobei Formation in the Huainan region of North China and their
1923 biostratigraphic significance. Precambrian Research 236, 157–181.
1924 Tang, Q., Pang, K., Yuan, X., Wan, B., Xiao, S., 2015. Organic-walled microfossils from the
1925 TonianGouhou Formation, Huaibei region, North China Craton, and their biostratigraphic
1926 implications. Precambrian Research 266, 296–318.
1927 Tang, D., Shi, X., Wang, X., Jiang, G., 2016. Extremely low oxygen concentration in mid-Proterozoic
1928 shallow seawaters. Precambrian Research, 276, 145-157.
1929 Tang, Q., Pang, K., Yuan, X., Xiao, S., 2020. A one-billion-year-old multicellular chlorophyte. Nature
1930 Ecology and Evolution, doi: 10.1038/s41559-020-1122-9.
1931 Teixeira, W., Geraldes, M.C., Matos, R., Salina Ruiz, A., Saes, G., Vargas-Mattos, G., 2010. A review
1932 of the tectonic evolution of the Sunsas Belt, SW Amazonian craton. Journal of South American Earth
1933 Sciences, 29, 47-60.
1934 Thomazo, C., Pinto, D.L., Busigny, V., Ader, M., Hashizume, K., Philippot, P., 2009. Biological
1935 activity and the Earth's surface evolution: insights from carbon, sulfur, nitrogen and iron stable
1936 isotopes in the rock record. Comptes Rendus Palevol, 8, 665-678.
1937 Thomson, J., 1871. On the stratified rocks of Islay. Report of the 41st Meeting of the British Association
1938 for the Advancement of Science, Edinburgh, John Murray, London, pp. 110-111.
1939 Thomson, J., 1877. On the geology of the island of Islay. Transactions of the Geological Society of
1940 Glasgow 5, 200-222.
1941 Thomson, D., Rainbird, R.H., Planavsky, N., Lyons, T.W., Bekker, A., 2015. Chemostratigraphy of the
1942 Shaler Supergroup, Victoria Island, NW Canada: a record of ocean composition prior to the
1943 Cryogenian glaciations. Precambrian Research, 263, 232-245.
1944 Torres, M.A., Paris, G., Adkins, J.F., Fischer, W.W., 2018. Riverine evidence for isotopic mass balance
1945 in the Earth's early sulfur cycle. Nature Geoscience, 11, 661-664.
1946 Trendall, A.F., 1966. Towards rationalism in Precambrian stratigraphy. Geol. Soc. Austr. J., 13, 517-
1947 522.
1948 Trendall, A.F., 1991. The "Geological Unit" (g.u.) – A suggested new measure of geologic time.
1949 Geology, 19, 195.
1950 Trendall et al. (2004)
1951 Tsikos, H., Matthews, A., Erel, Y., Moore, J.M., 2010. Iron isotopes constrain biogeochemical redox
1952 cycling of iron and manganese in a Palaeoproterozoic stratified basin. Earth and Planetary Science
1953 Letters, 298, 125-134.
1954 Tyrell, T. 1999. The relative influences of nitrogen and phosphorus on oceanic primary production.
1955 Nature 400, 525–531.
1956 Van Kranendonk, M.J., Altermann, W., Beard, B.L., Hoffman, P.E., Johnson, C.J., Kasting, J.F.,
1957 Melezhik, V.A., Nutman, A.P., Papineau, D., Pirajino, F., 2012. A chronostratigraphic division of the

1958 Precambrian: possibilities and challenges. In: Gradstein, F.M., Ogg, J.G., Schmitz, M., Ogg, G.,
1959 (Coordinators). The Geologic Time Scale 2012. Elsevier Publ., pp. 299-392.
1960 Van Kranendonk, M.J., Kirkland, C.L., 2016. Conditioned duality of the Earth system: Geochemical
1961 tracing of the supercontinent cycle through Earth history. Earth-Science Reviews, 160: 171-187.
1962 Veizer, J., 1989. Strontium isotopes in seawater through time. Annual Reviews of Earth and Planetary
1963 Sciences, 17, 141-167.
1964 Vermeesch, P., Resentini, A., and Garzanti, E., 2016. An R package for statistical provenance analysis:
1965 Sedimentary Geology, 336, 14–25, https://doi.org/10.1016/j.sedgeo.2016.01.009
1966 Walker, J.C.G., Hays, P.B., and Kasting, J.F., 1981. A negative feedback mechanism for the long-term
1967 stabilization of Earth's surface temperature: Journal of Geophysical Research, 86, 9776,
1968 doi:10.1029/JC086iC10p09776.
1969 Walter, M. R., Oehler, J. H., and Oehler, D. Z. 1976. Megascopic algae 1300 million years old from the
1970 Belt Supergroup, Montana: a reinterpretation of Walcott's Helminthoidichnites. Journal of
1971 Paleontology 50, 872–881.
1972 Wang, X. C., Li, Z. X., Li, X. H., Li, Q. L., Zhang, Q.-R., 2011. Geochemical and Hf-Nd isotope data
1973 of Nanhua rift sedimentary and volcaniclastic rocks indicate a Neoproterozoic continental flood basalt
1974 provenance. Lithos, 427–440.
1975 Wang, C., Peng, P., Wang, X., Yang, S., 2016. Nature of three Proterozoic (1680 Ma, 1230 Ma and 775
1976 Ma) mafic dyke swarms in North China: Implications for tectonic evolution and paleogeographic
1977 reconstruction. Precambrian Research, 285, 109-126.
1978 Wang, D., Zhu, X.-K., Zhao, N., Yan, B., Li, X.-H., Shi, F., Zhang, F., 2019. Timing of the termination
1979 of Sturtian glaciation: SIMS U-Pb zircon dating from South China. Journal of Asian Earth Sciences
1980 177, 287–294.
1981 Ward, L.M., Kirschvink, J.L., Fischer, W.W., 2016. Timescales of oxygenation following the evolution
1982 of oxygenic photosynthesis. Origin of Life and Evolution of the Biosphere, 46, 51-65.
1983 Warke, M.R., Strauss, H., Schröder, S., 2020a. Positive cerium anomalies imply pre-GOE redox
1984 stratification and manganese oxidation in Paleoproterozoic shallow marine environments.
1985 Precambrian Research, 344, 105767.
1986 Warke, M.R., Di Rocco, T., Zerkle, A.L., Lepland, A., Prave, A.R., Martin, A.P., Ueno, Y., Condon,
1987 D.J., Claire, M.W., 2020b. The Great Oxidation Event preceded a Paleoproterozoic Snowball Earth.
1988 Proceedings of the National Academy of Sciences, 117, 13314-13320.
1989 Whitmeyer, S.J., Karlstrom, K.E., 2007. Tectonic model for the Proterozoic growth of North Americ.
1990 Geosphere, 3: 220-259.
1991 Worsley, T.R., Nance, R.D., Moody, J.B., 1985. Proterozoic to recent tectonic tuning of biogeochemical
1992 cycles. In: Sunquist, E.T., Broecker, W.S. (Eds.), The Carbon Cycle and Atmospheric CO_2: Natural
1993 Variations Archean to Present. American Geophysical Union, Geophysical Monographs, 32: 561-572.

1994 Xiao, S., Narbonne, G.M., 2020. The Ediacaran Period. From: F.M. Gradstein, J.G. Ogg, M.D. Schmitz,
1995 G.M. Ogg (Eds.). The Geologic Time Scale 2020 volume 1. Elsevier Science Limited 521-560pp.
1996 Xiao, S., Tang, Q., 2018. After the boring billion and before the freezing millions: evolutionary patterns
1997 and innovations in the Tonian Period: Emerging Topics in Life Sciences, 2, 161-171, doi:
1998 10.1042/ETLS20170165.
1999 Yang, B., Collins, A.S., Blades, M.L., Capogreco, N., Payne, J.L., Munson, T.J., Cox, G.M., 2019.
2000 Middle-late Mesoproterozoic tectonic geography of the North Australia Craton: U–Pb and Hf isotopes
2001 of detrital zircons in the Beetaloo Sub-basin, Northern Territory, Australia. Journal of the Geological
2002 Society, London, 176, 771-784.
2003 Yang, B., Collins, A.S., Cox, G.M., Jarrett, A.J.M., Denyszyn, S., Blades, M.L., Farkaš, J., Glorie, S.,
2004 2020. Using Mesoproterozoic Sedimentary Geochemistry to Reconstruct Basin Tectonic Geography
2005 and Link Organic Carbon Productivity to Nutrient Flux from a Northern Australian Large Igneous
2006 Province. Basin Research, 2020; 00: 1–17. https://doi.org/10.1111/bre.12450.
2007 Yin, L. 1997. Acanthomorphic acritarchs from Meso-Neoproterozoic shales of the Ruyang Group,
2008 Shanxi, China. Rev. Palaeobot. Palynol., 98: 15-25.
2009 Yin, L., Changtai, N., Kong, F.-F. 2018. A Review of Proterozoic Organic walled Microfossils –
2010 *Tappania* and Its Biologic and Geologic Implication. Acta Palaeontol. Sinica, 57: 147-156.
2011 Young, G.M., 2013. Precambrian supercontinents, glaciations, atmospheric oxygenation, metazoan
2012 evolution and an impact that may have changed the second half of Earth history. Geoscience Frontiers,
2013 4: 247-261.
2014 Young, G.M., 2019. Aspects of the Archean-Proterozoic transition: How the great Huronian Glacial
2015 Event was initiated by rift-related uplift and terminated at the rift-drift transition during break-up of
2016 Lauroscandia. Earth Science Reviews, 190, 171-189.
2017 Zalasiewicz, J. Smith, A., Brenchley, P., Evans, J., Knox, R., Riley, N., Gale, A., Gregory, F.J.,
2018 Rushton, A., Gibbard, P., Hesselbo, S., Marshall, J., Oates, M., Rawson, P., Trewin, N., 2004.
2019 Simplifying the stratigraphy of time. Geology, 32, 1-4.
2020 Zhai, M.G., Hu, B., Zhao, T.P., Peng, P., Meng, Q.R., 2015. Late Paleoproterozoic-Neoproterozoic
2021 multi-rifiting events in the North China craton and their geological significance: a study advance and
2022 review. Tectonophysics, 662, 153-166.
2023 Zhang, K., Zhu, X., Wood, R.., Shi, Y., Gao, Z., Poulton, S.W., 2018. Oxygenation of the
2024 Mesoproterozoic ocean and the evolution of complex eukaryotes. Nature Geoscience, 11: 345-350.
2025 Zhang, S., Wang, X., Wang, H., Bjerrum, C.J., Hammerlund, E.U., Mafalda Costa, M., Connelly, J.N.,
2026 Zhang, B., Su, J., Canfield, D.E., 2016. Sufficient oxygen for animal respiration 1,400 million years
2027 ago. Proceedings of the National Academy of Science, 113, 1731-1736.
2028 Zhang, S., Ernst, R.E., Pei, J., Zhao, Y., Zhou, M., Hu, G., 2018. A temporal and causal link between
2029 c. 1380 Ma large igneous provinces and black shale: Implications for the Mesoproterozoic time scale
2030 and paleoenvironment. Geology, 46: 963-966.

Zhao, G., Cawood, P.A., 2012. Precambrian geology of China. Precambrian Research, 222-223, 13-54.

Zhao, G., Cawood, P.A., Wilde, S.A., Sun, M., 2002. Review of global 2.1-1.8 Ga orogens: implications for a pre-Rodinia supercontinent. Earth-Science Reviews, 59, 125-162.

Zhou, C.M., Huyskens, M.H., Lang, X.G., Xiao, S.H., Yin, Q.Z., 2019. Calibrating the terminations of Cryogenian global glaciations: Geology, 47, 251–254, doi: 10.1130/G45719.1.

Zhou, Y., Pogge von Strandmann, P.A.E., Zhu, M., Ling, H., Manning, C., Li, D., He, T., Shields, G.A., 2020. Reconstructing Tonian seawater $^{87}Sr/^{86}Sr$ using calcite microspar. Geology, doi: 10.1130/G46756.1.

Zhu, S., Zhu, M., Knoll, A.H., Yin, Z., Zhao, F., Sun, S., Qu, Y., Shi, M., Liu, H., 2016. Decimetre-scale multicellular eukaryotes from the 1.56-billion-year-old Gaoyuzhuang Formation in North China. Nature Communications, doi: 10.1038/ncomms11500.

Zumberge, J.A., Rocher, D., Love, G.D., 2019. Free and kerogen-bound biomarkers from late Tonian sedimentary rocks record abundant eukaryotes in mid-Neoproterozoic marine communities. Geobiology, doi: 10.1111/gbi.12378.

2047 **Figure captions**
2048
2049 **Fig. 1A.** Current geological time scale; **1B**. Timescale proposal of van Kranendonk et al. (2012). Golden
2050 spike symbols represent ratified (yellow) and potential (pale) GSSP levels. Clock symbols represent
2051 ratified Proterozoic and recommended Archean GSSAs.
2052
2053 **Fig. 2.** Evolution of stratigraphic terminology for the Neoproterozoic Era. Note that age ranges for
2054 earlier subdivisions are based on current age estimates. Triangle symbol (Δ) denotes the approximate
2055 levels of glaciations relevant to the time scale subdivisions. * Denotes the term "Ediacarian" introduced
2056 by Cloud and Glaessner (1982).
2057
2058 **Fig. 3.** Peaks in the distribution (1σ error) of U–Pb zircon ages for orogenic granitoids and detrital
2059 zircon grains match intervals of supercontinent assembly, whereas troughs correspond to intervals of
2060 supercontinent tenure and break-up (from Condie and Aster 2010; Condie, 2014). Black: Total ages (n
2061 = 37,830); Green: detrital ancient sedimentary rocks (n = 21,849); Blue: detrital modern sediments (n
2062 = 7053; 2x); Red: orogenic granitoids (n = 8928). N (vertical axis) is the number of zircon ages as a
2063 function of time for a Gaussian kernel bandwidth of three standard deviations (30 m.y.).
2064
2065 **Fig. 4.** The Neoproterozoic geological time scale (after Halverson et al., 2020). Negative
2066 carbon isotope anomalies (BSA = Bitter Springs Anomaly; RA = Russøya anomaly; GA =
2067 Garvellach anomaly; TA = Trezona Anomaly; SA = Shuram Anomaly; E-CA = Ediacaran-
2068 Cambrian boundary anomaly). Minimum biostratigraphic ranges are also shown for
2069 *Trachyhystrichosphaera aimika*, *Cerebrosphaera globosa* (*C. buickii*), and the *Cycliocyrillium*
2070 *simplex* assemblage. Geochronological age constraints for the Tonian and Cryogenian periods
2071 (along with ages from the early Ediacaran Period that provide minima on the Cryogenian-
2072 Ediacaran boundary) are shown (in open squares) by type of age determination. **4B.** Expanded
2073 view of the age constraints that establish the synchronous onset and end of the Cryogenian
2074 glaciations.
2075
2076 **Fig. 5.** Neoproterozoic seawater strontium isotope curve (blue line) superimposed on known large
2077 igneous provinces (red bars) and the carbon isotope record (after Zhou et al., 2020).

2078 **Fig. 6A.** Current geological time scale; **6B.** Proposed chronostratigraphic subdivision of the geological
2079 time scale – this paper. Note that era and period boundary ages are approximate ages only and would
2080 inevitably change in any internationally agreed chronostratigraphic scheme. Period names in italics
2081 represent suggested changes to existing nomenclature. If the first period of the Paleoproterozoic Era

2082 were renamed (here as the *Scourian* Period, cf. Oxygenian Period of van Kranendonk et al., 2012), we
2083 note that the term ‘Siderian’ would likely be retained for the final period of the Archean Eon.

2084
2085

Figure 1

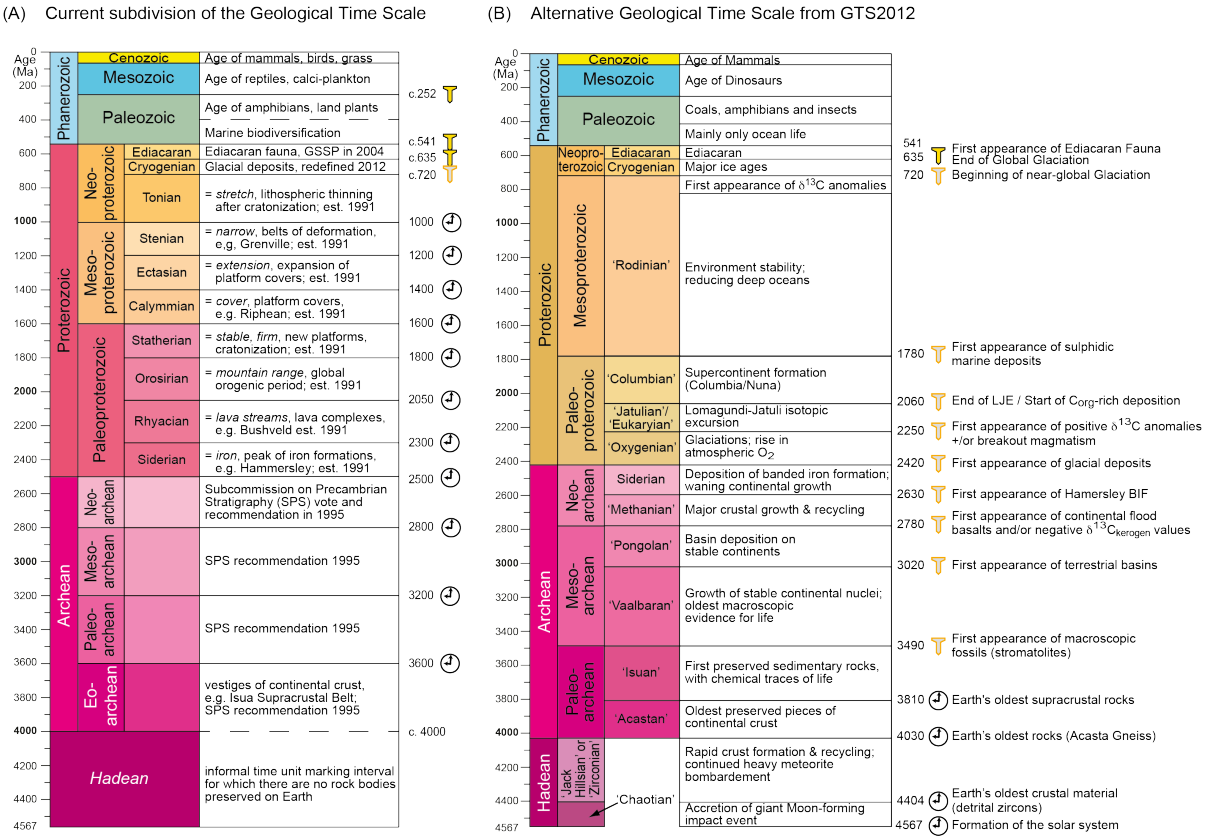
(A) Current subdivision of the Geological Time Scale
(B) Alternative Geological Time Scale from GTS2012
Age (Ma)
Phanerozoic
Proterozoic
Archean
Hadean
Cenozoic
Mesozoic
Paleozoic
Neo-proterozoic
Meso-proterozoic
Paleoproterozoic
Neo-archean
Meso-archean
Paleo-archean
Eo-archean
Ediacaran
Cryogenian
Tonian
Stenian
Ectasian
Calymmian
Statherian
Orosirian
Rhyacian
Siderian
Age of mammals, birds, grass
Age of reptiles, calci-plankton
Age of amphibians, land plants
Marine biodiversification
Ediacaran fauna, GSSP in 2004
Glacial deposits, redefined 2012
= stretch, lithospheric thinning after cratonization; est. 1991
= narrow, belts of deformation, e.g, Grenville; est. 1991
= extension, expansion of platform covers; est. 1991
= cover, platform covers, e.g. Riphean; est. 1991
= stable, firm, new platforms, cratonization; est. 1991
= mountain range, global orogenic period; est. 1991
= lava streams, lava complexes, e.g. Bushveld est. 1991
= iron, peak of iron formations, e.g. Hammersley; est. 1991
Subcommission on Precambrian Stratigraphy (SPS) vote and recommendation in 1995
SPS recommendation 1995
SPS recommendation 1995
vestiges of continental crust, e.g. Isua Supracrustal Belt; SPS recommendation 1995
informal time unit marking interval for which there are no rock bodies preserved on Earth
c.252
c.541
c.635
c.720
1000
1200
1400
1600
1800
2050
2300
2500
2800
3200
3600
c. 4000
Age of Mammals
Age of Dinosaurs
Coals, amphibians and insects
Mainly only ocean life
Neopro-terozoic
Ediacaran
Cryogenian
Mesoproterozoic
Paleo-proterozoic
Neo-archean
Meso-archean
Paleo-archean
Hadean
'Rodinian'
'Columbian'
'Jatulian'/ 'Eukaryian'
'Oxygenian'
Siderian
'Methanian'
'Pongolan'
'Vaalbaran'
'Isuan'
'Acastan'
'Chaotian'
Ediacaran
Major ice ages
First appearance of δ13C anomalies
Environment stability; reducing deep oceans
Supercontinent formation (Columbia/Nuna)
Lomagundi-Jatuli isotopic excursion
Glaciations; rise in atmospheric O2
Deposition of banded iron formation; waning continental growth
Major crustal growth & recycling
Basin deposition on stable continents
Growth of stable continental nuclei; oldest macroscopic evidence for life
First preserved sedimentary rocks, with chemical traces of life
Oldest preserved pieces of continental crust
Rapid crust formation & recycling; continued heavy meteorite bombardement
Jack Hillsian' or Zirconian
Accretion of giant Moon-forming impact event
541 First appearance of Ediacaran Fauna / End of Global Glaciation
635
720 Beginning of near-global Glaciation
1780 First appearance of sulphidic marine deposits
2060 End of LJE / Start of Corg-rich deposition
2250 First appearance of positive δ13C anomalies +/or breakout magmatism
2420 First appearance of glacial deposits
2630 First appearance of Hamersley BIF
2780 First appearance of continental flood basalts and/or negative δ13Ckerogen values
3020 First appearance of terrestrial basins
3490 First appearance of macroscopic fossils (stromatolites)
3810 Earth's oldest supracrustal rocks
4030 Earth's oldest rocks (Acasta Gneiss)
4404 Earth's oldest crustal material (detrital zircons)
4567 Formation of the solar system

Figure 2

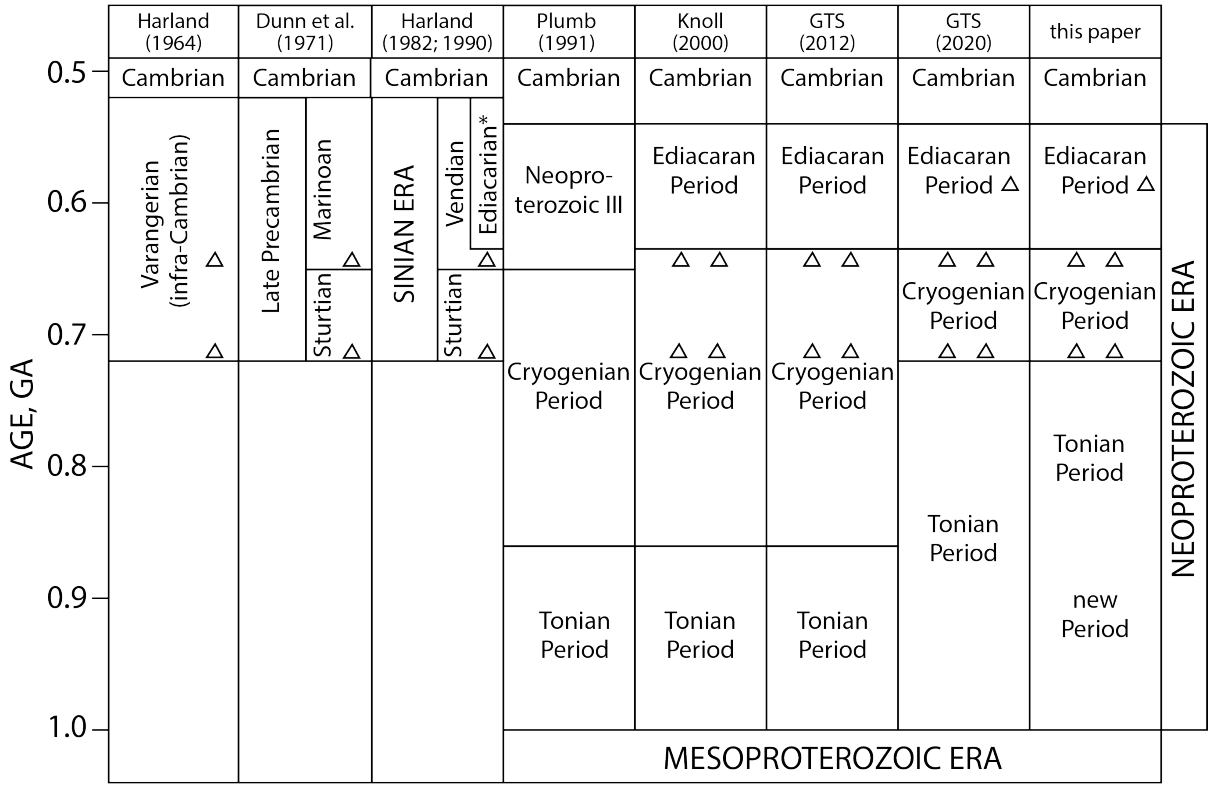
Harland (1964)
Dunn et al. (1971)
Harland (1982; 1990)
Plumb (1991)
Knoll (2000)
GTS (2012)
GTS (2020)
this paper
Cambrian
Varangerian (infra-Cambrian)
Late Precambrian
Marinoan
Sturtian
SINIAN ERA
Vendian
Ediacarian*
Sturtian
Neopro-terozoic III
Cryogenian Period
Tonian Period
Ediacaran Period
Cryogenian Period
Tonian Period
Ediacaran Period
Cryogenian Period
Tonian Period
Ediacaran Period
Cryogenian Period
Tonian Period
new Period
NEOPROTEROZOIC ERA
MESOPROTEROZOIC ERA
AGE, GA
0.5
0.6
0.7
0.8
0.9
1.0

Figure 3

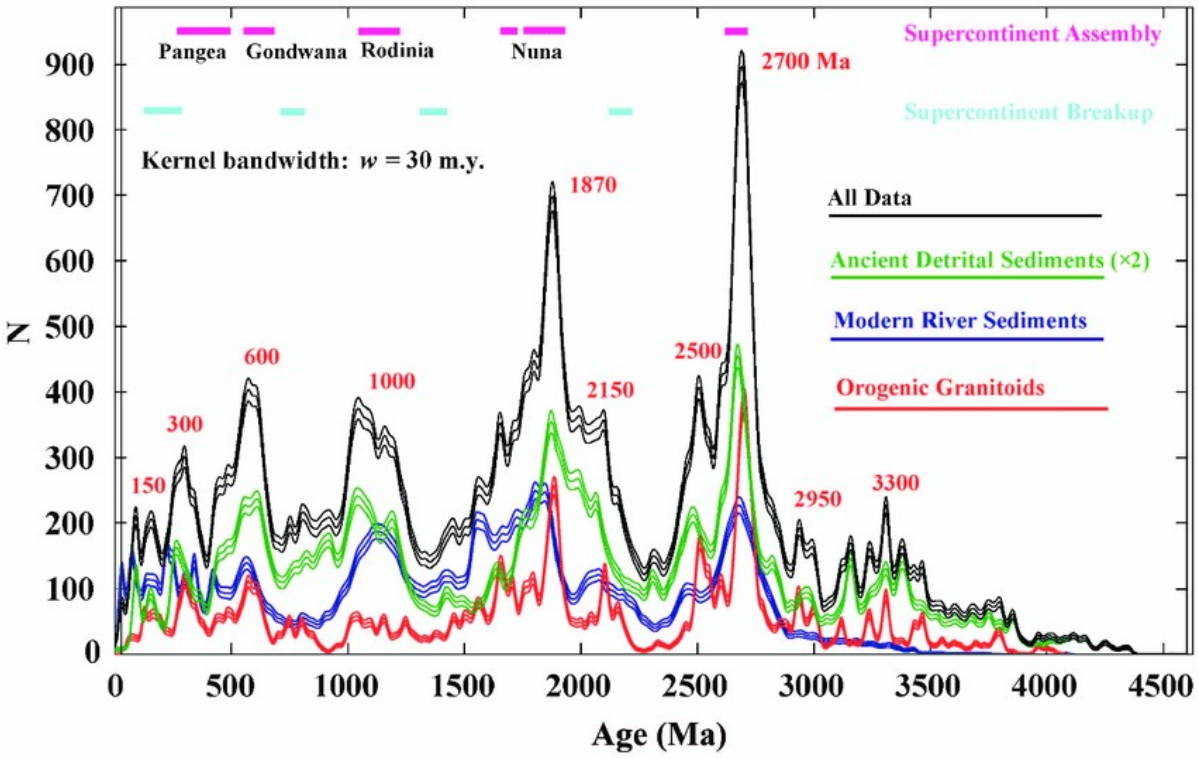
Pangea
Gondwana
Rodinia
Nuna
Supercontinent Assembly
Supercontinent Breakup
2700 Ma
Kernel bandwidth: w = 30 m.y.
1870
All Data
Ancient Detrital Sediments (×2)
Modern River Sediments
Orogenic Granitoids
600
1000
2500
300
2150
150
2950
3300
N
900
800
700
600
500
400
300
200
100
0
0
500
1000
1500
2000
2500
3000
3500
4000
4500
Age (Ma)

2101 Figure 4

2102

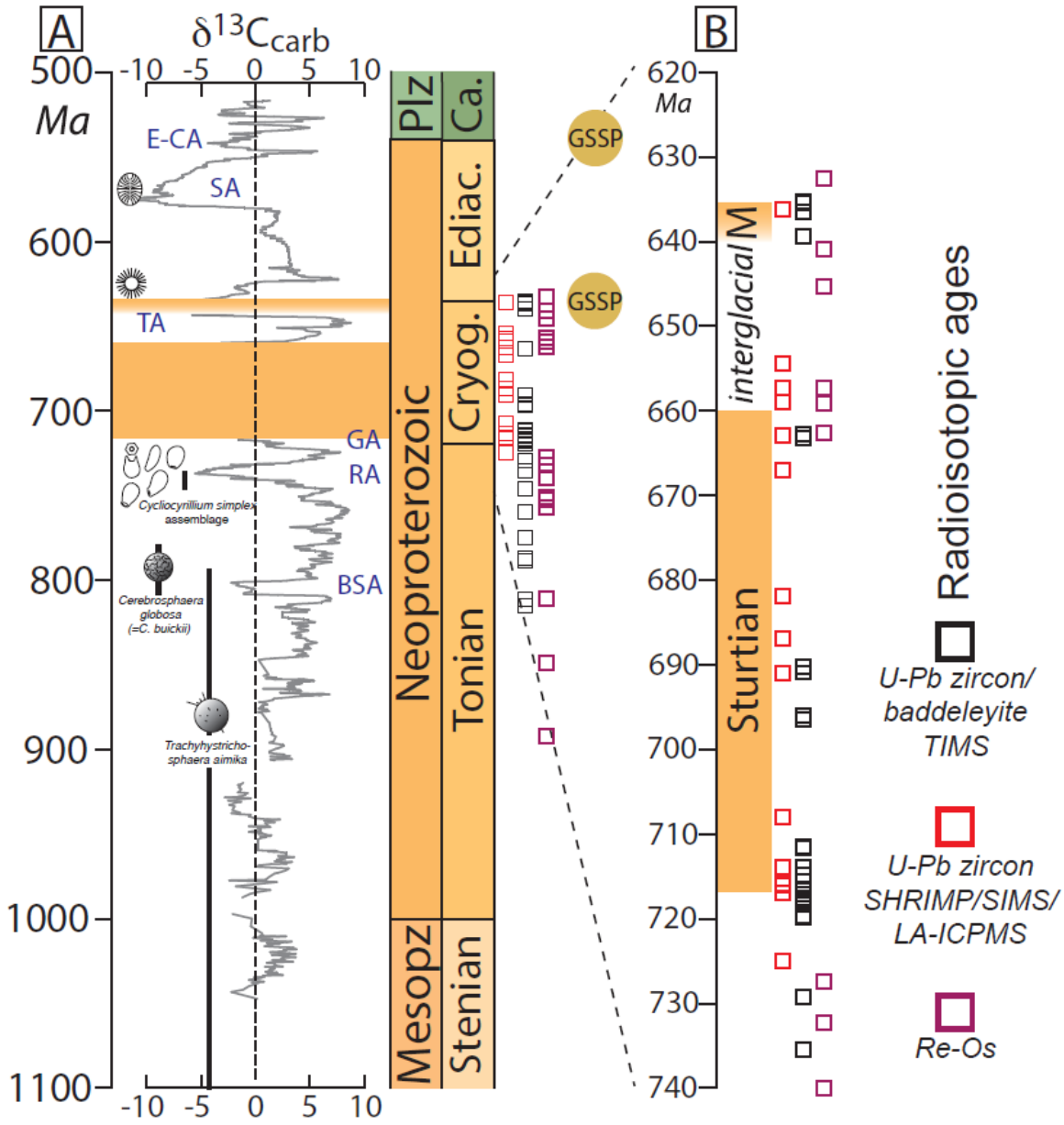

2103

2104

2105

2106 Figure 5
2107
2108

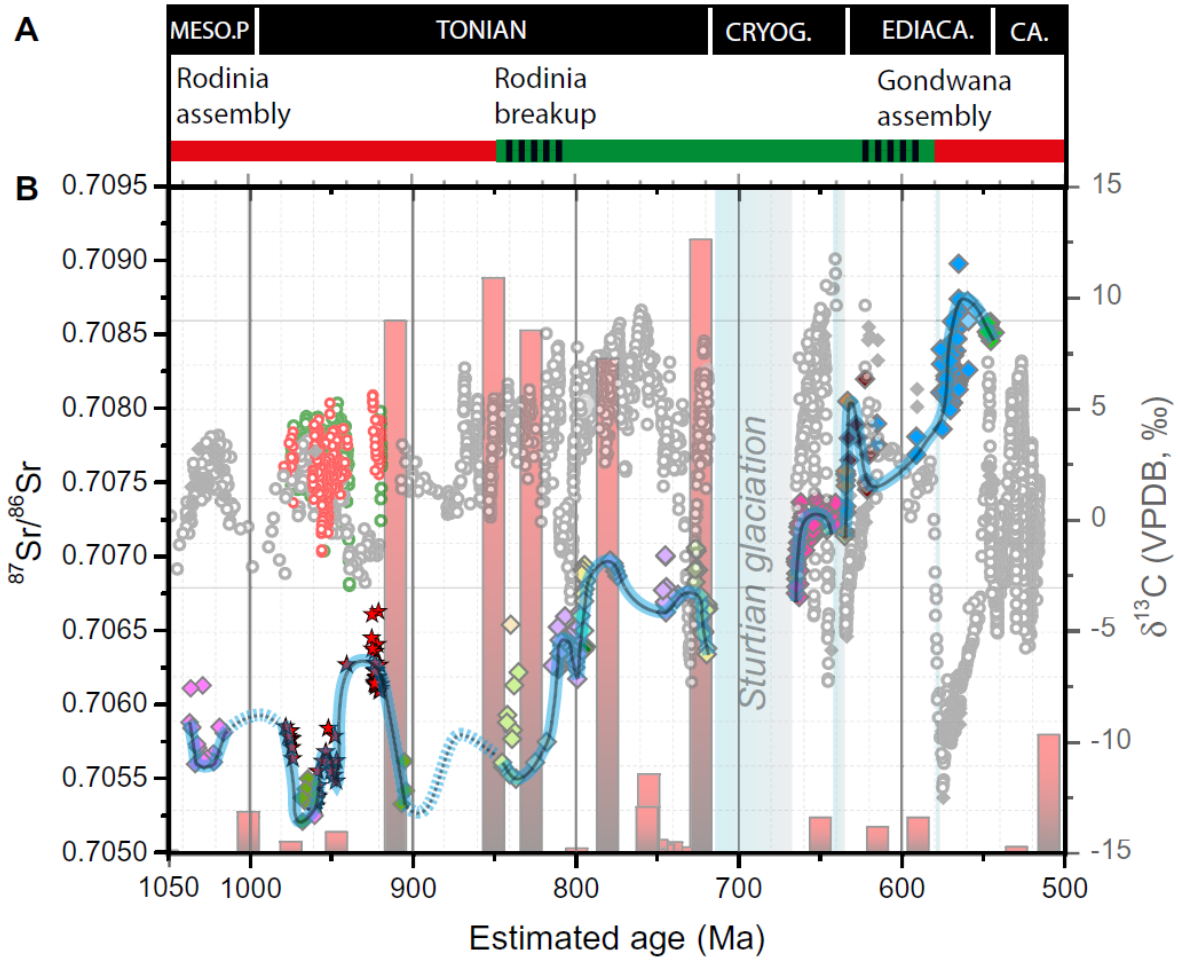

2109
2110

2111 Figure 6

2112

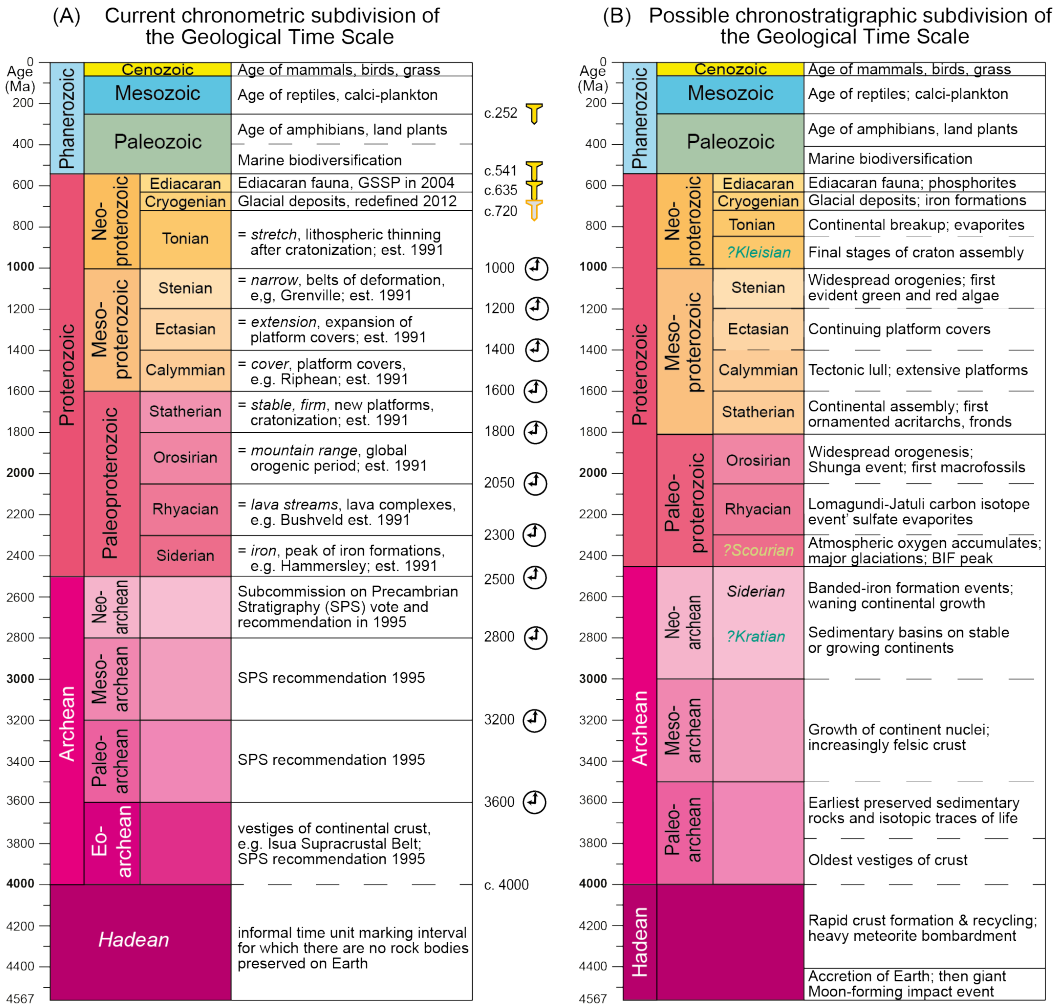

2113

2114

2115